Methods[1]

Expedition 320/321 Scientists[2]

Chapter contents

Introduction 1
Reconstruction of geologic age during Expedition 320/321 4
Lithostratigraphy 5
Biostratigraphy 8
Paleomagnetism 11
Geochemistry 13
Physical properties 17
Stratigraphic correlation and composite section 22
Downhole measurements 24
References 28
Figures 34
Tables 62

Introduction

The Pacific Equatorial Age Transect (PEAT) program, which includes Integrated Ocean Drilling Program (IODP) Expeditions 320 and 321, was the first scientific program following the complete refit of the R/V *JOIDES Resolution*. During this process, scientific facilities on the ship were replaced with a completely new structure and all major drilling and ship systems were completely refurbished. All laboratory equipment used on these first two expeditions was new, refurbished, upgraded, or replaced. This was also the first scientific use of the new software controlling the instruments and new database system.

Information assembled in this chapter will help the reader understand the basis for our shipboard observations and preliminary conclusions. It will also enable the interested investigator to identify data and select samples for further analysis. Information presented here concerns only shipboard operations and analyses described in the site chapters. Methods used by various investigators for shore-based analyses of Expedition 320/321 data will be described in individual publications in various professional journals and the **"Expedition research results"** of this *Proceedings* volume. This introductory section provides an overview of operations, curatorial conventions, and general core handling and analysis.

Site locations

At all Expedition 320/321 sites, Global Positioning System (GPS) coordinates from precruise site surveys were used to position the vessel on site. The only seismic system used during the cruise was the Syquest Bathy 2010 CHIRP Subbottom Profiler, which was monitored on the approach to each site to reconfirm the seafloor depth with those from the precruise survey. Once the vessel was positioned at a site, the thrusters were lowered and a positioning beacon was dropped to the seafloor. The dynamic positioning control of the vessel uses navigational input from the GPS and triangulation to the seafloor beacon, weighted by the estimated positional accuracy (Fig. **F1**). The final hole position was the mean position calculated from the GPS data collected over the time that the hole was occupied.

Drilling operations

The advanced piston corer (APC) and the extended core barrel (XCB) were used during Expedition 320/321. These standard cor-

[1] Expedition 320/321 Scientists, 2010. Methods. *In* Pälike, H., Lyle, M., Nishi, H., Raffi, I., Gamage, K., Klaus, A., and the Expedition 320/321 Scientists, *Proc. IODP,* 332/321: Tokyo (Integrated Ocean Drilling Program Management International, Inc.). doi:10.2204/iodp.proc.320321.102.2010
[2] **Expedition 320/321 Scientists' addresses.**

doi:10.2204/iodp.proc.320321.102.2010

ing systems and their characteristics are summarized in Graber et al. (2002). The APC system cuts soft sediment cores with minimal coring disturbance relative to other IODP coring systems. After the APC core barrel is lowered through the drill pipe and lands near the bit, the drill pipe is pressured up until the two shear pins that hold the inner barrel attached to the outer barrel fail. The inner barrel then advances into the formation and cuts the core. The driller can detect a successful cut, or "full stroke," from the pressure gauge on the rig floor. The XCB system is deployed when the formation becomes either too stiff for the APC system, or when drilling harder substrate such as chert. The XCB cutting shoe (bit) extends ~30.5 cm ahead of the main bit in soft sediments but retracts into the main bit if hard formations are encountered.

The standard bottom-hole assembly (BHA) used at Expedition 320/321 sites was composed of an 11⅞ inch (~29.05 cm) drill bit, a bit sub, a seal bore drill collar, a landing saver sub, a modified top sub, a modified head sub, a nonmagnetic drill collar, seven 8 inch (~20.32 cm) drill collars, a tapered drill collar, six joints (two stands) of 5½ inch (~13.97 cm) drill pipe, and one crossover sub. A lockable flapper valve was used so that we could collect downhole logs without dropping the bit.

APC refusal is conventionally defined in two ways: (1) the piston fails to achieve a complete stroke (as determined from the pump pressure reading) because the formation is too hard or (2) excessive force (>60,000 lb; ~267 kN) is required to pull the core barrel out of the formation. In the case where full or partial stroke can be achieved but excessive force cannot retrieve the barrel, the core barrel can be "drilled over;" after the inner core barrel is successfully shot into the formation, the drill bit is advanced to total depth to free the APC barrel. This strategy allows a hole to be advanced much farther with the APC, the preferred coring tool. Nonmagnetic core barrels were used during all conventional APC coring, but the APC drillover technique was not used in the first hole at each site because chert was expected at these sites. Standard steel core barrels were used when utilizing the drillover technique because they are stronger than the nonmagnetic barrels.

Most APC/XCB cored intervals were ~9.5 m long, which is the length of a standard core barrel. In some cases, the drill string was drilled or "washed" ahead without recovering sediments to advance the drill bit to a target depth where core recovery needed to be resumed. Such advances were necessary in multiple holes at a site to ensure that coring gaps in one hole were covered by cored intervals in adjacent holes. The amount of advance was typically 1–4 m and accounted for drilling depth shift caused by tides, heave, and other factors (see **"Stratigraphic correlation and composite section"**). After chert horizons were established in Hole A at each site by coring and logging, these intervals were often drilled through using a center bit, so as to obtain piston cores below. Core recovery information is shown in the "Operations" section of each site chapter.

All APC cores taken during Expedition 321 and some APC cores taken during Expedition 320 were oriented using the FlexIt tool (see **"Paleomagnetism"**). Formation temperature measurements were made in Hole B of each site (see **"Downhole measurements"**) so we could use the formation information from Hole A to avoid any chert layers that might damage the tools. Downhole logging was conducted in one hole at each site.

IODP depth conventions

For the last few decades, Deep Sea Drilling Project, Ocean Drilling Program (ODP), and IODP Phase 1 reports, diagrams, and publications used three primary designations to reference depth: meters below rig floor (mbrf), meters below seafloor (mbsf), and meters composite depth (mcd). These designations were combinations of origin of depth scales (rig floor or seafloor), measurement units (m), and method of construction (composite). The designations evolved over many years based on the needs of individual science parties.

Over the course of ODP and IODP scientific drilling, issues with the existing depth scale designations and the lack of a consistent framework became apparent. For example, application of the same designation to scales created with distinctly different tools and methods was common (e.g., mbsf for scales measured by drill string tally and those measured with the wireline). Consequently, new scale-type designations were created ad hoc to differentiate the wireline logging scale from the core depth scale depth-mapping procedures and products could be adequately described. Management and use of multiple maps, composite scales, or splices for a hole or a site was problematic and the requirement to integrate scientific procedures among three IODP implementing organizations amplified the need to establish a standardized and versatile depth framework.

Given the opportunity offered by the hiatus in IODP drilling operations, a new classification and a nomenclature for depth scale types were defined in 2006–2007 (see IODP Depth Scales Terminology at **www.iodp.org/program-policies/**) (Table **T1**). The framework forms a basis upon which the implementing organizations could address more specific issues of how to manage depth scales, depth maps, and

splices. This new depth framework has been implemented within the context of the new Laboratory Information Management System (LIMS) aboard the *JOIDES Resolution*.

The new methods and nomenclature of calculating sample depth in a hole has changed to be method-specific. This will ensure that data acquisition, mapping of scales, and construction of composite scales and splices are unequivocal.

The primary scales are measured by the length of drill string (e.g., drilling depth below rig floor [DRF], drilling depth below seafloor [DSF]), length of core recovered (e.g., core depth below seafloor [CSF], core composite depth below seafloor [CCSF]), and logging wireline (e.g., wireline log depth below rig floor [WRF], wireline log depth below seafloor [WSF]). All units are in meters.

Core handling and analysis

As soon as cores arrived on deck, headspace samples were taken using a syringe for immediate hydrocarbon analysis as part of the shipboard safety and pollution prevention program. Core catcher samples were taken for biostratigraphic analysis. Whole-round samples were taken from some core sections for shipboard interstitial water examinations and waters for postcruise analyses. Rhizon interstitial water samples were taken for selected intervals in addition to whole rounds (see **"Geochemistry"**). In addition, samples were immediately taken from the ends of cut sections for shore-based microbiological analysis.

To facilitate real-time drilling decisions to maximize stratigraphic overlap between holes, whole-round core sections were run through the Special Task Multisensor Logger (STMSL), which collects magnetic susceptibility and gamma ray attenuation (GRA) bulk density immediately after entering the core laboratory (see **"Stratigraphic correlation and composite section"**). After the cores reached equilibrium with laboratory temperature (typically after 4 h), whole-round core sections were run through the Whole-Round Multisensor Logger (WRMSL; *P*-wave velocity, density, magnetic susceptibility, and resistivity) and the natural gamma loggers. Thermal conductivity measurements were also taken, typically in Section 3 of each core.

The cores were then split lengthwise into working and archive halves, from bottom to top. Investigators should be aware that older material could have been transported upward on the split face of each section during splitting. The working half of each core was sampled for shipboard biostratigraphy, physical properties, carbonate, paleomagnetism, bulk X-ray diffraction (XRD) mineralogy, and shore-based studies. Shipboard sampling was kept to a minimum during Expedition 320/321 to allow construction of a detailed sampling plan after the composite section was built. Archive-half sections were scanned on the Section-Half Multisensor Logger (SHMSL), measured for color reflectance on the Section-Half imaging logger (SHIL), described visually and by means of smear slides, and finally run through the cryogenic magnetometer. No core sampling was done on board other than for shipboard analyses and personal samples for research focusing on ephemeral properties. Both halves of the core were then put into labeled plastic tubes, sealed, and transferred to cold storage space aboard the ship. At the end of the expedition, the cores were transferred from the ship into refrigerated trucks and then to cold storage at the IODP Gulf Coast Repository in College Station, Texas (USA).

Drilling-induced core deformation

When cores are split significant sediment disturbance may be observed. This might include a concave-downward appearance of originally horizontal bedding, haphazard mixing of lumps of different lithologies (mainly at the tops of cores), fluidization, and flow-in (primarily at the bottoms of cores). The "Lithology" section in each site chapter presents the observations of core disturbance. Core deformation may also occur during retrieval because of changes in pressure and temperature as the core is raised and during cutting and core handling on deck.

Curatorial procedures and sample depth calculations

Numbering of sites, holes, cores, and samples followed the standard IODP procedure. A full curatorial identifier for a sample consists of the following information: expedition, site, hole, core number, core type, section number, and interval in centimeters measured from the top of the core section, and also the sampling tools and volumes taken. For example, a sample identification of "320-U1331A-1H-2, 10–12 cm" represents a sample taken from the interval between 10 and 12 cm below the top of Section 2 of Core 1 ("H" designates that this core was taken with the APC system) of Hole A of Site U1331 during Expedition 320. The "U" preceding hole numbers indicates the hole was drilled by the United States Implementing Organization platform, the *JOIDES Resolution*.

Core intervals are defined by the length of drill string, the seafloor depth, and the amount the driller advances the core barrel, reported in DSF. Once a core is recovered on board, the length of core is measured and this is the "curated" length. The depth of a sample below seafloor (CSF) is calculated by adding

the depth of the sample below the section top and the lengths of all higher sections in the core to the core-top depth measured with the drill string (DSF). A soft to semisoft sediment core from less than a few hundred meters below seafloor expands upon recovery (typically a few percent to as much as 15%), so the recovered interval does not match the cored interval. In addition, a coring gap typically occurs between cores, as shown by composite depth construction (see **"Stratigraphic correlation and composite section"**). Thus, a discrepancy can exist between the DSF depth and the CSF depth.

For instance, when a recovered core measures >100% of the cored interval, the CSF depth of a sample taken from the bottom of that core will be deeper than that from a sample from the top of the subsequent core. For this expedition we report all results in the core depth below seafloor method with allowing these overlaps (CSF) (Table **T1**), chiefly to avoid confusion during core description and sampling. The primary focus of Expedition 320/321 was obtaining complete sections, so multiple APC/XCB holes (typically three) were drilled at a site to construct a continuous composite sections; these are reported as CCSF. CCSF depths were reported in two manners. CCSF-A is the depth based on a simple alignment of cores from multiple adjacent holes. CCSF-A is generally longer than CSF. CCSF-B is the CCSF-A depth divided by a linear scaling factor to "compress" the depth scale to approximate CSF.

If a core has incomplete recovery, all cored material is assumed to originate from the top of the drilled interval as a continuous section for curation purposes. The true depth interval within the cored interval is not known. This should be considered as a sampling uncertainty in age-depth analysis and correlation of core data with downhole logging data.

Reconstruction of geologic age during Expedition 320/321

A major task aboard the *JOIDES Resolution* during the PEAT expedition was to establish an age model for each site. These age models will be further refined during postcruise shore-based work. It is anticipated that the final limit of resolution in the PEAT site age models will depend mainly on sedimentation rate and thickness of the bioturbated layer at each site. Under these premises, and assuming average sedimentation rates of 1–2 cm/k.y. for the PEAT biogenic sediments, a sample resolution of 10 cm offers a relative time resolution of 5–10 k.y. Ultimately, after postcruise work the goal is to constrain the geologic age of any such sample to a precision that is better than ±50 k.y. in any part of the age span of the PEAT cores (i.e., from ~53 Ma to the present). The age resolution provided during the shipboard work is considerably less precise and depends on how well sedimentation rates can be constrained.

The reconstruction of geologic age and sedimentation rates in PEAT sediments involves several different data sets. The first crucial step in this process was to select a framework timescale for Eocene through recent times, the age span of the PEAT sediments. Geologic timescales are being constantly improved and refined as new methods and approaches are developed and new data are generated. This also holds true for Cenozoic timescales. Existing timescales for the Cenozoic era are built using a combination of geomagnetic polarity data and biostratigraphy (e.g., Berggren et al., 1995) and, more recently, cyclostratigraphy tuned to the orbital metronome (e.g., Shackleton et al., 1995; Lourens et al., 2004; Pälike et al., 2006b). The chosen timescale for the Pacific Equatorial Age Transect has been pieced together from three different timescales because at present this combination is considered to represent the best available organization and subdivision of Cenozoic time for marine sediments. The three data sets are arranged chronologically to encompass the past 60 m.y.: Neogene time (0–23 Ma) is based on work presented by Lourens et al. (2004), Oligocene and Eocene time (23–42.5 Ma) is based on work presented by Pälike et al. (2006b), and Eocene through late Paleocene time (42.5–60 Ma) is based on work presented by Cande and Kent (1995). Details about how these three data sets were merged are discussed in **"Magnetostratigraphy."**

The PEAT timescale is summarized in a series of figures (Figs. **F2, F3, F4**). These graphs show how the geomagnetic polarity zones (chrons and subchrons) are correlated to formal geochronologic units, Cenozoic epochs (Pleistocene through Paleocene), and standard, albeit informal, subdivisions of these epochs (early, middle, late; see Salvador, 1994). In order to avoid overloading the figures, we have omitted corresponding chronostratigraphic units (series) as well as the next higher rank (above epoch) in the geochronologic hierarchy (period) and the next lower rank (age).

Another key data set used during shipboard work for reconstruction of geologic age consists of micropaleontological bioevents. Shipboard PEAT expertise covers benthic and planktonic foraminifers, calcareous nannofossils, diatoms, and radiolarians. Biostratigraphers acquired whole-assemblage data in terms of abundance and preservation for the different microfossil groups. The rate of taxonomic evolution, defined as the number of evolutionary appearances and extinctions per unit time, determines the bio-

stratigraphic resolution attainable. In a few cases, distinct abundance crossovers among two taxa at the species or genus level, often ancestor/descendant, are employed as biostratigraphic marker events as well as coiling direction changes (in planktonic foraminifers). All bioevents used during the PEAT expeditions have been calibrated either to magnetostratigraphic polarity zones (chrons and subchrons) and/or astrochronologically tuned cyclostratigraphies in numerous marine sediment cores/sections gathered at different geographic locations. Subsequently, calibration ages have been integrated into a single age estimate considered to be presently the best available age for each bioevent. Original calibration ages of some bioevents are derived from different (pre-PEAT) timescales. We have therefore recalculated these, using linear interpolation, in order to adjust them to our chosen PEAT framework timescale. Each bioevent thus has a given age estimate expressed in Ma. All bioevents used during the PEAT expeditions are shown in Figures F2 and F3, which also show how individual bioevents relate to geochronologic epochs and geomagnetic polarity zones. Bioevents and their associated best-age estimates are listed in Tables T2, T3, T4, and T5. References presenting published calibrations (in some cases prior to adjustment to the corrected PEAT timescale) can be found in BIOSTRAT in "Supplementary material."

Biostratigraphic data are unique in the sense that they represent a continuum of organic evolution among the planktonic and benthic assemblages. The various assemblages and their component taxa are thus uniquely confined to certain geological time intervals. Thus, we can arrange the stratigraphic column in terms of relative time based on the order in which microfossil taxa appear and become extinct. This crucial biostratigraphic character is employed to guide the interpretation of magnetostratigraphic and cyclostratigraphic data, which in contrast can only be used to tell geologic age if we know to which part of the stratigraphic column they belong. Biostratigraphers provided this guiding input to cyclo- and magnetostratigraphers.

Geologic age information derived from bio- and magnetostratigraphers is integrated by stratigraphic correlators, who in turn generate age-depth plots and calculate sedimentation rates (see "Stratigraphic correlation and composite section") for each PEAT site. The core depth below seafloor is estimated using a core composite depth scale (CCSF-A) (see "Stratigraphic correlation and composite section").

A few days after the PEAT expedition phase ended in late June 2009, the International Union of Geological Sciences Executive Committee decided to ratify the suggestion by the International Commission on Stratigraphy to make the following changes to the subdivision of Cenozoic time: (1) the Quaternary is established as a third system/period; (2) the Quaternary is divided into two series/epochs (Pleistocene and Holocene); (3) the lower boundary of the Pleistocene series is moved to encompass the Gelasian stage, which previously belonged to the Pliocene series, thereby shortening the Pliocene epoch and Neogene period by 782 k.y.; and (4) the Neogene/Quaternary (Pliocene/Pleistocene) boundary has an age of 2.588 Ma according to the August 2009 version of the International Stratigraphic Chart (www.stratigraphy.org). As these changes occurred after the PEAT timescale was established and extensively used by the two expeditions, we adhere to the PEAT subdivision of late Cenozoic time, following Lourens et al. (2004).

Lithostratigraphy

The lithostratigraphy of sediments recovered during Expedition 320/321 was determined by a combination of core description, smear slide and thin section analyses, and digital color imaging. The methods employed were based on those used during ODP Leg 199 (Shipboard Scientific Party, 2002), which recovered sediments similar to those drilled during Expedition 320/321, and IODP Expedition 320T, the first expedition to use the new IODP core description and database systems employed here (Expedition 320T Scientists, 2009).

New core description process and database

A new core description process and database, first implemented and assessed during Expedition 320T, was used during Expedition 320/321 using DESClogik software. Prior to drilling operations, two spreadsheet templates were constructed in Tabular Data Capture and customized for Expedition 320 using the lithostratigraphic results of ODP Legs 199 and 138 as a guide (Shipboard Scientific Party, 2002; Mayer, Pisias, and Janecek, et al., 1992). The first of these spreadsheet templates was used to record core descriptions (Fig. F5). The second template was used to record descriptions of smear slides and thereby quantify the texture and relative abundance of biogenic and nonbiogenic components (Fig. F6).

Visual core description and barrel sheets

Visual core descriptions of the archive half of the split cores provide a summary of the data obtained during shipboard analysis. Visual core description data were recorded digitally in real time using DESClogik. DESClogik includes a graphic display mode of core data display (e.g., aligned digital

images of section halves and various measurement data) that can be used to aid core description. During Expedition 320/321, the STRATER software package was used to compile the visual core descriptions for each core. Site, hole, and core number are given at the top of the visual core description together with a summary core description (Fig. F7). Core depth below seafloor, core length, and section breaks are indicated along the left side of the digital color image of the core and Graphic Lithology column. Columns to the right of the Graphic Lithology column show data collected by the WRMSL and SHMSL (see "Physical properties"). These include GRA densitometer bulk density, corrected magnetic susceptibility, and lightness as determined by color reflectance (L*). Columns to the right of these data show stratigraphic age, shipboard samples taken, sedimentary structures (bioturbation intensity and sedimentary structure type), lithologic accessories, and sediment disturbance.

Digital color image

The SHIL imaged the flat face of split cores using a line scan camera. Sediment cores are imaged as soon as possible after splitting to minimize color changes that occur through oxidation and drying. The flat face of the archive-half section was scraped with the edge of a glass slide to provide a "clean" surface for imaging. Images are taken at an interval of 10 lines/mm. Camera height is adjusted so that image pixels are square. Light is provided by three pairs of Advanced Illumination high-current focused light emitting diode line lights with fully adjustable angles to the lens axis. Note that compression of line-scanned images into compiled stacks may result in artifacts (e.g., false appearance of lamination).

Graphic lithology

Each recovered lithology is shown in the Graphic Lithology column on the visual core description (Figs. F7, F8). For intervals composed of more than one lithology, symbols are arranged within the column from left to right in order of their relative abundance. Graphic lithologies are used for all components that compose 25% or more of the total sediment. The width of each pattern in the column approximates the relative abundance of that component.

Sedimentary structures

Sedimentary structures formed by natural processes (i.e., not a result of drilling disturbance) are represented on the barrel sheet with symbols in the Structures column. Structures formed by both biogenic and physical processes are included. An estimate of bioturbation intensity is indicated on the left side of the Structures column. Bioturbation intensity is classified as nonvisible, indicating either the complete absence of bioturbation (0% of the surface area) or a completely bioturbated sediment (100% of the surface area); minor (<30% of the surface area); moderate (30–60% of the surface area); and intense (>60% of the surface area) following Droser and Bottjer (1986) and Kemp (1995). When identifiable, ichnofossils of *Zoophycos, Skolithos, Chondrites,* and *Planolites* burrows were reported in the lithologic description; however, during Expedition 320 these were included in the electronic database "comments." Sedimentary structure types are indicated on the right side of the Structures column (e.g., nodules and soft-sediment deformation structures). All contacts between lithologies are gradational unless otherwise specified.

Drilling disturbance

Sediment disturbance resulting from the coring process is illustrated in the Drilling Disturbance column on the visual core description (e.g., flow-in, biscuits, and drilling breccia) (Fig. F8). If the feature extends over an interval, the symbol appears centered on a vertical line to denote the extent of occurrence. Blank regions indicate an absence of drilling disturbance.

Sample types

Visual core descriptions display where sample material was taken for shipboard analysis (all whole rounds and all samples taken to aid core description). Whole rounds consist of samples taken for interstitial pore water and micropaleontology samples. Samples taken to aid core description including "toothpick" samples were analyzed for smear slides, thin section billets, and discrete samples for mineralogical analysis by XRD (Fig. F8). Typically, three or four smear slides were made per core, but more samples were selected in cores showing a high degree of lithologic variability. Interstitial pore water samples were taken at designated intervals, and a micropaleontology sample was obtained from the core catcher of most cores. XRD samples were taken only where needed to assess the lithologic components.

Color

In addition to the digital color image captured by the SHIL, visual core descriptions show sediment color and the corresponding hue, value, and chroma data as determined qualitatively using Munsell Soil Color Charts (Munsell Color Company, 1994). These data were recorded immediately after cores were split to avoid color changes associated with drying and redox reactions.

Core summary

The written description for each core contains a brief overview of both major and minor lithologies, their Munsell color, and notable features such as sedimentary structures and major disturbances resulting from the coring process.

Smear slide descriptions

Smear slide samples were taken by toothpick sampling of the split core to establish major and minor lithologies. Visual percentage estimates of biogenic, nonbiogenic, and textural features were made from each slide (Fig. F6). Biogenic components were divided into major microfossil groups (e.g., nannofossils, radiolarian, fish debris). Basic mineralogies were identified. The zeolite minerals phillipsite and clinoptilite were identified and tabulated individually in the smear slide template; however, they are depicted in the final visual core description as "zeolites."

Sediment classification

Lithologic names consist of a principal name based on composition, degree of lithification, and/or texture as determined from visual core description, smear slide, and thin section observations. For a mixture of components, the principal name is preceded by major modifiers (in order of increasing abundance) that refer to components making up ≥25% of the sediment. Minor components that represent between 10% and 25% of the sediment follow the principal name (after a "with") in order of increasing abundance. For example, an unconsolidated sediment containing 30% nannofossils, 25% clay minerals, 20% foraminifers, 15% quartz silt, and 10% manganese nodules would be described as a clayey nannofossil ooze with manganese nodules, quartz silt, and foraminifers. Sedimentary components that make up <25% of the total sediment are not designated in the Graphic Lithology column. Our naming conventions follow the ODP sediment classification scheme (Mazzullo et al., 1988).

Sediments were divided into lithostratigraphic units on the basis of composition and abundance of different grain types estimated from visual examination of the core, smear slides, thin sections, shipboard measurements of carbonate content (see below), and shipboard XRD analyses (see below) (Fig. F9). When encountered, fragments of pumice are noted in each visual core description. Size divisions for grains are those of Wentworth (1922) (Fig. F9).

Terms that describe lithification vary depending upon the dominant composition, as described below:

1. Sediments derived predominantly from calcareous pelagic organisms (e.g., calcareous nannofossils and foraminifers): the lithification terms "ooze," "chalk," and "limestone" reflect whether the sediment can be deformed with a finger (ooze), can be scratched easily by a fingernail (chalk), or cannot be scratched easily (limestone).
2. Sediments derived predominantly from siliceous microfossils (e.g., diatoms and radiolarians): the lithification terms "ooze," "diatomite/radiolarite," "porcellanite," and "chert" reflect whether the sediment can be deformed with a finger (ooze), cannot be easily deformed manually (diatomite/radiolarite), or displays a glassy luster (chert). We use the term porcellanite as defined by Keene (1975) to describe a siliceous limestone/claystone that has a dull luster and is less hard and compact than chert. It may contain a mix of opal, quartz, clay minerals, and carbonate. Note that the terms "porcellanite" and "chert" do not imply crystallinity of the silica.
3. Sediments derived predominantly from siliciclastic material: if the sediment can be deformed easily with a finger, no lithification term is added and the sediment is named for the dominant grain size. For more consolidated material, the lithification suffix "-stone" is appended to the dominant size classification (e.g., "clay" versus "claystone").

Core curation and shipboard sampling of igneous rocks

We examined core sections containing igneous rocks prior to cutting the core with a diamond-impregnated saw to describe important mineralogic and structural features. Each piece was numbered sequentially from the top of the core section and labeled on the outside surface. Pieces that could be fit together were assigned the same number and lettered consecutively (e.g., 1A, 1B, 1C, etc.). Plastic spacers were placed between pieces with different numbers. The presence of a spacer may represent a substantial interval of no recovery. If it was evident that an individual piece had not rotated about a horizontal axis during drilling, an arrow was added pointing to the top of the section.

Visual core descriptions and barrel sheets for igneous rocks

The few fragments of basalt recovered during Expedition 320/321 were described in the database templates and annotated visual core descriptions of the core were used for the sediments.

X-ray diffraction analyses

Because of technical difficulties, only a handful of XRD analyses were conducted during Expedition

320/321. Bulk sample analyses were performed using a Bruker D-4 Endeavor X-ray diffractometer with a Vantec detector using Ni-filtered CuKα radiation. Instrument conditions were as follows: voltage = 40 kV, current = 40 mA, goniometer scan = 2–70°2θ (air-dried samples), step size = 0.01°2θ, scan speed = 1.2°2θ/min, and count time = 0.5 s.

Biostratigraphy

Preliminary age assignments were based on biostratigraphic analyses of calcareous nannofossils, planktonic foraminifers, radiolarians, and diatoms. Paleodepth interpretations were based on benthic foraminifers. The biostratigraphy is tied to the geomagnetic polarity timescale (GPTS) used for Expedition 320/321, which is based upon a composite of several timescales (Table **T6**) (Cande and Kent, 1995; Lourens et al., 2004; Pälike et al., 2006b). Planktonic foraminifer, calcareous nannofossil, radiolarian, and diatom bioevents for the middle Eocene to Pleistocene were recalibrated to Lourens et al. (2004) and Pälike et al. (2006b) (Tables **T2, T3, T4, T5**). Neogene calcareous bioevents are reported to a 10 k.y. resolution, Paleogene calcareous bioevents are reported to a 100 k.y. resolution, and biosiliceous bioevents are reported to a 10 k.y. resolution.

Calcareous nannofossil datum depths were determined by examining core catcher samples and, where appropriate, additional section samples (sampling spacing of 1.5–0.25 m). Planktonic and benthic foraminifers, radiolarians, and diatoms were examined in core catcher samples and additional section samples (sampling spacing of ~2–4 m). Preservation, abundance, and zonal assignment for selected samples and for each microfossil group were initially recorded and saved in Microsoft Excel and subsequently entered through DESCLogik into the LIMS database. Biostratigraphic analyses were focused on Hole A, allowing greater sampling density. Samples were taken from the composite splice to provide more complete stratigraphic coverage, where appropriate.

Calcareous nannofossils

Calcareous nannofossil zonal scheme and taxonomy

The zonal scheme of Martini (1971), zonal code numbers NP and NN, was used for Cenozoic calcareous nannofossil biostratigraphy. These zonations represent a general framework for the biostratigraphic classification of mid- to low-latitude nannofossil assemblages and are presented in Figure **F2.** Top *Sphenolithus ciperoensis* is used for recognizing the base of Zone NN1, following Perch-Nielsen (1985). The base of Zone NN2 (base of *Discoaster druggii*) cannot be differentiated because of the rare and sporadic occurrences of the marker fossil. Ages and calibration sources for calcareous nannofossil datums are presented in Table **T2.** The age estimates presented are all adjusted to the Expedition 320/321 timescale (see **"Reconstruction of geologic age during Expedition 320/321"**). Nannofossil taxonomy follows Bown (1998, 2005) and Perch-Nielsen (1985), where full taxonomic lists can be found. A taxonomic list of nannofossil species from Table **T2** is given in BIOSTRAT in **"Supplementary material."**

Methods of study for calcareous nannofossils

Calcareous nannofossils were examined in smear slides using standard light microscope techniques under crossed polarizers, transmitted light, and phase contrast at 1000× magnification.

Total calcareous nannofossil abundance within the sediment is recorded as follows:

D = dominant (>90% of sediment particles).
A = abundant (>50%–90% of sediment particles).
C = common (>10%–50% of sediment particles).
F = few (1%–10% of sediment particles).
R = rare (<1% of sediment particles).
B = barren (none present).

Abundance of individual calcareous nannofossil taxa is recorded as follows:

D = dominant (>100 specimens per field of view).
A = abundant (>10–100 specimens per field of view).
C = common (>1–10 specimens per field of view).
F = few (1 specimen per 1–10 fields of view).
R = rare (<1 specimen per 10 fields of view).

Preservation of the calcareous nannofossils is recorded as follows:

G = good (little or no evidence of dissolution and/or recrystallization, primary morphological characteristics only slightly altered, and specimens were identifiable to the species level).
M = moderate (specimens exhibit some etching and/or recrystallization, primary morphological characteristics somewhat altered; however, most specimens were identifiable to the species level).
P = poor (specimens were severely etched or overgrown, primary morphological characteristics largely destroyed, fragmentation has occurred, and specimens often could not be identified at the species and/or generic level).

Foraminifers

Planktonic foraminifer zonal scheme and taxonomy

The tropical planktonic foraminifer zonal scheme for the Paleocene (P zones) follows Olsson et al. (1999).

The Eocene and Oligocene (P and O zones, respectively) scheme follows Berggren and Pearson (2005). The Neogene (M, PL, and PT zones) scheme follows Berggren et al. (1995). The planktonic foraminifer zonal scheme used during Expedition 320/321 is illustrated in Figure **F4.** Ages and calibration sources of planktonic foraminifer datums are from multiple sources (Table **T3**). The age estimates presented are adjusted to the Expedition 320/321 timescale. Lourens et al. (2004) reports the astronomical calibration for the Neogene and we have incorporated additional recalibrated datums from Berggren et al. (1995), Berggren and Pearson (2005), and recent studies with biomagnetostratigraphy. For a more detailed discussion of the planktonic foraminifer zonation and revised calibrations to the PEAT timescale see Wade et al. (2007). Zone division of the middle Miocene is provided by the fohsellid lineage. However, we are unable to differentiate the base of Zone M9 because of the lack of calibration of *Globorotalia* (*Fohsella*) *lobata* to the astronomical timescale. Therefore, throughout this interval we employ both the M zones of Berggren et al. (1995) and the N zones of Blow (1969) (Fig. **F2B**). Planktonic foraminifer taxonomic concepts selectively follow those of Kennett and Srinivasan (1983), Bolli and Saunders (1985), Toumarkine and Luterbacher (1985), Loeblich and Tappan (1988), Spezzaferri and Premoli Silva (1991), Chaisson and Leckie (1993), Leckie et al. (1993), Spezzaferri (1994), Pearson (1995), Chaisson and Pearson (1997), Pearson and Chaisson (1997), and Pearson et al. (2006). A taxonomic list of planktonic foraminifer datum species from Table **T3** is given in BIOSTRAT in **"Supplementary material."**

Benthic foraminifer taxonomy and paleodepth determination

Taxonomic assignments follow Tjalsma and Lohmann (1983), van Morkhoven et al. (1986), Miller and Katz (1987), Thomas (1990), Katz and Miller (1991), Kaminski et al. (1993), Jones (1994), Nomura (1995), Holbourn and Henderson (2002), Kuhnt et al. (2002), and Ortiz and Thomas (2006). The generic classification of Loeblich and Tappan (1988) was used and updated in some instances, in particular for uniserial taxa (Hayward, 2002). A taxonomic list of benthic foraminifers recorded during Expedition 320/321 is given in BIOSTRAT in **"Supplementary material."**

Paleodepth estimates are based on van Morkhoven et al. (1986) using the following categories:

Neritic = <200 m.
Bathyal = 200–2000 m.
Abyssal = >2000 m.

Methods of study for foraminifers

Sediments were washed with distilled/tap water over a 63 µm wire mesh sieve. Indurated samples were soaked in a 3% hydrogen peroxide solution (with a small amount of sodium borate added) prior to washing. All samples were then dried in the sieves or on filter papers in a low-temperature oven (~50°C) and subsequently examined under a binocular light microscope. To minimize contamination of foraminifers between samples, the sieve was placed into a sonicator for several minutes and thoroughly checked or dipped in a dilute solution of methyl blue dye between samples to enable identification of contaminants from previous samples. Species identification for planktonic foraminifers were generally made on the >250 and >150 µm size fractions. The 63–150 µm size fraction was scanned for distinctive taxa. Planktonic foraminifer species distribution and range charts are presented in each site chapter. Benthic foraminifer assemblage composition and paleodepth estimates were based on counts of ~200 specimens from the >250 and >150 µm size fractions, where possible. Relative percentages of benthic to planktonic tests were determined by counting specimens in four adjacent quadrants in three different locations on the picking tray during Expedition 321.

The following abundance categories were estimated from visual examination of the dried sample for planktonic and benthic foraminifers:

D = dominant (>30% of foraminifer assemblage).
A = abundant (>10%–30% of foraminifer assemblage).
F = few (>5% to <10% of foraminifer assemblage).
R = rare (>1% to <5% of foraminifer assemblage).
P = present (<1% of foraminifer assemblage).
B = barren.

The preservation status of planktonic and benthic foraminifers was estimated as follows:

VG = very good (no evidence of overgrowth, dissolution, or abrasion).
G = good (little evidence of overgrowth, dissolution, or abrasion).
M = moderate (calcite overgrowth, dissolution, or abrasion are common but minor).
P = poor (substantial overgrowth, dissolution, or fragmentation).

Radiolarians

Radiolarian zonal scheme and taxonomy

The taxonomy for radiolarians studied during Expedition 320/321 is taken from Nigrini et al. (2006) and Nigrini and Sanfilippo (2001), with a few species from additional sources as noted in the taxonomic list (see BIOSTRAT in **"Supplementary material"**).

The radiolarian zonal scheme used is described in Sanfilippo and Nigrini (1998) and Nigrini et al. (2006). The species considered are based on the biostratigraphy developed for the tropical Pacific by Nigrini et al. (2006) (Leg 199) and Moore (1995) (Leg 138) (see BIOSTRAT in **"Supplementary material;"** Fig. **F3**). These ODP legs were restricted to the equatorial zone of the Pacific and had good paleomagnetic control through much of the recovered sections. All age estimates for the radiolarian datums are based on the material collected during Legs 138 and 199 and conform to the timescale used during Expedition 320/321. This entailed recalibration of ages for individual datums based on the more recent calibration of the paleomagnetic timescale (Lourens et al., 2004; Pälike et al., 2006b). Leg 138 samples have been reviewed, and in some cases datums were shifted to conform with more accurate taxonomic concepts. In addition, new datums from the Leg 138 material have been added to those reported in the Leg 138 *Scientific Results* volume (Pisias, Mayer, Janecek, Palmer-Julson, and van Andel, 1995).

Methods of study for radiolarians

Samples were disaggregated by warming in a solution of 10% H_2O_2. After effervescence subsided, calcareous components were dissolved by adding a 10% solution of hydrochloric acid. The solution was then sieved through a 63 µm sieve. A strewn slide was prepared by pipetting the microfossils onto a microscope slide, which was then covered with a 22 mm × 40 mm glass coverslip before the water was evaporated. To avoid crushing the radiolarians with the coverslip, in some cases adhesive tape with an 18 mm × 35 mm rectangular hole was placed on the microscope slide.

Abundance estimates of the radiolarian assemblage are qualitative estimates of the concentration of radiolarians in individual sediment samples, with categories as follows:

A = abundant.
C = common.
R = rare.
B = barren.

Abundance of individual radiolarian species was recorded as follows:

C = common (>100 specimens per slide).
F = few (>10–100 specimens per slide).
R = rare (<10 specimens per slide).
VR = very rare (1–2 specimens per slide).
(blank) = not found or not recorded.

Preservation of the radiolarian assemblage was recorded as follows:

G = good (majority of specimens complete, with minor dissolution, recrystallization, and/or breakage).
M = moderate (minor but common dissolution, with a small amount of breakage of specimens).
P = poor (strong dissolution, recrystallization, or breakage; many specimens unidentifiable).

Mixing of older radiolarian microfossils into younger sections frequently occurs in the tropical Pacific sediments. The amount of admixed older specimens in a sample was estimated as

(blank) = no mixing of older specimens detected.
1 = 1–3 reworked specimens were detected per slide.
2 = 3–10 reworked specimens were detected per slide.
3 = >10 reworked specimens were detected per slide.

Diatoms

Diatom zonal scheme and taxonomy

The taxonomy for the diatoms studied during Expedition 320/321 is taken largely from Burckle (1972), Akiba (1986), Akiba and Yanagisawa (1986), Baldauf and Iwai (1995), Barron (1981, 1985a, 2006), and Barron et al. (2004). The diatom zonal scheme used here mainly follows biostratigraphic studies by Baldauf and Iwai (1995) (Leg 138), Barron (1983, 1985a, 1985b, 2006), and Barron et al. (2004) (Leg 199), with additional information from Akiba (1986), Akiba and Yanagisawa (1986), Barron (1981, 1983), Barron and Gladenkov (1995), Burckle (1972, 1978), Burckle and Trainer (1979), Burckle et al. (1982), and Fenner (1985) (Table **T5;** Fig. **F4**). Legs 138 and 199 were restricted to the equatorial zone of the Pacific and had good paleomagnetic control through much of the recovered sections. Therefore, age estimates for diatom datums from Leg 138 and 199 data are adjusted to the timescale used during Expedition 320/321. A taxonomic list of diatom species in Table **T5** is given in BIOSTRAT in **"Supplementary material."**

Methods of study for diatoms

Samples examined from Expedition 320 were prepared using H_2O_2 and HCl as detailed in Baldauf and Iwai (1995). Slides for examination were prepared with optical adhesive similar to the procedures discussed below for Expedition 321. Strewn slides were prepared for samples examined from Expedition 321 by placing a small amount of raw sediment onto a slide and allowing the water to evaporate by heating on a hot plate for ~5 min. About 1–2 drops of optical adhesive were applied to the dry slide, which was

then covered with a 22 mm × 40 mm glass coverslip. The adhesive was solidified by placing the slide under ultraviolet light for ~10 min. Strewn slides were scanned at a maximum magnification of 1250× for stratigraphic markers and other common taxa.

Abundance estimates of the diatom assemblage are qualitative estimates of the concentration of diatoms in individual sediment samples, with categories as follows:

D = dominant (>90% of sediment particles).
A = abundant (>50%–90% of sediment particles).
C = common (>10%–50% of sediment particles).
F = few (1%–10% of sediment particles).
R = rare (<1% of sediments particles).
B = barren (none present).

Abundance of individual diatom species was recorded as follows:

D = dominant (>50 valves per counted transect).
A = abundant (>20–50 valves per counted transect).
C = common (>10–20 valves per counted transect).
F = few (>1–10 valves per counted transect).
R = rare (≤1 valve per counted transect).

Preservation of the diatom assemblage was recorded as follows:

G = good (majority of specimens complete with minor dissolution and/or breakage and no significant enlargement of the areolae or dissolution of the frustules rim detected, the sample generally has a high diatoms per gram concentration).
M = moderate (minor but common areolae enlargement and dissolution of the frustule rim with a considerable amount of breakage of specimens).
P = poor (strong dissolution or breakage, some specimens unidentifiable, strong dissolution of the frustule rim and areolae enlargement the sample generally has lower diatoms per gram concentration).

Paleomagnetism

Samples, instruments, and measurements

Paleomagnetic investigations during Expedition 320/321 focused mainly on measuring the natural remanent magnetization (NRM) of archive-half sections before and after alternating-field (AF) demagnetization. We typically collected one discrete sample per section from working-half sections for use in AF or thermal demagnetization experiments. Discrete samples were taken from the first deep hole cored at a site (typically Hole A). These samples were only taken from APC cores during Expedition 321 but were taken from both APC and XCB cores during Expedition 320. We collected them by inserting a hollow extruder into the middle of the split-core sections and then extruding the sediments into plastic cubes (2 cm × 2 cm × 2 cm, with an internal volume of 7 cm^3) (Fig. **F10**) as described in Richter et al. (2007).

All remanence measurements were made using a 2G Enterprises Model-760R Superconducting Rock Magnetometer (SRM) equipped with direct-current superconducting quantum interference devices (SQUIDs) and an inline, automated AF demagnetizer capable of reaching a peak field of 80 mT. The coordinate systems for the SRM and the archive and working halves are shown in Figure **F11.** A new software package was being developed for the SRM during Expedition 320T with alterations continuing during Expeditions 320 and 321, resulting in some evolution in data acquisition as the expeditions progressed. We continuously tested and assessed the software in order to minimize any impact that these changes might have on data quality. The principal disadvantages of the current software are the limitation of the demagnetization schedule that cannot, at this time, be used to enter more than one measurement or demagnetization step, and the numerous "Cancel" and "Continue" toggles that freeze the software. Once a well-trodden path is established through the software, measurements can be made with a minimum of surprises.

The SRM and other instruments used, tested, or available in the paleomagnetism laboratory during Expedition 320/321 are listed in Table **T7.** In the table, we also give quality assessment information (e.g., sensitivity, accuracy, and precision) of the instruments determined by experimentation or based on past experience and information provided by the instrument vendors. For example, experimentation with the SRM indicates that the noise level is $<2 \times 10^{-10}$ Am^2 based on tests conducted at the beginning of Expedition 320/321. For split core samples, where the effective volume of material measured is ~100 cm^3, this permits samples with intensities as low as $\sim 2 \times 10^{-5}$ A/m to be measured.

NRM measurements were usually made every 5 or 2.5 cm along the split-core sections as well as over a 15 cm long interval before the sample passed the center of the pick-up coils of the SQUID sensors and a 15 cm long interval after the samples had passed through it. These are referred to as the header and trailer measurements and serve the dual functions of monitoring the background magnetic moment and allowing for future deconvolution analysis. In a few selected intervals and when time allowed, we increased the measurement resolution to 1 cm. Typically, we measured NRM after 0 and 20 mT AF demagnetization. Because core flow (the analysis of one core after

the other) through the laboratory dictates the available time for measurements, ~2–3 h per core, we did not always have time for the optimal number of demagnetization steps. During part of Expedition 320/321, we were able to measure a 10 mT demagnetization and occasionally even 5 and 15 mT steps. These additional demagnetization steps did not prove to be as beneficial as using the extra time to measure the core sections at higher resolution following 20 mT demagnetization, so we opted to cease the additional demagnetization steps and increase the resolution when time permitted. The 2.5 cm measurement spacing became standard during Expedition 321. We also did not measure those sections that were entirely visibly disturbed. Similarly, in analyzing the data, we culled measurements within 5 cm (Expedition 320) or 7.5 cm (Expedition 321) of section ends and within intervals with drilling-related core disturbance, usually the top few to tens of centimeters of most cores.

During Expedition 320, a suite of discrete samples distributed evenly downhole (typically one sample from each core) was subjected to progressive AF demagnetization and measured at 5 mT steps to a peak field of 40 mT and then 10 mT steps to 60 mT, with a few samples demagnetized up to 80 mT. This was done to determine whether a characteristic remanent magnetization could be resolved and, if so, what level of demagnetization was required to resolve it. We also evaluated the NRM using thermal demagnetization on 13 samples from Site U1331. After measuring their NRM at room temperature, these samples were progressively demagnetized at 90°C and then from 150°C to 600°C at 50°C intervals. During Expedition 321, AF demagnetization of discrete samples was conducted at peak fields of 0, 10, and 20 mT, the same as the demagnetization sequence applied to half-core sections, in order to check whether the radial-inward drilling-induced magnetization that has occasionally been reported from previous ODP/IODP expeditions is present or not.

Low-field magnetic susceptibility was measured on all whole-core sections using the WRMSL and the STMSL (see **"Physical properties"** and **"Stratigraphic correlation and composite section"**). The susceptibility meters are Bartington loop meters (model MS2 with an MS2C sensor, a coil diameter of 88 mm, and an operating frequency of 0.565 kHz). They have a nominal resolution of 2×10^{-6} SI (Blum, 1997). The "units" option for the meters was set on SI units, and the values were stored in the database in raw meter units. To convert to true SI volume susceptibilities, these should be multiplied by ~0.68×10^{-5} (Blum, 1997).

We measured the bulk magnetic susceptibility of each discrete sample using a Kappabridge KLY-4S susceptibility meter, except for samples from Site U1338. During Expedition 320, because the plastic cube that holds the discrete sample is occasionally incompletely filled with sediments, we measured the mass of each sample and then estimated the true volume by using this mass and the bulk (wet) density of nearby samples, which are part of the moisture and density (MAD) data collected by the physical property scientists.

Coring and core orientation

Cores were collected using nonmagnetic core barrels, except at depths where overpull was apparent during core recovery and the more expensive nonmagnetic barrel was endangered. In addition, the BHA included a Monel (nonmagnetic) drill collar when the FlexIt core orientation tool was used (Sites U1331 and U1332 of Expedition 320 and Sites U1337 and U1338 of Expedition 321). Because much of the drill pipe had not been used for several years, rust was a concern. An effort was made to clean the interior of the pipe prior to the first core during Expedition 320 by running a drilling tool, called a pig, up and down the pipe.

During Expedition 320, the FlexIt orientation tool appeared to yield anomalous orientation data on deployment for APC cores at Sites U1331 and U1332, and the instrument was not used at other Expedition 320 sites. During Expedition 321, the FlexIt tool was considered to perform satisfactorily and was used to orient all APC cores at Sites U1337 and U1338. In a few cases the FlexIt orientation data were accidentally lost, in part because of bugs in the FlexIt software.

The FlexIt tool uses three orthogonally mounted fluxgate magnetometers to record the orientation of the double lines scribed on the core liner with respect to magnetic north. The tool also has three orthogonally mounted accelerometers to monitor the movement of the drill assembly and help determine when the most stable and thus useful core orientation data were gathered. The tool declination, inclination, total magnetic field, and temperature are recorded internally at a regular interval until the tool's memory capacity is filled (Fig. **F12**). For a measurement interval of 6 s, which is what we used, the tool can typically be run for ~24 h, although we aimed to switch tools at least every 8–12 h. Three FlexIt tools (serial numbers 936, 937, and 938) were available.

Standard operating procedure was to set up a tool as described in the IODP "Core Orientation Standard Operating Procedure" manual (20 January 2009, available from the IODP Cumulus database). This involves synchronizing the instrument to a PC running the FlexIt software (version 3.5) and inserting the tool inside a pressure casing. The enclosed tool is

then given to a core technician, who installs it on the sinker bars that reside above the core barrel. The double lines on the core liner are aligned relative to the tool. Prior to firing the APC, the core barrel is held stationary (along with the pipe and BHA) for several minutes. During this time, the data recorded are those used to constrain the core orientation. When the APC fires, the core barrel is assumed to maintain the same orientation, although this and past cruises have found evidence that the core barrel can rotate and/or the core liner can twist as it penetrates the sediments. Generally, the core barrel is pulled out after a few minutes except for cores collected with the advanced piston corer temperature tool (APCT-3) (see **"Downhole measurements"**), for which the core barrel remains in the sediments for ≥10 min.

The procedure for determining polarity differed for the two expeditions. During Expedition 321, the FlexIt tool was used for core orientation and was judged to generate reliable orientation data. During Expedition 320, azimuthal core orientation was determined indirectly by correlating distinct geomagnetic reversal patterns, as recorded by the paleomagnetic declination in each hole, with the GPTS. A feasible polarity pattern was interpreted using biostratigraphic constraints, and the mean paleomagnetic direction for stable polarity intervals from each core was then determined using (1) Fisher statistics, with data from reversed polarity intervals inverted for Sites U1331, U1333, U1334, and Hole U1336A or (2) Bingham statistics for data from Sites U1332 and U1335. By subtracting this core mean declination from each observed declination obtained from the respective core, the azimuth of the core can be approximately reoriented from "sample" coordinates into "geographic" coordinates. After this reorientation, normal polarity intervals have ~0° declination and reversed polarity intervals have ~180° declination. This orientation method can break down when significant coring gaps occur within the composite stratigraphic section, which is rare when multiple holes are cored at a site. Paleomagnetic inclination was shallow at these paleoequatorial sites and rarely useful in constraining polarity.

For all cores collected with the XCB, rotation occurs between pieces of core within a single core. Hence, XCB cores are not reoriented nor can we confidently determine polarity as the inclination is generally too shallow to be diagnostic.

Magnetostratigraphy

Magnetic polarity zones (magnetozones) were assigned based on distinct ~180° alternations in declination and subtle changes in inclination that occur along each stratigraphic section. Magnetostratigraphy for each site was then constructed by correlating these magnetozones with GPTS. Biostratigraphic age constraints significantly limit the range of possible correlations with the GPTS.

The GPTS used for Expedition 320/321 is based upon a composite of several timescales (Table **T6**) (Cande and Kent, 1995; Lourens et al., 2004; Pälike et al., 2006a, 2006b). Its construction follows the procedure described by Backman et al. (2008), which is excerpted here: "Global Cenozoic timescales are still under development. Orbitally tuned cyclostratigraphic data are the chronological backbone in the most recent Neogene timescale, which includes 'Quaternary' times (Lourens et al., 2004). Their synthesis is considered to fairly well reflect the true progress of Neogene time. The Paleogene timescale, on the other hand, is less sharp and definitive, owing to the lack of a continuous Milankovitch-based Paleogene cyclostratigraphy, and it will therefore continue to develop and change over some years to come." The PEAT expedition age model is based on the following three timescales:

1. Interval 0.000–23.030 Ma: the Neogene timescale of Lourens et al. (2004) is used. They placed the Paleogene/Neogene boundary at 23.030 Ma, based on an astronomically derived age for the base of Chron C6Cn.2n (Shackleton et al., 2000), updated to the new astronomical solution of Laskar et al. (2004) by Pälike et al. (2006a). Pälike et al. (2006b) estimated an age of 23.026 Ma for this reversal boundary (i.e., 4 k.y. younger than the Lourens et al., 2004, estimate).
2. Interval 23.278–41.510 Ma: the Pälike et al. (2006b, table S1) timescale is used from the top of Chron C6Cn.3n at 23.278 Ma to the base of Chron C19n at 41.510 Ma. This implies that the 248 k.y. long Chron C6Cn.2r is artificially shortened by 4 k.y. (1.6%) when shifting from the Miocene to the Oligocene timescale.
3. Interval 42.536–83.000 Ma: the Cande and Kent (1995) timescale is used from the top of Chron C20n to the top of Chron C34n. This implies that the 1.026 m.y. long Chron C19r is artificially lengthened by 11 k.y. (1.1%) when shifting from the Pälike et al. (2006b) timescale to the Cande and Kent (1995) timescale. The impact of these two artificial timescale jumps (4 and 11 k.y., respectively) on the data and discussions presented here is negligible.

Geochemistry

The geochemistry program included characterization of volatile gases, interstitial water composition, sedi-

mentary inorganic geochemistry including inorganic carbon, and sedimentary organic carbon. These analyses were carried out to satisfy routine shipboard safety and pollution prevention requirements, to characterize interstitial waters and sediment geochemistry for shipboard interpretation, and to provide sampling frameworks for shore-based research.

Sediment gases sampling and analysis

The organic geochemistry program monitored the compositions and concentrations of volatile hydrocarbons (C_1–C_6) and other gases (i.e., O_2 and N_2) in the sediments from headspace gas samples at typical intervals of one per core. The IODP gas sampling protocol for pollution prevention and safety as required by IODP safety regulations was modified to better constrain the concentrations of dissolved gases. The routine headspace procedure involved placing ~5 cm^3 of sediment sample in a 21.5 cm^3 glass serum vial that was sealed with a septum and metal crimp cap and heated at 70°C for 30 min. A 5 cm^3 volume of gas from the headspace in the vial was removed with a glass syringe for analysis by gas chromatography.

Headspace gas samples were analyzed using an Agilent 6890 gas chromatograph equipped with a 2.4 m × 3.2 mm stainless steel column packed with 100–120 mesh HayeSep R and a flame ionization detector. This instrument quickly measures concentrations of methane (C_1), ethane (C_2), ethene (C_2=), propane (C_3), and propene (C_3=). The gas syringe was directly connected to the gas chromatograph via a 1 cm^3 sample loop. Helium was used as the carrier gas, and the gas chromatograph oven temperature was programmed to ramp at 30°C/min from 90° to 100°C, 15°C/min from 100° to 110°C, and remain at 110°C for 4.5 min before ramping at 50°C/min to 150°C with a final holding time of 1.8 min. Data were collected and evaluated with an Agilent Chemstation data-handling program. Chromatographic response was calibrated against preanalyzed standards. Gas void samples were not taken during Expedition 320/321 because gas voids were not present in the core.

Interstitial water sampling and chemistry

Interstitial waters were extracted from 5 or 10 cm long whole-round sections that were cut and capped immediately after core retrieval on deck. In one hole at each site, two samples per core were taken from the upper 50 to 60 m CSF and from every core thereafter to total depth. When possible, a whole-round section at least 10 cm long was taken near (~1 m above) the sediment/basement contact. Occasionally, samples from more than one hole were treated as constituting a single depth profile ("splice") using CCSF-A as the depth reference if possible. Before squeezing, samples were removed from the core liner and the outer surfaces were carefully scraped off with spatulas to minimize potential contamination by the coring process. Whole rounds were placed into a titanium and steel squeezing device and squeezed at ambient temperature with a hydraulic press at pressures typically up to 20 MPa and occasionally as high as 40 MPa, if needed. Interstitial water samples were collected in acid-cleaned plastic syringes, filtered through 0.45 µm Whatman polyethersulfone disposable filters, and stored in plastic sample tubes for shipboard analyses or archived in either glass ampoules or plastic vials for shore-based analysis.

Interstitial waters were also sampled at higher resolution (up to every 10 cm) across selected lithologic transitions or in zones of pronounced interstitial chemical gradients with Rhizon samplers. These were originally developed as soil moisture samplers for root zones and they consist of thin tubes of hydrophilic porous polymer that pull water from sediment under vacuum. Rhizon samplers have recently been applied to sampling of sediment interstitial water, including during Expedition 302 (Dickens et al., 2007). Rhizon CSS-F 5 cm Core Solution Samplers (Rhizosphere Research Products) were soaked in distilled water for ~1 h before use. Rhizon samplers were wiped clean of excess water and carefully inserted through holes either drilled in the end cap or drilled through the core liner at a 55° angle so that the 5 cm porous tube was in contact with presumably undisturbed sediment away from the core liner on either side. Rhizon samples collected through the end cap were taken before the core was run through the STMSL and samples collected through the core liner were taken after the core was run through the STMSL. Acid-washed 10 mL syringes were attached to each Rhizon sampler, pulled to generate vacuum, and held open with wooden spacers. The first ~1 mL of water was discarded, with the rest collected and split for shore-based and shipboard analyses. Collection of 10–12 mL typically took 20–40 min.

Interstitial water analyses followed the procedures outlined by Gieskes et al. (1991), Murray et al. (2000), and user manuals for the new shipboard instrumentation with modifications as indicated (see "Geochemistry" in each site chapter). Interstitial water samples were analyzed for salinity with a handheld refractometer, for pH and alkalinity by Gran titration with a Brinkman pH electrode and Metrohm autotitrator, for Cl^- concentrations by titration, and for SO_4^{2-} concentrations by ion chromatography with a Dionex ICS-3000 ion chromatograph. H_4SiO_4 and HPO_4^{2-} concentrations were analyzed by an OI Analytical

Discrete Analyzer (DA3500) spectrophotometer unit during Expedition 320. H_4SiO_4 concentrations were analyzed by inductively coupled plasma–atomic emission spectroscopy (ICP-AES) with minor elements (see below) during Expedition 321.

Major and minor elements were determined by ICP-AES with the newly installed Teledyne Prodigy high-dispersion ICP-AES. ICP-AES techniques for the major cations Na^+, Mg^{2+}, Ca^{2+}, and K^+ used dilutions of International Association for the Physical Sciences of the Ocean (IAPSO) standard seawater as calibration standards. Standards and samples were diluted 1:5 with distilled water and then diluted 1:10 with a 2.5% HNO_3 (by volume) solution with Sc at 10 ppm as an internal standard during Expedition 320 and with Y at 10 ppm as an internal standard during Expedition 321. Sc was used as an internal standard during Expedition 320 because we did not have sufficient Y standard solution, which was acquired for Expedition 321. For Site U1336, major cations Mg^{2+}, Ca^{2+}, and K^+ were determined by ion chromatography on the 1:200 dilutions used for sulfate determinations. These values were later confirmed by ICP-AES. ICP-AES techniques for the minor elements Mn^{2+}, Fe^{2+}, B, Sr^{2+}, Ba^{2+}, and Li^+ were modified from those described by Murray et al. (2000) by preparing calibration standards in an acidified (2.5% HNO_3, by volume) sodium chloride matrix (35 g NaCl/L) and by using 2.5% HNO_3 solution with Sc or Y at 10 ppm as an internal standard. Standards and acidified interstitial water samples were diluted for each analytical run to 1:10 at Sites U1331–U1333 and 1:5 at Sites U1334–U1338. For Sites U1331–U1335 (Expedition 320), we applied an internal drift correction using Sc for major element analyses. Interferences on both Sc lines occurred in the standard calibration for minor elements, so we did not apply an internal drift correction using Sc for minor element analyses. During Expedition 321, drift of the instrument during even long (>100 samples) runs was only on the order of a few percent and was element (wavelength line) specific. Therefore drift correction was made when necessary for both major and minor elements using the factor from a drift monitor solution (middle value standard solution) that was analyzed every 5 or 10 samples. The measured Y intensity was still useful for checking whether sample dilutions had been conducted successfully.

IAPSO standard seawater was used for calibration and quality control purposes when applicable. To assess precision of the ICP-AES technique for elements not present in IAPSO seawater at high enough concentrations and to facilitate the direct comparison of data generated during both PEAT expeditions, some interstitial water samples, including three samples analyzed during Expedition 320, were analyzed multiple times. These data and those from repeat measurements of IAPSO seawater are summarized in Table **T8.** Agreement is generally good between the data generated by the different expeditions except for silicic acid, which was determined by different techniques during the different expeditions (DA3500 during Expedition 320 and ICP-AES during Expedition 321). This inconsistency resulted from the failure of the DA3500 during Expedition 321 and will require shore-based measurements to be resolved. Na^+ was also determined by charge balance, neglecting contributions by ammonium and bromide. Chemical data for interstitial water are reported in molar concentration units in each site report.

Bulk sediment geochemistry

Major and minor elements

Bulk sediment samples were taken for the determination of selected major, minor, and trace element concentrations; calcium carbonate contents; and organic carbon contents. Samples were regularly taken at a frequency of one per section (every 1.5 m) adjacent to physical property samples (typically within 5 cm). Sample intervals were occasionally adjusted depending on the prevailing lithology, and not all samples were analyzed for every element in order to best approach the scientific questions during the available time and with the available resources. Taking sediment composition samples adjacent to physical property samples is most effective for using measured analytical data (e.g., calcium carbonate content) to calibrate higher resolution multisensor track data and for the calculation of mass accumulation rates. Samples were freeze-dried for 12–24 h and ground in a mortar for subsequent analyses.

Major, minor, and trace element analyses of solid bulk samples were carried out following modifications of the methods described in Murray et al. (2000) and following procedures applied during Leg 199 (Quintin et al., 2002; Shipboard Scientific Party, 2002). Approximately 100 mg of sample (or standard) powder was added to 400 mg of a $LiBO_2$ flux (preweighed onshore) in a platinum vial. As a wetting agent, 10 µL of a 0.172 mM LiBr solution was added. Sample and flux were mixed in the platinum vial and melted with a NT-2100 Bead Sampler at ~1050°C for ~10 min. After cooling, the sample glass was dissolved in 50 mL 10% HNO_3 (trace metal grade). Five milliliters of this sample solution was diluted with 35 mL 2.5% HNO_3, resulting in the dilution of the freeze-dried rock powder by a factor of 4000 before analysis. Na, Mg, Al, Si, P, K, Ca, Sc, Ti, V, Cr, Mn, Fe, Cu, Sr, Y, Zr, and Ba were measured with the ICP-AES. Calibration was achieved by analyzing

solutions of international powdered rock standards subjected to the same sample preparation (Table T9). Instrumental drift was externally monitored by repeated analyses of drift standards. Reproducibility was monitored by repeated measurement of limestone standards treated as samples (Table T10).

Sedimentary inorganic and organic carbon

Inorganic carbon (IC) concentrations were determined using a Coulometrics 5011 carbon dioxide coulometer. One carbonate determination was performed typically for each 1.5 m section of core. Samples of ~10 mg of freeze-dried ground sediment were reacted with 2N HCl. The liberated CO_2 was backtitrated to a colorimetric end point. Calcium carbonate content, as weight percent, was calculated from the IC content with the assumption that all IC is present as calcium carbonate:

$$\text{wt\% } CaCO_3 = \text{wt\% IC} \times 8.33$$

Reproducibility was determined by replicate measurements of selected samples and standards treated as samples, with typical absolute standard deviations of 0.3–0.4 wt% on sample and standard duplicates.

Total carbon (TC) content was determined using a Thermo Electron Flash EA 1112 element analyzer equipped with a Thermo Electron packed column CHNS/NCS (polytetrafluoroethylene; length = 2 m; diameter = 6 × 5) and thermal conductivity detector (TCD) on a subset of the samples used for inorganic carbon determinations. Aliquots of 10 mg of freeze-dried ground sediment in tin cups were combusted at 1800°C in a stream of oxygen. Nitrogen oxides were reduced to N_2, and the mixture of N_2, CO_2, H_2O, and SO_2 gases was separated by gas chromatograph and detection performed by the TCD. The gas chromatograph oven temperature was set at 65°C. H_2 values are not useful because they represent hydrogen from both organic matter and (clay) minerals. All measurements were calibrated by comparison to pure sulfanilamide as a standard. The reproducibility of TC measurements was determined to be ±0.03 – ±0.06 wt% (1σ; n = 5), with a typical detection limit of 0.03 wt%. Contents of total organic carbon (TOC), as weight percent, were calculated as the difference between TC and IC,

$$\text{wt\% TOC} = \text{wt\% TC} - \text{wt\% IC}.$$

The "acidification method" of TOC analysis was also applied to examine improving analytical precision of TOC in high-$CaCO_3$–low-TOC sediments. Freeze-dried samples (~30 mg) in precombusted silver capsules were treated with small aliquots (10 µL) of 2N HCl at room temperature to remove $CaCO_3$; samples were treated with repeated aliquots until no further reaction was visible and then dried. TOC concentration was determined using a Thermo Electron Flash EA 1112 element analyzer for TC, calibrated using solutions that contain 0.071–0.281 mg of cysteine hydrochloride. During Expedition 321 the mean TOC value measured for National Institute of Standards and Technology (NIST) 1646a estuarine Sediment reference material was 0.87 ± 0.01 wt% (1σ; N = 10).

Bulk carbonate geochemistry

The trace element content of bulk carbonate leachates was measured using the ICP-AES for selected samples from Sites U1336–U1338. About 20 mg of freeze-dried powdered sample was weighed, placed in acid-cleaned centrifuge tubes, and rinsed with 10 mL of 18.2 MΩ H_2O buffered to pH 10 with ammonium hydroxide (100 µL of 30% assay per liter of water) to remove any salts using agitation with a vortex stirrer followed by a wrist-action shaker for 20 min. Following rinsing, samples were centrifuged at 40,000 rpm for 10 min, and the supernatant was discarded. Approximately 3 mL of 18.2 MΩ H_2O was then added to each tube to rinse away the buffer before leaching. Samples were briefly vortex-stirred before centrifugation and the removal of all liquid with a disposable plastic pipet. Samples were then leached with 0.5 mL of 1M acetic acid (HOAc) adjusted to pH 5 with sodium acetate (NaOAc) while being ultrasonicated at room temperature for 60–120 min. After ultrasonication until the absence of visible air bubbles, samples were left overnight before the addition of 4.5 mL of 18.2 MΩ H_2O and centrifugation at 40,000 rpm for 10 min. Between 1 and 4 mL (average = 1.5 mL) of supernatant was transferred to a clean centrifuge tube and diluted to 400 ppm Ca using the $CaCO_3$ weight percent data for each sample. Samples were further diluted for analysis with Y-spiked 2% HNO_3 to a Ca concentration of 100 ppm. Calibration was achieved with matrix-matched standard solutions prepared from single-element solutions. Aliquots of the NIST 1C (National Bureau of Standards 1C) limestone reference material were treated as samples for quality control purposes and results are summarized in Table T11. Reproducibility of the technique is generally better than 2% relative standard deviation and values compare well to the only comparable published values from Kryc et al. (2003). Unfortunately, Sr was present at concentrations too low in the NIST 1C standard to be measured by the technique employed here, and Mg/Ca data are not available from the Kryc et al. (2003) study, as those authors used a $MgCl_2$ soak prior to carbonate leaching.

Physical properties

Shipboard measurements of physical properties provide information that assists in characterization of lithologic units, correlation of lithology with downhole geophysical logging data, assessment of the consolidation history, and interpretation of seismic reflection profiles. The primary objectives of the Expedition 320/321 physical properties program were to collect high-resolution data to

1. Provide bulk density data for determination of mass accumulation rates,
2. Facilitate hole to hole and site to site correlation and construction of composite stratigraphic sections,
3. Enable postcruise cyclostratigraphy studies,
4. Facilitate construction of synthetic seismic profiles, and
5. Investigate the characteristics of major seismic reflectors.

Physical properties were measured on whole-round sections and undisturbed intervals of split sections using two different track systems, the STMSL and the WRMSL. Sections from intervals that overlapped with those cored in earlier holes were run through the STMSL immediately after being brought in from the catwalk to aid in preliminary determinations of depth offsets in the composite section (see **"Stratigraphic correlation and composite section"**). Following STMSL measurements and prior to being run through the WRMSL, sections were allowed to thermally equilibrate to ambient room temperature (i.e., 20°–22°C) to ensure thermal homogeneity for the physical property measurements. The STMSL incorporates a GRA bulk densitometer and a magnetic susceptibility sensor. The WRMSL incorporates a GRA bulk densitometer, a magnetic susceptibility sensor, a compressional *P*-wave velocity sensor (PWL), and a noncontact resistivity (NCR) detector. The NCR detector did not operate properly during Expedition 320, was switched off after scanning cores from Site U1332, and was not used during Expedition 321. Natural gamma radiation (NGR) and thermal conductivity also were measured on whole-round sections using the NGR logger and the needle-probe method, respectively. Compressional wave velocity was measured on split-core sections, and MAD measurements were made on discrete samples taken from the split cores. Bulk properties determined by MAD analyses include wet bulk density, dry bulk density, grain density, water content, and porosity. Color reflectance was measured on the split-core archive sections with the SHMSL. A comprehensive discussion of all methodologies and calculations used in the *JOIDES Resolution* physical properties laboratory is presented in Blum (1997).

Special Task Multisensor Logger measurements

The principal aim of acquiring STMSL data during Expedition 320/321 was to obtain rapid, medium- to high-resolution data sets of GRA and magnetic susceptibility to determine offsets in the composite section during the drilling of multiple-hole sites. The GRA bulk densitometer and magnetic susceptibility loop incorporated in the STMSL are essentially identical to those of the WRMSL (see **"Whole-Round Multisensor Logger measurements"**). The STMSL GRA densitometer was not operational during Expedition 320. The typical measurement interval for the STMSL was 5 cm.

Whole-Round Multisensor Logger measurements

Collection of high-resolution data sets, especially of GRA bulk density and magnetic susceptibility, to facilitate shipboard core to core correlation and the construction of composite stratigraphic sections had to be completed within a reasonable time frame without compromising the shipboard processing of recovered core. The quality of the WRMSL data is highly dependent on the condition of the core.

GRA bulk density, magnetic susceptibility, compressional wave velocity, and NCR were measured nondestructively with the WRMSL on all whole-round core sections. To optimize WRMSL performance, sampling intervals and measurement residence times were the same for all sensors for any one core. Sampling intervals were set at 2.5 cm so that a 9.5 m long core would take ~3 h to pass through the WRMSL with a residence time of 3 s for each measurement. These sampling intervals are common denominators of the distances between the sensors installed on the WRMSL (30–50 cm) and allow a combination of sequential and simultaneous measurements optimize the total measurement time.

Gamma ray attenuation bulk density

Bulk density reflects the combined effect of variations in porosity, grain density (dominant mineralogy), and coring disturbance. Porosity is mainly controlled by lithology and texture, compaction, and cementation (controlled by both mechanical and chemical processes).

The GRA densitometer uses a 10 mCi ^{137}Cs capsule as the gamma ray source (with the principal energy peak at 0.662 MeV) and a scintillation detector. The narrow collimated peak is attenuated as it passes through the center of the core. Incident photons are scattered by the electrons of the sediment material by Compton scattering.

The attenuation of the incident intensity (I_0) is directly related to the electron density in the sediment core of diameter (D), which can be related to bulk density given the average attenuation coefficient (in micrometers) of the sediment (Evans, 1965; Harms and Choquette, 1965). Because the attenuation coefficient is similar for most common minerals and aluminum, bulk density is obtained through direct calibration of the densitometer using aluminum rods of different diameters mounted in a core liner that is filled with distilled water. The GRA densitometer has a spatial resolution of <1 cm.

Magnetic susceptibility

Magnetic susceptibility is a measure of the degree to which a material can be magnetized by an external magnetic field. It provides information on the magnetic composition of the sediments that often can be related to mineralogical composition (e.g., terrigenous versus biogenic materials) and diagenetic overprinting. Magnetite and a few other iron oxides with ferromagnetic characteristics have a specific magnetic susceptibility several orders of magnitude higher than clay, which has paramagnetic properties. Carbonate, silica, water, and plastics (core liner) have small negative values of magnetic susceptibility. Sediments rich in biogenic carbonate and opal therefore have generally low to negative magnetic susceptibility if practically no clay or magnetite is present. In such cases, measured values approach the detection limit of magnetic susceptibility sensors.

Magnetic susceptibility was measured with the Bartington Instruments MS2C system on the WRMSL and STMSL. The frequency at which the magnetic susceptibility loop operates is 621 Hz for the WRMSL and 513 Hz for the STMSL. The output of the magnetic susceptibility sensors can be set to centimeter-gram-second (cgs) units or SI units. The IODP standard is the SI setting. However, to actually obtain the dimensionless SI volume-specific magnetic susceptibility values, the instrument units stored in the IODP database must be multiplied by a correction factor to compensate for instrument scaling and the geometric ratio between core and loop dimensions.

Compressional wave velocity

The *P*-wave velocity sensor measures the ultrasonic *P*-wave velocity of the whole-round sample in the core liner. The PWL transmits a 500 kHz *P*-wave pulse through the core section at a specified repetition rate. This signal is coupled to the sample by the plastic pole pieces of the transducers and the pressure applied by the linear actuator. No water is used to improve coupling between the transducers and the liner. The pressure applied by the actuator is sufficient for reliable *P*-wave measurement. The transmitting and receiving ultrasonic transducers are aligned so that wave propagation is perpendicular to the section's long axis. Torque applied by the actuator can be set by the user to ensure good acoustic contact between the liner and the core material.

Traveltime is determined by signal processing software which automatically detects first arrival of the *P*-wave signal to a precision of 50 ns. It is a challenge for an automated routine to pick the first arrival of a potentially weak signal with significant background noise. The search method skips the first positive amplitude and finds the second positive amplitude using a detection threshold limit, typically set to 30% of the maximum amplitude of the signal. It then finds the preceding zero crossing and subtracts one period to determine the first arrival. To avoid extremely weak signals, minimum signal strength can be set (typically 0.02 V) and weaker signals are ignored. To avoid cross-talk signals at the beginning of the record from the receiver, a delay (typically 0.01 ms) can be set to force the amplitude search to begin in the quiet interval preceding the first arrival. In addition, a trigger (typically 4 V) is selected to initiate the arrival search process, and the number of waveforms to be stacked (typically five) can also be set. A linear voltage differential transformer is used to measure the separation of the transducer to derive a travel path length for the signal (i.e., the core diameter). After corrections for system propagation delay, liner thickness, and liner material velocity, the ultrasonic *P*-wave velocity is calculated.

P-wave velocity varies with lithology, porosity, and bulk density of material; state of stress; temperature; and fabric or degree of fracturing. In marine sediments and rocks, velocity is controlled by degree of consolidation and lithification, fracturing, and occurrence and abundance of free gas and gas hydrate. Together with bulk density, velocity data are used to derive porosities and to calculate acoustic impedance and reflection coefficients that can be used to construct synthetic seismic profiles and to estimate the depth of seismic horizons.

Noncontact resistivity

The NCR sensor measures the resistivity of the whole-core section. It can be used to investigate core properties in terms of the fluid/solid phases of the sediment or rock and type of porosity. The NCR induces a high-frequency magnetic field in the core from a transmitter coil that induces eddy currents in the core that are inversely proportional to the resistivity. A receiver coil measures very small magnetic fields that are regenerated by the eddy current. To accurately measure these very small magnetic fields, a

difference technique compares the readings generated from the core measuring coils to the readings from an identical set of coils operating in the air. Resistivities between 0.1 and 10 Ωm can be measured using this sensor.

Factors affecting noncontact resistivity results include magnetic susceptibility, pore water salinity, porosity, and mineral composition. Noncontact resistivity measurements provide important information that can be used to understand sediment facies and geochemical processes. Combination logs of resistivity and density provide lithologic information that cannot be achieved with other nondestructive measurement methods, such as grain size, permeability, and tortuosity. Because resistivity is influenced by salinity, NCR data are valuable as a continuous log for geochemical interpretation.

The NCR detector was not performing during Expedition 320 and was switched off after scanning cores from Site U1332. The nature of the problem is unclear, but it could not be remedied by moving the detector closer to the core. The NCR detector was kept switched off during Expedition 321.

Natural gamma radiation

The NGR logger was designed and built at the IODP-USIO Texas A&M University facility from 2006 to 2008. The NGR logger measures gamma rays emitted from whole-round core sections. Gamma rays arise primarily as a result of the decay of U, Th, and K isotopes. Data generated from this instrument are used to augment geologic interpretations and fine tune stratigraphic correlations.

The main NGR detector unit consists of 8 NaI scintillator detectors, 7 plastic scintillator detectors, 22 photomultipliers, and passive lead shielding. The NaI detectors are covered by at least 8 cm of lead shielding. In addition, lead separators (~7 cm of low-background lead) are positioned between the NaI detectors. Half of the lead shielding closest to the NaI detectors is composed of low-background lead, whereas the outer half is composed of regular (virgin) lead. In addition to this passive lead shielding, the NGR employs a plastic scintillator to suppress the high-energy gamma and muon components of cosmic radiation by producing a veto signal when charged particles from cosmic radiation pass through the plastic scintillator.

A measurement run consists of two positions on each core section counted for at least 5 min each for a total of 16 measurements per section. Complete spectra for each measurement are uploaded to the LIMS.

NGR measurements collected from Holes U1331B and U1331C and all holes at Sites U1332–U1334 were measured without the use of the active shielding feature. This was unintentional and was caused by a power failure early during the expedition. The shield was turned back on before the cores from the last two sites (U1335 and U1336) were measured. Lack of active shielding resulted in elevated background counts. Furthermore, because nobody was initially aware of this situation, the routine data reduction on the ship used background data acquired with the active shielding on. This resulted in background-corrected values that were generally too high by ~4 cps, and the edge effect correction created additional, clearly visible artifacts in the form of "spikes" at the section ends.

The incorrectly processed data were reprocessed postcruise using appropriate background data collected without active shielding before the expedition. The incorrectly processed data were replaced with the correctly processed data in the LIMS database and the comment "Active shielding OFF" was added to each replacement record.

Thermal conductivity

Thermal conductivity was measured with the TK04 (Teka Bolin) system using the needle probe method in full-space configuration for soft sediments (Von Herzen and Maxwell, 1959). During Expedition 320/321 a foam insulating jacket was used to prevent temperature changes in the section being analyzed for thermal conductivity (a heating/ventilation/air conditioning vent is located directly over the thermal conductivity station in the core laboratory). The needle probe contains a heater wire and calibrated thermistor. Thermal transfer compound was used to improve the coupling between the needle and the sediment. The probe is assumed to be a perfect conductor because it is much more conductive than unconsolidated sediments. With this assumption, the temperature of the superconductive probe has a linear relationship with the natural logarithm of the time after the initiation of the heat,

$$T(t) = (q/4\pi k) \times \ln(t) + C,$$

where

- T = temperature (K),
- q = heat input per unit length per unit time (J/m/s),
- k = thermal conductivity (W/[m·K]),
- t = time after initiation of heat (s), and
- C = a constant.

Thermal conductivity was measured by inserting the needle into the unconsolidated sediment through a small, 2 mm hole drilled into the core liner. Five measuring cycles were automatically performed at each sampling location and used to calculate an av-

erage conductivity. A self-test, which included a drift study, was conducted at the beginning of each cycle. Once the samples were equilibrated, the heater circuit was closed and the temperature rise in the probes was recorded. Thermal conductivities were calculated from the rate of temperature rise while the heater current was flowing. Temperatures measured during the first 150 s of the heating cycle were fitted to an approximate solution of a constantly heated line source (for details see Kristiansen, 1982; Blum, 1997). Measurement errors were 5%–10%. At sites where in situ temperatures were measured, thermal conductivity was corrected for in situ temperature and pressure as part of the calculation of heat flow. Thermal conductivity measurements were taken with a frequency of one per core in soft sediments (typically in Section 3 of Hole A cores), into which the TK04 needles could be inserted without risk of damage.

Moisture and density

Wet and dry bulk density, grain density, water content, and porosity were determined from measurements of wet sediment mass, dry sediment mass, and dry sediment volume. In soft sediments, samples of ~10 cm^3 were extracted, usually from the middle of each core section, and placed in preweighed 16 mL Wheaton beakers. Stiff sediments drilled with XCB were sampled, where appropriate, by extracting ~10 cm^3 blocks of in situ sections using a spatula and placed into a beaker as above. One sample was routinely collected in each undisturbed section from Hole A. Samples were taken in subsequent holes when gaps in Hole A needed to be spliced.

Sample mass was determined to a precision of 0.005 g using two Mettler Toledo electronic balances and a computer averaging system to compensate for the ship's motion. Sample volumes were determined using a hexapycnometer system that consists of six custom-configured Micromeritics AccuPyc 1330TC helium-displacement pycnometers with a precision of 1% of the nominal full-scale volume. Volume measurements were preceded by three purges of the sample chambers with helium warmed to ~25°C. Three acquisition cycles were used for each sample. A reference volume was included within each sample set and rotated sequentially among the cells to check for instrument drift and systematic error. Sample beakers used for discrete determination of moisture and density were calibrated before the cruise. Dry mass and volume were measured after samples were heated in an oven at 105° ± 5°C for 24 h and allowed to cool in a desiccator. Procedures for the determination of these properties comply with the American Society for Testing and Materials (ASTM) designation (D) 2216 (ASTM, 1990). Fundamental phase relationships and assumptions for the calculations of all physical property parameters are discussed by Blum (1997) and summarized in **"Mass and volume calculation"** and **"Calculation of bulk properties."**

Mass and volume calculation

Wet mass (M_{wet}), dry mass (M_{dry}), and dry volume (V_{dry}) are measured in the laboratory. The mass ratio (rm) is a computational constant of 0.965 (i.e., 0.965 g of freshwater per 1 g of seawater). Salt precipitated in sediment pores during the drying process is included in the M_{dry} and V_{dry} values. The mass of the evaporated water (M_{water}) and the salt (M_{salt}) in the sample are given by

$$M_{water} = M_{wet} - M_{dry}$$

and

$$M_{salt} = M_{water}\,[s/(1 - s)],$$

where s is the assumed saltwater salinity (0.035) corresponding to a pore water density (ρ_{pw}) of 1.024 g/cm^3 and a salt density (ρ_{salt}) of 2.22 g/cm^3. The corrected mass of pore water (M_{pw}), volume of pore water (V_{pw}), mass of solids excluding salt (M_{solid}), volume of salt (V_{salt}), volume of solids excluding salt (V_{solid}), and wet volume (V_{wet}) are, respectively,

$$M_{pw} = (M_{wet} - M_{dry})/\mathrm{rm},$$

$$V_{pw} = M_{pw}/\rho_{pw},$$

$$M_{solid} = M_{wet} - M_{pw},$$

$$M_{salt} = M_{pw} - (M_{wet} - M_{dry}),$$

$$V_{salt} = M_{salt}/\rho_{salt},$$

$$V_{wet} = V_{dry} - V_{salt} + V_{pw},$$

and

$$V_{solid} = V_{wet} - V_{pw}.$$

Calculation of bulk properties

For all sediment samples, water content (w) is expressed as the ratio of the mass of pore water to the wet sediment (total) mass,

$$w = M_{pw}/M_{wet}.$$

Wet bulk density (ρ_{wet}), dry bulk density (ρ_{dry}), sediment grain density (ρ_{solid}), porosity (ϕ), and void ratio (VR) are calculated from

$$\rho_{wet} = M_{wet}/V_{wet},$$

$$\rho_{dry} = M_{solid}/V_{wet},$$

$$\rho_{solid} = M_{solid}/V_{solid},$$

$$\phi = V_{pw}/V_{wet},$$

and

$$VR = V_{pw}/V_{solid}.$$

P-wave velocity

The Section Half Velocity Gantry measures the ultrasonic velocity of materials placed between its transducers in the *x*-, *y*-, and *z*-directions on undisturbed working-half split-core sections from Hole A. Routine sampling frequency for *P*-wave measurements on the *x*-, *y*-, and *z*-axes was one per section, positioned next to MAD discrete samples. Velocity is measured in the *x*-direction using a caliper velocimeter (the contact probe) and in the *y*-, and *z*-directions using pairs of piezoelectric transducers (the insertion probe). The method of measurement is to derive an estimate of the traveltime and accurately measure the path length of the ultrasonic *P*-wave through the sample, with velocity (m/s) = path length (m)/traveltime (s) = dS/dt.

Traveltime measurement is estimated by an algorithm for graphical first arrival pick. An ultrasonic pulser generates a high-impulse voltage which is applied to the ultrasonic transmitter to induce oscillation of the crystal element at the required frequency. A trigger pulse from the pulser is applied to the oscilloscope to start the recording of the waveform from the receiving transducer. By recognizing unique features of the waveform, an estimate of the time for the ultrasonic pulse to propagate through the system is derived. This time includes traveltime through the sample and propagation system delays introduced by various components. A system delay time is calculated during the calibration process. Subtraction of the system delay time (and liner material propagation time, if required) from the total traveltime gives the traveltime for the ultrasonic pulse through the sample. Precise lengths for the sample are derived from a linear variable displacement transducer. The transducer converts changes in physical position into an alternating current electrical output and requires calibration, which is performed at the same time as the system delay is derived. The chisel transducers are fixed at 8.2 cm for the *z* (downhole)-axis and 3.44 cm for the *y*-axis (IODP axis designation). The *x*-axis separation is derived from a linear differential voltage transformer and calibration constants.

Section-Half Multisensor Logger measurements

The sensors included in the SHMSL are reflectance spectroscopy and colorimetry and magnetic susceptibility. Magnetic susceptibility data were not captured on this system during Expedition 320/321 because the magnetic properties of the brackets upon which the track is mounted cause artifacts in the data that cannot be corrected automatically using the software currently available. Not collecting susceptibility data allowed the collection of color reflectance data at a higher resolution than would otherwise have been possible in the time available. Two spectrophotometers were used during Expedition 320/321. A Minolta spectrophotometer (model CM-202) was used at Sites U1331–U1334, and an Ocean Optics spectrophotometer (model USB4000) was used at Sites U1335–U1338. Both spectrophotometers provide a high-resolution stratigraphic record of color variations. At each measurement depth the Minolta spectrophotometer records a spectra of 31 determinations at 10 nm intervals over the 400 to 700 nm wavelength band. The Ocean Optics spectrophotometer records a spectra with 3840 determinations spaced at ~0.2 nm between 177 and 925 nm at each measurement depth. The switch to the Ocean Optics spectrophotometer occurred after initial concerns about the linearity of the Ocean Optics data were alleviated.

Measurements were made on the archive halves of freshly split cores that were covered with clear plastic wrap. The SHMSL skips empty intervals and intervals where the core surface is well below the level of the core liner but does not recognize relatively small cracks or disturbed areas of core. Thus, SHMSL data may contain spurious measurements that should, to the extent possible, be edited out of the data set before use. Data are generated using the L*a*b* color system (Fig. **F13**), which describes colors by their position along three axes: (1) L*, which represents the white to black content (high to low values); (2) a*, which ranges from blue (negative) to yellow (positive); and (3) b*, which ranges from green (negative) to red (positive). During Expedition 320/321, data were captured at a minimum sample spacing of 2.5 cm, but through critical intervals this spacing was reduced to achieve higher resolution data (1 cm).

Percentage reflectance and color spectral data can support lithology description (Balsam et al., 1997; Balsam and Damuth, 2000). Color parameters may be used to obtain a detailed time series of relative changes in composition that can be used to correlate sections and analyze cyclicity. Spectral data can be used to estimate the abundances of certain compounds: visible range provides a semiquantitative estimate of hematite and goethite, whereas near-infrared and

near-ultraviolet ranges allow estimation of carbonate, opal, organic matter, chlorite, and some combinations of clay minerals.

Stratigraphic correlation and composite section

The scientific objectives of Expedition 320/321 required the recovery of complete stratigraphic sections, yet it has been demonstrated that a continuous section is rarely recovered from a single borehole because of core recovery gaps between successive APC and XCB cores despite 100% or more nominal recovery and other offsets (tides, core expansion, and deformation) (e.g., Ruddiman et al., 1987; Hagelberg et al., 1995; Lisiecki and Herbert, 2007). Construction of a complete stratigraphic section, referred to as a composite splice, requires combining stratigraphic intervals from two or more holes cored at the same site. To maximize the probability of bridging core recovery gaps in successive holes, the depths below the seafloor from which cores are recovered are offset between the holes. This practice ensures that most between-core intervals missing within a given hole are recovered in at least one of the adjacent holes. During Expedition 320/321, at least two holes were cored at all sites and used to construct composite sections.

Our composite sections and splice construction methodology follows one which has been successfully employed during a number of previous ODP legs and IODP expeditions (e.g., Hagelberg et al., 1992; Curry, Shackleton, Richter, et al., 1995; Jansen, Raymo, Blum, et al., 1996; Lyle, Koizumi, Richter, et al., 1997; Wefer, Berger, Richter, et al., 1998; Wang, Prell, Blum, et al., 2000; Lyle, Wilson, Janecek, et al., 2002; Mix, Tiedemann, Blum, et al., 2003; Zachos, Kroon, Blum, et al., 2004; Channell, Kanamatsu, Sato, et al., 2006). Assembly and verification of a complete composite stratigraphic section requires construction of a composite depth scale. Other depth scales (discussed below) can be implemented using downhole logging data and/or combining splicing and drill pipe depths.

Once a composite depth scale has been completed, a stratigraphically continuous and complete composite splice can be created from representative intervals from the multiple holes. Ideally, both core recovery gaps and intervals with coring deformation are absent in the spliced section. The continuity and completeness of the spliced section are dependent on avoiding coeval core recovery gaps in multiple holes, which can be done through real-time adjustments to the depths at which a core is collected, as discussed below.

Core composite depth scale

The goal of constructing a composite depth scale is to place coeval, laterally continuous stratigraphic features into a common frame of reference by depth shifting the CSF depth scales (see Table **T1**) of individual cores to maximize correlation between holes. In the composite depth scale used by IODP, referred to as the core composite depth below seafloor (CCSF-A) the depths of the individual cores can only be shifted by a constant amount without permitting expansion or contraction of the relative depth scale within any core (Fig. **F14**). Ultimately, this provides good first-order correlation between cores from different holes while also avoiding more subjective, and potentially erroneous, interpretations that might arise without applying this restriction first. The CCSF-A scale, once established, provides a basis upon which higher order depth composite scales can be built. The CCSF-A depth scale also allows a direct translation between lengths as measured in cores that are ordered in the splice and the new depth scale.

In essence, the CCSF-A scale overcomes many of the inadequacies of the CSF depth scale, which is based on drill pipe measurements and is unique to each hole. The CSF depth scale is based on the length that the drill string is advanced on a core by core basis and is often inaccurate because of ship heave (which is not compensated for in APC coring), tidal variations in sea level, and other sources of error. In contrast, the CCSF-A scale is built by assuming that the uppermost sediment (mudline) in the first core from a given hole is the sediment/water interface. This core becomes the "anchor" in the composite depth scale and is typically the only one in which depths are the same on both the CSF and CCSF-A scales. From this anchor, physical property core logging data (e.g., bulk density and magnetic susceptibility) are correlated among holes downsection. For each core, a depth offset (a constant) that best aligns the physical property variations to the equivalent cores in adjacent holes is added to the CSF depth in sequence down the holes. Depth offsets are often chosen to optimize correlation of specific features that define splice levels in cores from adjacent holes.

For Expedition 320/321, the CCSF-A scale and the splice are based on the stratigraphic correlation of data from the IODP STMSL core track, WRMSL, SHMSL, and long-core magnetometer (STMSL data were only used for real-time continuity assessment and are not presented in this report). For each of these track instruments, data were collected every 2.5 or 5 cm. We used magnetic susceptibility (Fig. **F14**), GRA bulk density, NGR, reflectance (L*, a*, and b*), and the intensity of magnetization following

20 mT AF demagnetization. All of these measurements are described in "Physical properties" and "Paleomagnetism." Other data were used as appropriate (see "Biostratigraphy" and "Lithostratigraphy").

The raw stratigraphic data were imported into Correlator (versions 1.43 for Expedition 320 and 1.61 for Expedition 321) and culled as necessary to avoid incorporating anomalous data influenced by edge effects at section boundaries and by coring disturbance. Correlator was used to assess the stratigraphic continuity of the recovered sedimentary sequences at each drill site and to construct the CCSF-A scale and composite splice.

Because depth intervals within cores are not squeezed or stretched by Correlator, all correlative features cannot be aligned. Stretching or squeezing between cores from different holes may reflect small-scale differences in sedimentation and/or distortion caused by the coring and archiving processes. The tops of APC cores are generally stretched and the bottoms are compressed, although this effect is lithology dependent. In addition, sediment (especially unconsolidated mud, ash, sand, and gravel) occasionally falls from higher levels in the borehole onto the tops of cores as they are recovered, and as a result the top 0–100 cm of many cores are not part of the stratigraphically contiguous section.

Correlations among cores from adjacent holes are evaluated visually and statistically by cross-correlation within a 2 m depth interval, which can be adjusted in length when appropriate. Depth-shifted data are denoted by CCSF-A. A table is presented in each site chapter that summarizes the depth offsets for each core. These tables are necessary for converting CSF to CCSF-A scales. The CCSF-A depth for any point within a core equals the CSF depth plus the cumulative offset. Correlation at finer resolution is not possible with Correlator because depth adjustments are applied linearly to individual cores; no adjustments, such as squeezing and stretching, are made within cores. Such fine-scale adjustment is possible postcruise (e.g., Hagelberg et al., 1995; Pälike et al., 2005).

Splicing

Once all cores have been depth shifted and stratigraphically aligned, a composite section is built by splicing segments together from multiple holes to form a complete record at a site (Fig. F14). The record is composed of core sections from adjacent holes so that coring gaps in one hole are filled with core intervals from an adjacent hole. The splice should contain no coring gaps, and an effort has been made to minimize inclusion of disturbed sections. The shipboard splice is ideally suited to guide core sampling for detailed paleoceanographic studies. A table and a figure presented in each site chapter summarize the intervals from each hole used to construct the splice. Additional splices may be constructed postcruise as needed.

The choice of tie points (and hence of a splice) is partly a subjective exercise. Our method in the construction of a splice followed three rules. First, where possible we avoided using the top and bottom ~0.5 m of cores, where disturbance resulting from drilling artifacts (even if not apparent in core logging data) is most likely. Second, we attempted to incorporate those portions of the recovered core that were most representative of the overall stratigraphic section of the site. Third, we tried to minimize the number of tie points to simplify postcruise sampling.

The length of the spliced section (on the CCSF-A scale) at a given site is typically ~5%–15% greater than the length of the cored section in any one hole as indicated by the CSF scale (Fig. F15). This increase is commonly attributed to sediment expansion resulting from elastic rebound, stretching during the coring process, gas expansion during the core recovery process, and curation practices, in which soupy core material commonly occurring at the top of many cores is curated as part of the core (e.g., Moran, 1997; Acton et al., 2001; Lisiecki and Herbert, 2007). In reality, much of the soupy material results from sediment falling into the hole or from sediment being stirred at the bottom of the hole as the BHA is advanced.

Ideally, the base of the CCSF-A scale is the bottom of the deepest core recovered from the deepest hole. In practice, however, the base often occurs where core recovery gaps align across all holes or the data quality does not allow reliable correlations between holes. Cores below this interval cannot be directly tied into the overlying and continuous CCSF-A scale. However, below the base of the continuous CCSF-A scale, cores from two or more holes can sometimes be correlated with each other to create a floating splice. In this case a CCSF-A depth was assigned to the section below the splice by adding the greatest cumulative offset to the first core below the splice and beginning the floating splice from that point in the section.

Corrected core composite depth scale

To correct the CCSF-A scale for empirically observed core expansion, a growth factor is calculated by fitting a line to CSF versus CCSF-A depth. By dividing the CCSF-A scale by the growth factor a corrected core composite depth scale (CCSF-B) can be evaluated that is a close approximation of the actual drilling depth scale. It should be noted, however, that

the actual growth factor is not linear and varies with lithology.

Special Task Multisensor Core Logger

To permit rapid stratigraphic correlation for real-time drilling adjustments, the STMSL was used. The STMSL is a simple track system with a magnetic susceptibility loop and a GRA sensor (see **"Physical properties"**). The GRA sensor failed after use at Site U1331 during Expedition 320, was repaired during the Honolulu port call, and used again during Expedition 321. To avoid interference with the susceptibility loop installed on the WRMSL, the STMSL operates at a different frequency (513 versus 621 Hz). It was developed to permit rapid measurement of susceptibility and GRA on whole-core sections as soon as possible following recovery. The concept was first attempted during ODP Leg 202 using a similar instrument from Oregon State University (Mix, Tiedemann, Blum, et al., 2003).

We ran the track for all sections measured using a sampling interval of 5 cm on all cores from the second and third hole at each site. Three measurements were made at each interval using SI units and the short (~1 s) measurement setting on the Bartington susceptibility meter. Using these settings, we could log a typical 9.5 m long core in ~30 min.

STMSL susceptibility is used in Correlator for preliminary stratigraphic correlation with the goal of determining if between-core gaps in one hole correspond with those in a hole that is being cored. If so, drilling adjustments can be made to ensure that coeval coring gaps are avoided in subsequent cores. These preliminary susceptibility and GRA data sets are then superseded by the same measurements collected on the WRMSL, which is done after the cores have equilibrated to room temperature and generally at higher resolution than on the STMSL. Likewise, the preliminary stratigraphic correlation is superseded by more careful evaluation following the collection of a suite of physical property data and core descriptions.

Depths in splice tables versus LIMS depths

The depth of a core interval recorded for a tie point in a splice table is not always the same as the depth for the same core interval returned by most database queries. This is because the tie point depth is based on the liner length, measured when the cores are cut into sections on the catwalk. The cores are analyzed on the STMSL almost immediately after this liner length measurement. At some later time, typically 10–36 h after being analyzed by the WRMSL, core sections are split and analyzed further (see **"Core handling and analysis"**). At this time, section lengths are measured again and archived as "curated lengths." General database queries return depths based on curated liner lengths. Because the sections may have expanded during the period between the two measurements or shifted during splitting and handling, the curated length is almost always longer than the initial liner length. Thus, depths associated with the WRMSL data used to construct the splice table are not identical to the final depths assigned to a given interval by the database. This leads to small differences, usually between 0 and 5 cm, between the CSF and CCSF-A depths recorded in a splice table and the depths reported in other places for the same core interval. We have chosen not to change these depths to be compatible with the LIMS database because this would not improve their accuracy. For consistency, we recommend that all postcruise depth models use or build on CCSF-A values provided in the LIMS database.

Downhole measurements

Downhole logs are used to determine physical, chemical, and structural properties of the formation penetrated by a borehole. Data are rapidly collected, continuous with depth, and measured in situ; they can be interpreted in terms of the stratigraphy, lithology, mineralogy, and geochemical composition of the penetrated formation. Where core recovery is incomplete or disturbed, log data may provide the only way to characterize the borehole section. Where core recovery is good, log and core data complement each other and may be interpreted jointly.

Downhole logs measure formation properties on a scale that is intermediate between those obtained from laboratory measurements on core samples and geophysical surveys. They are useful in calibrating the interpretation of geophysical survey data (e.g., through the use of synthetic seismograms) and provide a necessary link for the integrated understanding of physical properties on all scales.

Wireline logging

During wireline logging, logs are made with a variety of Schlumberger and Lamont-Doherty Earth Observatory Borehole Research Group (LDEO-BRG) logging tools combined into "tool strings," which are run down the hole after coring operations are complete. Four wireline tool strings were used during Expedition 320/321: a triple combination (triple combo: gamma ray, density, and resistivity); a modified triple combo, termed the "paleocombo" (gamma ray, density, and magnetic susceptibility); the Formation MicroScanner (FMS)-sonic (resistivity image of the borehole wall and elastic wave velocities); and

the Versatile Seismic Imager (VSI) (Fig. F16; Table T12). Each tool string also contains a telemetry cartridge for communicating through a seven-conductor wireline cable to the Schlumberger data acquisition system (MAXIS unit) on the drillship.

In preparation for logging, the boreholes were flushed of debris by circulating a "pill" of viscous drilling fluid (sepiolite mud mixed with seawater; approximate density = 8.8 lb/gal, or 1.055 g/cm^3) through the drill pipe to the bottom of the hole. The BHA was pulled up to a depth of 60–80 m drilling depth below seafloor (DSF). The tool strings were lowered downhole on a wireline cable during sequential runs and pulled up at constant speed, typically 250–300 m/h, to provide continuous measurements of several properties simultaneously. A new wireline heave compensator (WHC) was employed to minimize the effect of ship's heave on the tool position in the borehole (see below).

Logged sediment properties and tool measurement principles

The logged properties and the methods that the tools use to measure them are briefly described below. The main logs taken by the tools are listed in Table T13. More detailed information on individual tools and their geological applications may be found in Ellis and Singer (2007), Goldberg (1997), Lovell et al. (1998), Rider (1996), Robinson et al. (2008), Schlumberger (1989, 1994), and Serra (1984, 1986, 1989). A complete online list of acronyms for the Schlumberger tools and measurement curves is at www.apps.slb.com/cmd/.

Natural radioactivity

Two wireline gamma ray tools were used to measure and classify natural radioactivity in the formation. The Hostile Environment Natural Gamma Ray Sonde (HNGS) is a spectral gamma ray tool, and the Scintillation Gamma Ray Tool (SGT-N) is a total gamma ray tool.

The HNGS uses two bismuth germanate scintillation detectors and five-window spectroscopy to determine concentrations of K, Th, and U. The radioactive isotopes of these three elements dominate the natural radiation spectrum. The HNGS filters out gamma ray energies below 500 keV, eliminating sensitivity to bentonite or KCl in the drilling mud and improving measurement accuracy.

The SGT-N uses a sodium iodide scintillation detector to measure the total natural gamma ray emission, combining the spectral contributions of K, U, and Th concentrations in the formation. The SGT-N is not a spectral tool but provides high-resolution total gamma ray data for depth correlation between logging strings. It was included in the VSI tool string for this purpose.

Density

Formation density was determined with the Hostile Environment Litho-Density Sonde (HLDS). The sonde contains a radioactive cesium (^{137}Cs) gamma ray source (622 keV) and far and near gamma ray detectors mounted on a shielded skid, which is pressed against the borehole wall by a hydraulically activated eccentralizing arm. Gamma rays emitted by the source undergo Compton scattering, in which gamma rays are scattered by electrons in the formation. The number of scattered gamma rays that reach the detectors is proportional to the density of electrons in the formation, which is in turn related to bulk density. Porosity may also be derived from this bulk density if the matrix (grain) density is known. Good contact between the tool and borehole wall is essential for good HLDS logs; poor contact results in underestimation of density values.

The HLDS also measures photoelectric absorption as the photoelectric effect (PEF). Photoelectric absorption of the gamma rays occurs when their energy is reduced below 150 keV after being repeatedly scattered by electrons in the formation. Because PEF depends on the atomic number of the elements in the formation, it also varies according to the chemical composition of the minerals present. For example, the PEF of calcite = 5.08 barns/e$^-$, illite = 3.03 b/e$^-$, quartz = 1.81 barns/e$^-$, and kaolinite = 1.49 b/e$^-$.

Electrical resistivity

The phasor dual induction–spherically focused resistivity tool (DITE-SFL) was used to measure electrical resistivity. The DITE-SFL provides three measures of electrical resistivity, each with a different depth of investigation into the formation. The two induction devices (deep and medium depths of penetration) transmit high-frequency alternating currents (10–40 kHz) through transmitter coils, creating magnetic fields that induce secondary currents in the formation. These currents produce a new inductive signal, proportional to the conductivity of the formation, which is measured by the receiving coils. The measured conductivities are then converted to resistivity (in units of ohm-meters). The spherically focused resistivity is measured by an electrode device that sends a current into the formation. The amount of current needed to maintain a constant drop in voltage gives a direct measure of resistivity. This device uses several electrodes to focus the current flow into the formation so that equipotential surfaces are spherical, and has a higher vertical resolution than

the induction measurements. Calcite, silica, and hydrocarbons are electrical insulators, whereas ionic solutions like pore water are conductors. Electrical resistivity, therefore, can be used to evaluate porosity (via Archie's equation) for a given resistivity of the pore water, which depends on salinity and temperature.

Magnetic susceptibility

The Magnetic Susceptibility Sonde (MSS), a new wireline tool designed by the LDEO-BRG, was run for the first time in IODP during Expedition 320. It measures the magnetic susceptibility of the formation, which depends on the concentration and composition (size, shape, and mineralogy) of magnetic minerals, principally magnetites. These measurements provide one of the best methods for investigating stratigraphic changes in mineralogy and lithology because the measurement is quick, repeatable, and nondestructive and because different lithologies often have strongly contrasting susceptibilities. High-resolution susceptibility measurements aid significantly in paleoclimatic and paleoceanographic studies, where an accurate and complete stratigraphic framework is critical to reconstruct past climatic changes.

The MSS measures at two vertical resolutions (Fig. F17). A single-coil sensor provides high-resolution measurements (~10 cm) but reads shallow; therefore, bowsprings are used to push the tool against the borehole wall (additionally, the HLDS caliper arm aids in eccentralizing the tool). A dual-coil sensor provides lower resolution (~40 cm) and deeper reading measurements and is minimally affected by standoff; therefore, it acts as a quality control for the high-resolution readings. It also measures the electrical conductivity of the formation with an induction measurement similar to that provided by the DITE-SFL described above. The MSS can be run as a component of a Schlumberger tool string using a specially developed data translation cartridge (ELIC), saving hours of operation time. For quality control and environmental corrections, the MSS also measures internal temperature and *z*-axis acceleration.

Elastic wave velocity

The Dipole Sonic Imager measures the transit times between sonic transmitters and an array of eight receivers. It combines replicate measurements, thus providing a measurement of compressional velocity through sediments that is relatively free from the effects of formation damage and an enlarged borehole (Schlumberger, 1989). Along with the monopole transmitters found on most sonic tools, it also has two cross-dipole transmitters, which allow an additional measurement of shear wave velocity. Dipole measurements are necessary to measure shear velocities in slow formations, in which shear velocity is less than the compressional velocity of the borehole fluid. Such slow formations are typically encountered in deep-ocean drilling.

Formation MicroScanner

The FMS provides high-resolution electrical resistivity images of borehole walls. The tool has four orthogonal arms and pads, each containing 16 button electrodes that are pressed against the borehole wall during the recording. The electrodes are arranged in two diagonally offset rows of eight electrodes each. A focused current is emitted from the button electrodes into the formation, with a return electrode near the top of the tool. Resistivity of the formation at the button electrodes is derived from the intensity of current passing through the button electrodes. Processing transforms these measurements into oriented images with a resolution of ~0.5 cm that reveal the geologic structures of the borehole wall.

The development of the FMS tool has added a new dimension to wireline logging (Luthi, 1990; Lovell et al., 1998; Salimullah and Stow, 1992). Features such as bedding, fracturing, slump folding, and bioturbation can be resolved; images are oriented to magnetic north so that fabric analysis can be carried out and the dip and direction (azimuth) of planar features in the formation can be measured.

The maximum extension of the FMS caliper arms is 15 inches. In holes with a diameter >15 inches, the pad contact will be inconsistent and the FMS images may appear out of focus and too conductive. Irregular (rough) borehole walls will also adversely affect the images if contact with the wall is poor.

Accelerometry and magnetic field measurement

Three-component acceleration and magnetic field measurements were made with the General Purpose Inclinometry Tool (GPIT). The primary purpose of this tool, which incorporates a three-component accelerometer and a three-component magnetometer, is to determine the acceleration and orientation of the FMS-sonic tool string during logging. Thus, the FMS images can be corrected for irregular tool motion, and the dip and direction (azimuth) of features in the FMS image can be determined.

Vertical seismic profiling

The VSI is a borehole seismic tool optimized for vertical seismic profiles (VSPs) in open or cased holes that are vertical or deviated. The VSI consists of mul-

tiple shuttles (each containing a three-axis geophone) separated by acoustically isolating spacers. During Expedition 321, we used the VSI tool with a single shuttle. In a VSP experiment, the VSI records the full waveform of elastic waves generated by a seismic source positioned just below the sea surface. As a seismic source during Expedition 321, we used a Sercel G. Gun Parallel Cluster, which is composed of two 250 inch^3 air guns separated by 1 m. The source was positioned on the port side of the *JOIDES Resolution* at a water depth of ~7 m with a borehole offset of ~30 m. The VSI was clamped against the borehole wall at 15 m intervals, and 1–5 recordings were typically taken at each station. The recorded waveforms were stacked and a one-way traveltime was determined from the median of the first breaks for each station. These "check shot" measurements relate depth in the hole to traveltime in reflection seismic lines.

Log data quality

The principal influence on log data quality is the condition of the borehole wall. If the borehole diameter varies over short intervals because of washouts during drilling or ledges made of layers of harder material, the logs from those tools that require good contact with the borehole wall (i.e., FMS and density tools) may be degraded. Deep investigation measurements such as resistivity and sonic velocity, which do not require contact with the borehole wall, are generally less sensitive to borehole conditions. Very narrow ("bridged") sections will also cause irregular log results. Borehole quality is improved by minimizing the circulation of drilling fluid while drilling, flushing the borehole to remove debris, and logging as soon as possible after drilling and conditioning are completed.

The quality of the logging depth determination depends on several factors. The depth of the wireline-logged measurement is determined from the length of the logging cable paid out at the winch on the ship. The seafloor is identified on the natural gamma log by the abrupt reduction in gamma ray count at the water/sediment boundary (mudline). Discrepancies between the drillers depth and the wireline log depth occur because of core expansion, incomplete core recovery, incomplete heave compensation, and drill pipe stretch in the case of drillers depth. In the case of log depth, discrepancies occur because of incomplete heave compensation, incomplete correction for cable stretch, and cable slip. Tidal changes in sea level will also have an effect. To minimize the wireline tool motion caused by ship heave, a new hydraulic wireline heave compensator adjusts for rig motion during wireline logging operations.

Wireline heave compensator

For the first time during a full expedition, the new WHC was used aboard the *JOIDES Resolution* during Expedition 320/321. The WHC system is designed to compensate for the vertical motion of the ship and to maintain a steady motion of the logging tools. It uses vertical acceleration measurements made by a motion reference unit (MRU; located under the rig floor near the center of gravity of the ship) to calculate the vertical position of the ship and adjusts the length of the wireline by varying the distance between two pulleys that the wireline cable passes through. Real-time measurements of uphole (surface) and downhole acceleration are made simultaneously by the MRU and GPIT, respectively. A LDEO-developed software package allows these data to be analyzed and compared in real time, displaying the actual motion of the logging tool string and enabling the efficiency of the compensator to be evaluated. In addition to an improved design and smaller footprint compared to the previous system, its location with the winch unit on the starboard side of the derrick contributed to a significant reduction in the time necessary to prepare for logging operations. The WHC was nonoperational during Expedition 320.

Logging data flow and log depth scales

Data for each wireline logging run were monitored in real time and recorded using the Schlumberger MAXIS 500 system. The initial logging data are referenced to the WRF depth scale. After logging was completed, data were shifted to a seafloor reference (WSF) based on the step in NGR at the sediment/water interface. These initial data were made available to the science party.

Downhole log data were also transferred onshore to LDEO for standardized data processing. The main part of the processing is depth matching to remove depth offsets between different logging runs, which results in a new depth scale, wireline matched depth below seafloor (WMSF). Also, corrections are made to some tools and logs, documentation for the logs (with an assessment of log quality) is prepared, and data are converted to ASCII for the conventional logs and GIF for the FMS images. Schlumberger GeoQuest's GeoFrame software package is used for most of the processing. Data were transferred back to the ship within a few days of logging and were made available (in ASCII and DLIS formats) through the shipboard IODP logging database.

Measurements such as magnetic susceptibility, natural gamma radiation, and density are taken both downhole and on cores. They can be correlated using the Correlator software, which allows shifting of the core depths onto the wireline depth

scale (see **"Stratigraphic correlation and composite section"**).

Core-log-seismic integration

A depth-traveltime relationship must be determined at each site to correlate core and log data acquired in depth with seismic reflection measurements that are a function of traveltime. A direct measurement of the depth-traveltime relationship is given by the first arrival times in a VSP experiment (see above). This relationship can also be estimated by constructing synthetic seismograms, which are computed from reflection coefficients obtained from contrasts in *P*-wave velocity and density. These velocities and densities may be measured in situ with downhole logs or on cores in the physical property laboratory. The synthetic seismograms were calculated using the IESX seismic interpretation package (part of the Schlumberger GeoFrame software suite), which allows for interactively adjusting the depth-traveltime relationship until a good match is achieved between features in the synthetic seismogram and in the measured seismic data. A calibrated depth-traveltime relationship allows for correlating hole stratigraphy with seismic reflection features (e.g., to assign ages to prominent seismic horizons that can be correlated away from the drill site).

In situ temperature measurements

During Expedition 320/321, in situ temperature measurements were made with the APCT-3 and the sediment temperature (SET) tool. At least four in situ temperature measurements were made at each site using the APCT-3. The APCT-3 fits directly into the coring shoe of the APC and consists of a battery pack, data logger, and a platinum resistance-temperature device calibrated over a temperature range from 0° to 30°C. Before entering the borehole, the tool is first stopped at the mudline for 5 min to thermally equilibrate with bottom water. However, the lowest temperature recorded during the run down was occasionally preferred to the average temperature at the mudline as an estimate of the bottom water temperature because it was more repeatable, and bottom water is expected to have the lowest temperature in the profile. After the APC penetrated the sediment, it was held in place for 10 min as the APCT-3 recorded the temperature of the cutting shoe every second. When the APC is plunged into the formation, there is an instantaneous temperature rise from frictional heating. This heat gradually dissipates into the surrounding sediments as the temperature at the APCT-3 equilibrates toward the temperature of the sediments.

The SET tool was deployed for the first time on the *JOIDES Resolution* during Expedition 321, and except for an updated electronics section it is very similar to the Davis-Villinger Temperature Probe used extensively in previous IODP expeditions. The SET tool is run in semiconsolidated sediments that cannot be penetrated by the APCT-3 and measures temperature with a 1.4 m long probe that is pushed into the sediment below the drill bit and held in place for 10 min. The SET tool is run through the drill string on the coring wireline with the colleted delivery system, which allows the probe to be decoupled from the BHA and prevents the ship's heave from moving the probe and disturbing the measurement.

The equilibrium temperature of the sediments was estimated by applying a mathematical heat-conduction model to the temperature decay record (Horai and Von Herzen, 1985). The synthetic thermal decay curve for the APCT-3 and SET tool is a function of the geometry and thermal properties of the probe and the sediments (Bullard, 1954; Horai and Von Herzen, 1985). The equilibrium temperature must be estimated by applying a fitting procedure (Pribnow et al., 2000). However, where the APC has not achieved a full stroke, or where ship heave pulls the APC up from full penetration, the temperature equilibration curve will be disturbed and temperature determination is more difficult. The nominal accuracy of the APCT-3 and SET tool temperature measurements is ±0.05°C.

The APCT-3 and SET tool temperature data were combined with measurements of thermal conductivity (see **"Physical properties"**) obtained from whole-core samples to obtain heat flow values. Heat flow was calculated according to the Bullard method, to be consistent with the Leg 199 analyses and the synthesis of ODP heat flow data by Pribnow et al. (2000).

References

Acton, G.D., Borton, C.J., and the Leg 178 Shipboard Scientific Party, 2001. Palmer Deep composite depth scales for Leg 178 Sites 1098 and 1099. *In* Barker, P.F., Camerlenghi, A., Acton, G.D., and Ramsay, A.T.S. (Eds.), *Proc. ODP, Sci. Results,* 178: College Station, TX (Ocean Drilling Program), 1–35. **doi:10.2973/odp.proc.sr.178.202.2001**

Agnini, C., Fornaciari, E., Raffi, I., Rio, D., Röhl, U., and Westerhold, T., 2007. High-resolution nannofossil biochronology of middle Paleocene to early Eocene at ODP Site 1262: implications for calcareous nannoplankton evolution. *Mar. Micropaleontol.,* 64(3–4):215–248. **doi:10.1016/j.marmicro.2007.05.003**

Agnini, C., Muttoni, G., Kent, D.V., and Rio, D., 2006. Eocene biostratigraphy and magnetic stratigraphy from

Possagno, Italy: the calcareous nannofossil response to climate variability. *Earth Planet Sci. Lett.,* 241(3–4):815–830. **doi:10.1016/j.epsl.2005.11.005**

Akiba, F., 1986. Middle Miocene to Quaternary diatom biostratigraphy in the Nankai Trough and Japan Trench, and modified lower Miocene through Quaternary diatom zones for middle-to-high latitudes of the north Pacific. *In* Kagami, H., Karig, D.E., Coulbourn, W.T., et al., *Init. Repts. DSDP,* 87: Washington, DC (U.S. Govt. Printing Office), 393–481. **doi:10.2973/dsdp.proc.87.106.1986**

Akiba, F., and Yanagisawa, Y., 1986. Taxonomy, morphology and phylogeny of the Neogene diatom zonal marker species in the middle-to-high latitudes of the North Pacific. *In* Kagami, H., Karig, D.E., Coulbourn, W.T., et al., *Init. Repts. DSDP,* 87: Washington, DC (U.S. Govt. Printing Office), 483–554. **doi:10.2973/dsdp.proc.87.107.1986**

ASTM International, 1990. Standard test method for measurement of hydraulic conductivity of saturated porous materials using a flexible wall permeameter (Standard D5084–70). In *Annual Book of ASTM Standards:* Philadelphia (Am. Soc. Testing and Mater.), 63–70.

Backman, J., 1986. Late Paleocene to middle Eocene calcareous nannofossil biochronology from the Shatsky Rise, Walvis Ridge and Italy. *Palaeogeogr., Palaeoclimatol., Palaeoecol.,* 57(1):43–59. **doi:10.1016/0031-0182(86)90005-2**

Backman, J., 1987. Quantitative calcareous nannofossil biochronology of middle Eocene through early Oligocene sediment from DSDP Sites 522 and 523. *Abh. Geol. Bundesanst. (Austria),* 39:21–31.

Backman, J., Jakobsson, M., Frank, M., Sangiorgi, F., Brinkhuis, H., Stickley, C., O'Regan, M., Løvlie, R., Pälike, H., Spofforth, D., Gattacecca, J., Moran, K., King, J., and Heil, C., 2008. Age model and core-seismic integration for the Cenozoic Arctic Coring Expedition sediments from the Lomonosov Ridge. *Paleoceanography,* 23(1):PA1S03. **doi:10.1029/2007PA001476**

Baldauf, J.G., and Iwai, M., 1995. Neogene diatom biostratigraphy for the eastern equatorial Pacific Ocean, Leg 138. *In* Pisias, N.G., Mayer, L.A., Janecek, T.R., Palmer-Julson, A., and van Andel, T.H. (Eds.), *Proc. ODP, Sci. Results,* 138: College Station, TX (Ocean Drilling Program), 105–128. **doi:10.2973/odp.proc.sr.138.107.1995**

Balsam, W.L., and Damuth, J.E., 2000. Further investigations of shipboard vs. shore-based spectral data: implications for interpreting Leg 164 sediment composition. *In* Paull, C.K., Matsumoto, R., Wallace, P., and Dillon, W.P. (Eds.), *Proc. ODP, Sci. Results,* 164: College Station, TX (Ocean Drilling Program), 313–324. **doi:10.2973/odp.proc.sr.164.222.2000**

Balsam, W.L., Damuth, J.E., and Schneider, R.R., 1997. Comparison of shipboard vs. shore-based spectral data from Amazon-Fan cores: implications for interpreting sediment composition. *In* Flood, R.D., Piper, D.J.W., Klaus, A., and Peterson, L.C. (Eds.), *Proc. ODP, Sci. Results,* 155: College Station, TX (Ocean Drilling Program), 193–215. **doi:10.2973/odp.proc.sr.155.210.1997**

Barron, J.A., 1981. Late Cenozoic diatom biostratigraphy and paleoceanography of the middle-latitude eastern North Pacific, Deep Sea Drilling Project Leg 63. *In* Yeats, R.S., Haq, B.U., et al., *Init. Repts. DSDP,* 63: Washington, DC (U.S. Govt. Printing Office), 507–538. **doi:10.2973/dsdp.proc.63.113.1981**

Barron, J.A., 1983. Latest Oligocene through early middle Miocene diatom biostratigraphy of the eastern tropical Pacific. *Mar. Micropaleontol.,* 7:487–515. **doi:10.1016/0377-8398(83)90012-9**

Barron, J.A., 1985a. Late Eocene to Holocene diatom biostratigraphy of the equatorial Pacific Ocean, Deep Sea Drilling Project Leg 85. *In* Mayer, L., Theyer, F., Thomas, E., et al., *Init. Repts. DSDP,* 85: Washington, DC (U.S. Govt. Printing Office), 413–456. **doi:10.2973/dsdp.proc.85.108.1985**

Barron, J.A., 1985b. Miocene to Holocene planktic diatoms. *In* Bolli, H.M., Saunders, J.B., and Perch-Nielsen, K. (Eds.), *Plankton Stratigraphy:* Cambridge (Cambridge Univ. Press), 763–809.

Barron, J.A. 2006. Diatom biochronology for the early Miocene of the equatorial Pacific. *Stratigraphy,* 2(4):281–30.

Barron, J.A., Fourtanier, E., and Bohaty, S.M., 2004. Oligocene and earliest Miocene diatom biostratigraphy of ODP Leg 199 Site 1220, equatorial Pacific. *In* Wilson, P.A., Lyle, M., Janecek, T.R., and Firth, J.V. (Eds.), *Proc. ODP, Sci. Results,* 199: College Station (Ocean Drilling Program), 1–25. **doi:10.2973/odp.proc.sr.199.204.2004**

Barron, J.A., and Gladenkov, A.Y., 1995. Early Miocene to Pleistocene diatom stratigraphy of Leg 145. *In* Rea, D.K., Basov, I.A., Scholl, D.W., and Allan, J.F. (Eds.), *Proc. ODP, Sci. Results,* 145: College Station, TX (Ocean Drilling Program), 3–19. **doi:10.2973/odp.proc.sr.145.101.1995**

Berggren, W.A., and Pearson, P. N., 2005. A revised tropical to subtropical Paleogene planktonic foraminiferal zonation. *J. Foraminiferal Res.,* 35(4):279–298. **doi:10.2113/35.4.279**

Berggren, W.A., Kent, D.V., and Flynn, J.J., 1985. Jurassic to Paleogene, Part 2. Paleogene geochronology and chronostratigraphy. *In* Snelling, N.J. (Ed.), *The Chronology of the Geological Record.* Geol. Soc. London Mem., 10:141–195.

Berggren, W.A., Kent, D.V., Swisher, C.C., III, and Aubry, M.-P., 1995. A revised Cenozoic geochronology and chronostratigraphy. *In* Berggren, W.A., Kent, D.V., Aubry, M.-P., and Hardenbol, J. (Eds.), *Geochronology, Time Scales and Global Stratigraphic Correlation.* Spec. Publ.—SEPM (Soc. Sediment. Geol.), 54:129–212.

Blaj, T., Backman, J., and Raffi, I., 2009. Late Eocene to Oligocene preservation history and biochronology of calcareous nannofossils from paleo-equatorial Pacific Ocean sediments. *Rivista Italiana Paleontologia e Stratigrafia,* 115(1):67–84.

Blow, W.H., 1969. Late middle Eocene to Recent planktonic foraminiferal biostratigraphy. *In* Brönnimann, P.,

and Renz, H.H. (Eds.), *Proc. First Int. Conf. Planktonic Microfossils, Geneva, 1967:* Leiden (E.J. Brill), 1:199–422.

Blum, P., 1997. Physical properties handbook: a guide to the shipboard measurement of physical properties of deep-sea cores. *ODP Tech. Note,* 26. **doi:10.2973/odp.tn.26.1997**

Bolli, H.M., and Saunders, J.B., 1985. Oligocene to Holocene low latitude planktic foraminifera. *In* Bolli, H.M., Saunders, J.B., and Perch-Nielsen, K. (Eds.), *Plankton Stratigraphy:* Cambridge (Cambridge Univ. Press), 155–262.

Bown, P.R. (Ed.), 1998. *Calcareous Nannofossil Biostratigraphy:* Dordrecht, The Netherlands (Kluwer Academic Publ.)

Bown, P.R., 2005. Palaeogene calcareous nannofossils from the Kilwa and Lindi areas of coastal Tanzania (Tanzania Drilling Project sites 2003–4). *J. Nannoplankton Res.,* 27:21–95.

Bullard, E.C., 1954. The flow of heat through the floor of the Atlantic Ocean. *Proc. R. Soc. London, Ser. A,* 222:408–429.

Burckle, L.H., 1972. Late Cenozoic planktonic diatom zones from the eastern equatorial Pacific. *In* Simonsen, R. (Ed.), *First Symposium on Recent and Fossil Marine Diatoms*. Nova Hedwegia Beih., 39:217–246.

Burckle, L.H., 1978. Early Miocene to Pliocene diatom datum level for the equatorial Pacific. *Proc. Second Working Group Mtg. Biostratigraphic Datum Planes, Pacific Neogene, IGCP Proj. 114.* Spec. Publ.—Geol. Res. Dev. Ctr., 1:25–44.

Burckle, L.H., Keigwin, L.D., and Opdyke, N.D., 1982. Middle and late Miocene stable isotope stratigraphy: correlation to the paleomagnetic reversal record. *Micropaleontology,* 28(4):329–334. **doi:10.2307/1485448**

Burckle, L.H., and Trainer, J., 1979. Middle and late Pliocene diatom datum levels from the central Pacific. *Micropaleontology,* 25(3):281–293. **doi:10.2307/1485303**

Cande, S.C., and Kent, D.V., 1995. Revised calibration of the geomagnetic polarity timescale for the Late Cretaceous and Cenozoic. *J. Geophys. Res., [Solid Earth],* 100(B4):6093–6095. **doi:10.1029/94JB03098**

Chaisson, W.P., and Leckie, R.M., 1993. High-resolution Neogene planktonic foraminifer biostratigraphy of Site 806, Ontong Java Plateau (western equatorial Pacific). *In* Berger, W.H., Kroenke, L.W., Mayer, L.A., et al., *Proc. ODP, Sci. Results,* 130: College Station, TX (Ocean Drilling Program), 137–178. **doi:10.2973/odp.proc.sr.130.010.1993**

Chaisson, W.P., and Pearson, P.N., 1997. Planktonic foraminifer biostratigraphy at Site 925: middle Miocene–Pleistocene. *In* Shackleton, N.J., Curry, W.B., Richter, C., and Bralower, T.J. (Eds.), *Proc. ODP, Sci. Results,* 154: College Station, TX (Ocean Drilling Program), 3–31. **doi:10.2973/odp.proc.sr.154.104.1997**

Channell, J.E.T., Kanamatsu, T., Sato, T., Stein, R., Alvarez Zarikian, C.A., Malone, M.J., and the Expedition 303/306 Scientists, 2006. *Proc. IODP,* 303/306: College Station, TX (Integrated Ocean Drilling Program Management International, Inc.). **doi:10.2204/iodp.proc.303306.2006**

Curry, W.B., Shackleton, N.J., Richter, C., et al., 1995. *Proc. ODP, Init. Repts.,* 154: College Station, TX (Ocean Drilling Program). **doi:10.2973/odp.proc.ir.154.1995**

Dickens, G.R., Koelling, M., Smith, D.C., Schneiders, L., and the IODP Expedition 302 Scientists, 2007. Rhizon sampling of pore waters on scientific drilling expeditions: an example from the IODP Expedition 302, Arctic Coring Expedition (ACEX). *Sci. Drill.,* 4: 22–25. **doi:10.2204/iodp.sd.4.08.2007**

Droser, M.L., and Bottjer, D.J., 1986. A semiquantitative field classification of ichnofabric. *J. Sediment. Petrol.,* 56:558–559.

Ellis, D.V., and Singer, J.M., 2007. *Well Logging for Earth Scientists,* 2nd edition: Dordrecht, The Netherlands (Springer).

Evans, H.B., 1965. GRAPE—a device for continuous determination of material density and porosity. *Trans. SPWLA 6th Ann. Logging Symp.:* Dallas, 2:B1–B25.

Expedition 320T Scientists, 2009. USIO sea trials and assessment of readiness transit (START): Ontong Java Plateau. *IODP Prel. Rept.,* 320T. **doi:10.2204/iodp.pr.320T.2009**

Fenner, J., 1985. Late Cretaceous to Oligocene planktic diatoms. *In* Bolli, H.M., Saunders, J.B., and Perch-Nielsen, K. (Eds.), *Plankton Stratigraphy:* Cambridge (Cambridge Univ. Press), 713–762.

Gieskes, J.M., Gamo, T., and Brumsack, H., 1991. Chemical methods for interstitial water analysis aboard *JOIDES Resolution. ODP Tech. Note,* 15. **doi:10.2973/odp.tn.15.1991**

Goldberg, D., 1997. The role of downhole measurements in marine geology and geophysics. *Rev. Geophys.,* 35(3):315–342. **doi:10.1029/97RG00221**

Govindaraju, K., 1994. 1994 compilation of working values and sample description for 383 geostandards. *Geostand. Newsl.,* 18 (spec. iss.).

Graber, K.K., Pollard, E., Jonasson, B., and Schulte, E. (Eds.), 2002. Overview of Ocean Drilling Program engineering tools and hardware. *ODP Tech. Note,* 31. **doi:10.2973/odp.tn.31.2002**

Hagelberg, T., Shackleton, N., Pisias, N., and Shipboard Scientific Party, 1992. Development of composite depth sections for Sites 844 through 854. *In* Mayer, L., Pisias, N., Janecek, T., et al., *Proc. ODP, Init. Repts.,* 138: College Station, TX (Ocean Drilling Program), 79–85. **doi:10.2973/odp.proc.ir.138.105.1992**

Hagelberg, T.K., Pisias, N.G., Shackleton, N.J., Mix, A.C., and Harris, S., 1995. Refinement of a high-resolution, continuous sedimentary section for studying equatorial Pacific Ocean paleoceanography, Leg 138. *In* Pisias, N.G., Mayer, L.A., Janecek, T.R., Palmer-Julson, A., and van Andel, T.H. (Eds.), *Proc. ODP, Sci Results,* 138: College Station, TX (Ocean Drilling Program), 31–46. **doi:10.2973/odp.proc.sr.138.103.1995**

Hancock, H.J.L., Chaproniere, G.C., Dickens, G.R., and Henderson, R.A., 2002. Early Palaeogene planktonic foraminiferal and carbon isotope stratigraphy, Hole 762C, Exmouth Plateau, northwest Australian margin. *J. Micropalaeontol.,* 21(1):29–42.

Harms, J.C., and Choquette, P.W., 1965. Geologic evaluation of a gamma-ray porosity device. *Trans. SPWLA 6th Ann. Logging Symp.:* Dallas, C1–C37.

Hayward, B.W., 2002. Late Pliocene to middle Pleistocene extinctions of deep-sea benthic foraminifera ("*Stilostomella* extinction") in the southwest Pacific. *J. Foraminiferal Res.,* 32(3):274–307. **doi:10.2113/32.3.274**

Holbourn, A.E., and Henderson, A., 2002. Re-illustration and revised taxonomy for selected deep-sea benthic foraminifers. *Paleontologia Electronica,* 4.

Horai, K., and Von Herzen, R.P., 1985. Measurement of heat flow on Leg 86 of the Deep Sea Drilling Project. *In* Heath, G.R., Burckle, L.H., et al., *Init. Repts. DSDP,* 86: Washington, DC (U.S. Govt. Printing Office), 759–777. **doi:10.2973/dsdp.proc.86.135.1985**

Hunter Laboratory, 2008. CIE L*a*b* color scale. *Applications Note,* 8(7).

Jansen, E., Raymo, M.E., Blum, P., et al., 1996. *Proc. ODP, Init. Repts.,* 162: College Station, TX (Ocean Drilling Program). **doi:10.2973/odp.proc.ir.162.1996**

Jones, R.W., 1994. *The Challenger Foraminifera:* New York (Oxford).

Jovane, L., Florindo, F., Coccioni, R., Dinarès-Turell, J., Marsili, A., Monechi, S., Roberts, A.P., and Sprovieri, M., 2007. The middle Eocene climatic optimum event in the Contessa Highway section, Umbrian Appennines, Italy. *Geol. Soc. Am. Bull.,* 119(3):413–427. **doi:10.1130/B25917.1**

Kaminski, M.A., Geroch, S., and Kaminski, D.G. (Eds.), 1993. *The Origins of Applied Micropalaeontology: The School of Jozef Grzybowski*. Spec. Publ.– Grzybowski Found.

Katz, M.E., and Miller, K.G., 1991. Early Paleogene benthic foraminiferal assemblages and stable isotopes in the Southern Ocean. *In* Ciesielski, P.F., Kristoffersen, Y., et al., *Proc. ODP, Sci. Results,* 114: College Station, TX (Ocean Drilling Program), 481–512. **doi:10.2973/odp.proc.sr.114.147.1991**

Keene, J.B., 1975. Cherts and porcellanites from the North Pacific DSDP, Leg 32. *In* Larson, R.L., Moberly, R., et al. *Init. Repts. DSDP,* 32: Washington, DC (U.S. Govt. Printing Office), 429–507. **doi:10.2973/dsdp.proc.32.114.1975**

Kemp, A.E.S., 1995. Variation of trace fossils and ichnofacies in Neogene and Quaternary pelagic sediments from the eastern equatorial Pacific Ocean (Leg 138). *In* Pisias, N.G., Mayer, L.A., Janecek, T.R., Palmer-Julson, A., and van Andel, T.H. (Eds.), *Proc. ODP, Sci. Results,* 138: College Station, TX (Ocean Drilling Program), 177–190. **doi:10.2973/odp.proc.sr.138.110.1995**

Kennett, J.P., and Srinivasan, M.S., 1983. *Neogene Planktonic Foraminifera: A Phylogenetic Atlas:* Stroudsburg, PA (Hutchinson Ross).

Kristiansen, J.I., 1982. The transient cylindrical probe method for determination of thermal parameters of earth materials [Ph.D. dissert.]. Åarhus Univ.

Kryc, K.A., Murray, R.W., and Murray, D.W., 2003. Elemental fractionation of Si, Al, Ti, Fe, Ca, Mn, P, and Ba in five marine sedimentary reference materials: results from sequential extractions. *Anal. Chim. Acta,* 487(1):117–128. **doi:10.1016/S0003-2670(03)00492-6**

Kuhnt, W., Holbourn, A., and Zhao, Q., 2002. The early history of the South China Sea: evolution of Oligocene-Miocene deep water environments. *Rev. Micropaleontol.*

Laskar, J., Robutel, P., Joutel, F., Gastineau, M., Correia, A.C.M., and Levrard, B., 2004. A long-term numerical solution for the insolation quantities of the Earth. *Astron. Astrophys.,* 428(1):261–285. **doi:10.1051/0004-6361:20041335**

Leckie, R.M., Farnham, C., and Schmidt, M.G., 1993. Oligocene planktonic foraminifer biostratigraphy of Hole 803D (Ontong Java Plateau) and Hole 628A (Little Bahama Bank), and comparison with the southern high latitudes. *In* Berger, W.H., Kroenke, L.W., Mayer, L.A., et al., *Proc. ODP, Sci. Results,* 130: College Station, TX (Ocean Drilling Program), 113–136. **doi:10.2973/odp.proc.sr.130.012.1993**

Lisiecki, L.E., and Herbert, T.D., 2007. Automated composite depth scale construction and estimates of sediment core extension. *Paleoceanography,* 22(4):PA4213. **doi:10.1029/2006PA001401**

Loeblich, A.R., Jr., and Tappan, H., 1988. *Foraminiferal Genera and Their Classification:* New York (Van Nostrand Reinhold).

Lourens, L.J., Hilgen, F.J., Laskar, J., Shackleton, N.J., and Wilson, D., 2004. The Neogene period. *In* Gradstein, F.M., Ogg, J., et al. (Eds.), *A Geologic Time Scale 2004:* Cambridge (Cambridge Univ. Press), 409–440.

Lovell, M.A., Harvey, P.K., Brewer, T.S., Williams, C., Jackson, P.D., and Williamson, G., 1998. Application of FMS images in the Ocean Drilling Program: an overview. *In* Cramp, A., MacLeod, C.J., Lee, S.V., and Jones, E.J.W. (Eds.), *Geological Evolution of Ocean Basins: Results from the Ocean Drilling Program*. Geol. Soc. Spec. Publ., 131:287–303.

Luthi, S.M., 1990. Sedimentary structures of clastic rocks identified from electrical borehole images. *In* Hurst, A., Lovell, M.A., and Morton, A.C. (Eds.), *Geological Applications of Wireline Logs*. Geol. Soc. Spec. Publ., 48:3–10.

Lyle, M., Koizumi, I., Richter, C., et al., 1997. *Proc. ODP, Init. Repts.,* 167: College Station, TX (Ocean Drilling Program). **doi:10.2973/odp.proc.ir.167.1997**

Lyle, M., Wilson, P.A., Janecek, T.R., et al., 2002. *Proc. ODP, Init. Repts.,* 199: College Station, TX (Ocean Drilling Program). **doi:10.2973/odp.proc.ir.199.2002**

Martini, E., 1971. Standard Tertiary and Quaternary calcareous nannoplankton zonation. *In* Farinacci, A. (Ed.), *Proc. 2nd Int. Conf. Planktonic Microfossils Roma:* Rome (Ed. Tecnosci.), 2:739–785.

Mayer, L., Pisias, N., Janecek, T., et al., 1992. *Proc. ODP, Init. Repts.,* 138: College Station, TX (Ocean Drilling Program). **doi:10.2973/odp.proc.ir.138.1992**

Mazzullo, J.M., Meyer, A., and Kidd, R.B., 1988. New sediment classification scheme for the Ocean Drilling Program. *In* Mazzullo, J.M., and Graham, A.G. (Eds.), *Handbook for shipboard sedimentologists*. ODP Tech. Note, 8:45–67. **doi:10.2973/odp.tn.8.1988**

Miller, K.G., and Katz, M.E., 1987. Oligocene to Miocene benthic foraminiferal and abyssal circulation changes in

the North Atlantic. *Micropaleontology,* 33(2):97–149. doi:10.2307/1485489

Mix, A.C., Tiedemann, R., Blum, P., et al., 2003. *Proc. ODP, Init. Repts.,* 202: College Station, TX (Ocean Drilling Program). doi:10.2973/odp.proc.ir.202.2003

Moore, T.C., Jr., 1995. Radiolarian stratigraphy, Leg 138. *In* Pisias, N.G., Mayer, L.A., Janecek, T.R., Palmer-Julson, A., and van Andel, T.H. (Eds.), *Proc. ODP, Sci. Results,* 138: College Station, TX (Ocean Drilling Program), 191–232. doi:10.2973/odp.proc.sr.138.111.1995

Moran, K., 1997. Elastic property corrections applied to Leg 154 sediment, Ceara Rise. *In* Shackleton, N.J., Curry, W.B., Richter, C., and Bralower, T.J. (Eds.), *Proc. ODP, Sci. Results,* 154: College Station, TX (Ocean Drilling Program), 151–155. doi:10.2973/odp.proc.sr.154.132.1997

Munsell Color Company, Inc., 1994. *Munsell Soil Color Chart* (Revised ed.): Newburgh, MD (Munsell Color).

Murray, R.W., Miller, D.J., and Kryc, K.A., 2000. Analysis of major and trace elements in rocks, sediments, and interstitial waters by inductively coupled plasma–atomic emission spectrometry (ICP-AES). *ODP Tech. Note,* 29. doi:10.2973/odp.tn.29.2000

Nigrini, C., and Sanfilippo, A., 2001. Cenozoic radiolarian stratigraphy for low and middle latitudes with descriptions of biomarkers and stratigraphically useful species. *ODP Tech. Note,* 27. doi:10.2973/odp.tn.27.2001

Nigrini, C., Sanfilippo, A., and Moore, T.C., Jr., 2006. Cenozoic radiolarian biostratigraphy: a magnetobiostratigraphic chronology of Cenozoic sequences from ODP Sites 1218, 1219, and 1220, equatorial Pacific. *In* Wilson, P.A., Lyle, M., and Firth, J.V. (Eds.), *Proc. ODP, Sci. Results,* 199: College Station, TX (Ocean Drilling Program), 1–76. doi:10.2973/odp.proc.sr.199.225.2006

Nomura, R., 1995. Paleogene to Neogene deep-sea paleoceanography in the eastern Indian Ocean: benthic foraminifera from ODP Sites 747, 757, and 758. *Micropaleontology,* 41(3):251–290. doi:10.2307/1485862

Olsson, R.K., Hemleben, C., Berggren, W.A., and Huber, B.T. (Eds.), 1999. *Atlas of Paleocene Planktonic Foraminifera.* Smithson. Contrib. Paleobiol., Vol. 85.

Ortiz, S., and Thomas, E., 2006. Lower-middle Eocene benthic foraminifera from the Fortuna Section (Betic Cordillera, southeastern Spain). *Micropaleonotol.,* 52(2):97–150. doi:10.2113/gsmicropal.52.2.97

Pälike, H., Moore, T., Backman, J., Raffi, I., Lanci, L., Parés, J.M., and Janecek, T., 2005. Integrated stratigraphic correlation and improved composite depth scales for ODP Sites 1218 and 1219. *In* Wilson, P.A., Lyle, M., and Firth, J.V. (Eds.), *Proc. ODP, Sci. Results,* 199: College Station, TX (Ocean Drilling Program), 1–41. doi:10.2973/odp.proc.sr.199.213.2005

Pälike, H., Frazier, J., and Zachos, J.C., 2006a. Extended orbitally forced palaeoclimatic records from the equatorial Atlantic Ceara Rise. *Quat. Sci. Rev.,* 25(23–24):3138–3149. doi:10.1016/j.quascirev.2006.02.011

Pälike, H., Norris, R.D., Herrle, J.O., Wilson, P.A., Coxall, H.K., Lear, C.H., Shackleton, N.J., Tripati, A.K., and Wade, B.S., 2006b. The heartbeat of the Oligocene climate system. *Science,* 314(5807):1894–1898. doi:10.1126/science.1133822

Pearson, P.N., 1995. Planktonic foraminifer biostratigraphy and the development of pelagic caps on guyots in the Marshall Islands group. *In* Haggerty, J.A., Premoli Silva, I., Rack, F., and McNutt, M.K. (Eds.), *Proc. ODP, Sci. Results,* 144: College Station, TX (Ocean Drilling Program), 21–59. doi:10.2973/odp.proc.sr.144.013.1995

Pearson, P.N., and Chaisson, W.P., 1997. Late Paleocene to middle Miocene planktonic foraminifer biostratigraphy of the Ceara Rise. *In* Shackleton, N.J., Curry, W.B., Richter, C., and Bralower, T.J. (Eds.), *Proc. ODP, Sci. Results,* 154: College Station, TX (Ocean Drilling Program), 33–68. doi:10.2973/odp.proc.sr.154.106.1997

Pearson, P.N., Olsson, R.K., Huber, B.T., Hemleben, C., and Berggren, W.A. (Eds.), 2006. *Atlas of Eocene Planktonic Foraminifera.* Spec. Publ.—Cushman Found., 41.

Perch-Nielsen, K., 1985. Cenozoic calcareous nannofossils. *In* Bolli, H.M., Saunders, J.B., and Perch-Nielsen, K. (Eds.), *Plankton Stratigraphy:* Cambridge (Cambridge Univ. Press), 427–554.

Pisias, N.G., Mayer, L.A., Janecek, T.R., Palmer-Julson, A., and van Andel, T.H. (Eds.), 1995. *Proc. ODP, Sci Results,* 138: College Station, TX (Ocean Drilling Program). doi:10.2973/odp.proc.sr.138.1995

Pribnow, D.F.C., Kinoshita, M., and Stein, C.A., 2000. *Thermal Data Collection and Heat Flow Recalculations for ODP Legs 101–180:* Hanover, Germany (Inst. Joint Geosci. Res., Inst. Geowiss. Gemeinschaftsauf. [GGA]). http://www-odp.tamu.edu/publications/heatflow/ODPReprt.pdf

Quintin, L.L., Faul, K.L., Lear, C., Graham, D., Peng, C., Murray, R.W., and Shipboard Scientific Party, 2002. Geochemical analysis of bulk marine sediment by inductively coupled plasma–atomic emission spectroscopy on board the *JOIDES Resolution. In* Lyle, M., Wilson, P.A., Janecek, T.R., et al., *Proc. ODP, Init. Repts.,* 199: College Station, TX (Ocean Drilling Program), 1–14. doi:10.2973/odp.proc.ir.199.107.2002

Richter, C., Acton, G., Endris, C., and Radsted, M., 2007. Handbook for shipboard paleomagnetists. *ODP Tech. Note,* 34. doi:10.2973/odp.tn.34.2007

Rider, M.H., 1996. *The Geological Interpretation of Well Logs* (2nd ed.): Caithness (Whittles Publ.).

Robinson, S., Mrozewski, S., Hussain, T., Masterson, W., Meissner, E., Williams, T., Keogh, W., Myers, G., Bartington, G., and Goldberg, D., 2008. A new borehole magnetic susceptibility tool for high-resolution formation evaluation. *Trans. SPWLA 49th Annu. Log. Symp.*

Ruddiman, W.F., Cameron, D., and Clement, B.M., 1987. Sediment disturbance and correlation of offset holes drilled with the hydraulic piston corer: Leg 94. *In* Ruddiman, W.F., Kidd, R.B., Thomas, E., et al., *Init. Repts. DSDP,* 94: Washington, DC (U.S. Govt. Printing Office), 615–634. doi:10.2973/dsdp.proc.94.111.1987

Salimullah, A.R.M., and Stow, D.A.V., 1992. Application of FMS images in poorly recovered coring intervals: examples from ODP Leg 129. *In* Hurst, A., Griffiths, C.M., and Worthington, P.F. (Eds.), *Geological Application of Wireline Logs II.* Geol. Soc. Spec. Publ., 65:71–86.

Salvador, A. (Ed.), 1994. *International Stratigraphic Guide:* Boulder (Geol. Soc. Am.).

Sanfilippo, A., and Nigrini, C., 1998. Code numbers for Cenozoic low latitude radiolarian biostratigraphic zones and GPTS conversion tables. *Mar. Micropaleontol.,* 33(1–2):109–117. **doi:10.1016/S0377-8398(97)00030-3**

Schlumberger, 1989. *Log Interpretation Principles/Applications:* Houston (Schlumberger Educ. Services), SMP–7017.

Schlumberger, 1994. *IPL Integrated Porosity Lithology:* Houston (Schlumberger Wireline and Testing), SMP-9270.

Serra, O., 1984. *Fundamentals of Well-Log Interpretation* (Vol. 1): *The Acquisition of Logging Data:* Dev. Pet. Sci., 15A: Amsterdam (Elsevier).

Serra, O., 1986. *Fundamentals of Well-Log Interpretation* (Vol. 2): *The Interpretation of Logging Data*. Dev. Pet. Sci., 15B: Amsterdam (Elsevier).

Serra, O., 1989. *Formation MicroScanner Image Interpretation:* Houston (Schlumberger Educ. Services), SMP-7028.

Shackleton, N.J., Berger, A., and Peltier, W.A., 1990. An alternative astronomical calibration of the lower Pleistocene timescale based on ODP Site 677. *Trans. R. Soc. Edinburgh: Earth Sci.,* 81:251–261.

Shackleton, N.J., Crowhurst, S., Hagelberg, T., Pisias, N.G., and Schneider, D.A., 1995. A new late Neogene time scale: application to Leg 138 sites. *In* Pisias, N.G., Mayer, L.A., Janecek, T.R., Palmer-Julson, A., and van Andel, T.H. (Eds.), *Proc. ODP, Sci. Results,* 138: College Station, TX (Ocean Drilling Program), 73–101. **doi:10.2973/odp.proc.sr.138.106.1995**

Shackleton, N.J., Crowhurst, S.J., Weedon, G.P., and Laskar, J., 1999. Astronomical calibration of Oligocene–Miocene time. *In* Shackleton N.J., McCave, I.N., and Graham, P.W. (Eds.), *Astronomical (Milankovitch) Calibration of the Geological Time-Scale*. Philos. Trans. R. Soc., Ser. A., 357(1757):1907–1929.

Shackleton, N.J., Hall, M.A., Raffi, I., Tauxe, L., and Zachos, J., 2000. Astronomical calibration age for the Oligocene–Miocene boundary. *Geology,* 28(5):447–450. **doi:10.1130/0091-7613(2000)28<447:ACAFTO>2.0.CO;2**

Shipboard Scientific Party, 2002. Explanatory notes. *In* Lyle, M., Wilson, P.A., Janecek, T.R., et al., *Proc. ODP, Init. Repts.,* 199: College Station, TX (Ocean Drilling Program), 1–70. **doi:10.2973/odp.proc.ir.199.102.2002**

Shipboard Scientific Party, 2002b. Leg 199 summary. *In* Lyle, M., Wilson, P.A., Janecek, T.R., et al., *Proc. ODP, Init. Repts.,* 199: College Station, TX (Ocean Drilling Program), 1–87. **doi:10.2973/odp.proc.ir.199.101.2002**

Spezzaferri, S., 1994. Planktonic foraminiferal biostratigraphy and taxonomy of the Oligocene and lower Miocene in the oceanic record: an overview. *Palaeontographica Ital.,* 81:1–187.

Spezzaferri, S., and Premoli Silva, I., 1991. Oligocene planktonic foraminiferal biostratigraphy and paleoclimatic interpretation from Hole 538A, DSDP Leg 77, Gulf of Mexico. *Palaeogeogr., Palaeoclimatol., Palaeoecol.,* 83(1–3):217–263. **doi:10.1016/0031-0182(91)90080-B**

Srinivasan, M.S., and Sinha, D.K., 1992. Late Neogene planktonic foraminiferal events of the southwest Pacific and Indian Ocean: a comparison. *In* Tsuchi, R., and Ingle, J.C., Jr. (Eds.), *Pacific Neogene: Environment, Evolution and Events:* Tokyo (Univ. Tokyo Press), 203–220.

Thomas, E., 1990. Late Cretaceous through Neogene deep-sea benthic foraminifers (Maud Rise, Weddell Sea, Antarctica). *In* Barker, P.F., Kennett, J.P., et al., *Proc. ODP, Sci. Results,* 113: College Station, TX (Ocean Drilling Program), 571–594. **doi:10.2973/odp.proc.sr.113.123.1990**

Tjalsma, R.C., and Lohmann, G.P., 1983. *Paleocene–Eocene Bathyal and Abyssal Benthic Foraminifera from the Atlantic Ocean.* Micropaleontology, Spec. Publ., 4:1–90.

Toumarkine, M., and Luterbacher, H., 1985. Paleocene and Eocene planktic foraminifera. *In* Bolli, H.M., Saunders, J.B., and Perch-Nielsen, K. (Eds.), *Plankton Stratigraphy:* Cambridge (Cambridge Univ. Press), 87–154.

Turco, E., Bambini, A.M., Foresi, L., Iaccarino, S., Lirer, F., Mazzei, R., and Salvatorini, G., 2002. Middle Miocene high-resolution calcareous plankton biostratigraphy at Site 926 (Leg 154, equatorial Atlantic Ocean): palaeoecological and palaeobiogeographical implications. *Geobios,* 35:257–276. **doi:10.1016/S0016-6995(02)00064-5**

van Morkhoven, F.P.C.M., Berggren, W.A., and Edwards, A.S., 1986. *Cenozoic Cosmopolitan Deep-Water Benthic Foraminifera.* Bull. Cent. Rech. Explor.—Prod. Elf-Aquitaine, Mem. 11.

Villa, G., Fioroni, C., Pea, L., Bohaty, S., and Persico, P., 2008. Middle Eocene–late Oligocene climate variability: calcareous nannofossil response at Kerguelen Plateau, Site 748. *Mar. Micropaleontol.,* 69(2):173–192. **doi:10.1016/j.marmicro.2008.07.006**

Von Herzen, R., and Maxwell, A.E., 1959. The measurement of thermal conductivity of deep-sea sediments by a needle-probe method. *J. Geophys. Res.,* 64(10):1557–1563. **doi:10.1029/JZ064i010p01557**

Wade, B.S., 2004. Planktonic foraminiferal biostratigraphy and mechanisms in the extinction of *Morozovella* in the late middle Eocene. *Mar. Micropaleontol.,* 51(1–2):23–38. **doi:10.1016/j.marmicro.2003.09.001**

Wade, B.S., Berggren, W.A., and Olsson, R.K., 2007. The biostratigraphy and paleobiology of Oligocene planktonic foraminifera from the equatorial Pacific Ocean (ODP Site 1218). *Mar. Micropaleontol.,* 62(3):167–179. **doi:10.1016/j.marmicro.2006.08.005**

Wang, P., Prell, W.L., Blum, P., et al., 2000. *Proc. ODP, Init. Repts.,* 184: College Station, TX (Ocean Drilling Program). **doi:10.2973/odp.proc.ir.184.2000**

Wefer, G., Berger, W.H., and Richter, C., et al., 1998. *Proc. ODP, Init. Repts.,* 175: College Station, TX (Ocean Drilling Program). **doi:10.2973/odp.proc.ir.175.1998**

Wentworth, C.K., 1922. A scale of grade and class terms of clastic sediments. *J. Geol.,* 30:377–392.

Zachos, J.C., Kroon, D., Blum, P., et al., 2004. *Proc. ODP, Init. Repts.,* 208: College Station, TX (Ocean Drilling Program. **doi:10.2973/odp.proc.ir.208.2004**

Publication: 30 October 2010
MS 320321-102

Figure F1. IODP conventions for naming sites, holes, cores, and samples. CC = core catcher.

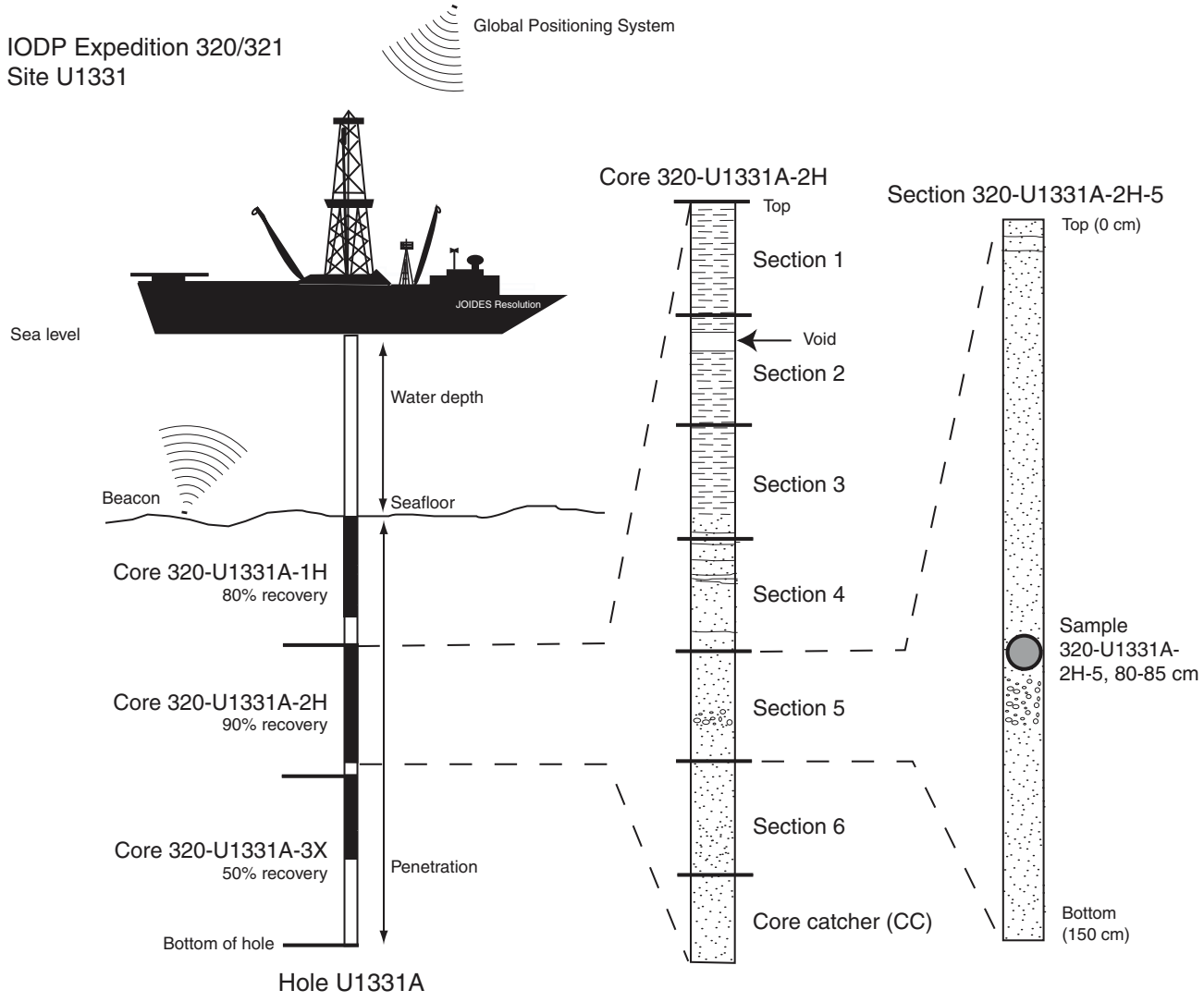

Figure F2. Timescale used for IODP Expedition 320/321 with calcareous nannofossil and planktonic foraminifer zones and datums through the interval 0 to 60 Ma. Underlined species are foraminifers. B = base, T = top, Tc = top common, Bc = base common, Br = base reentrance, X = abundance cross-over in nannofossils or a coiling change in planktonic foraminifer, s.l. = sensu lato. Subgenera within the genus *Globorotalia* (*Gr.*) are shown in parentheses, e.g., *Gr.* (*Truncorotalia*) *tosaensis*. **A.** 0–10 Ma. (**Continued on next three pages.**)

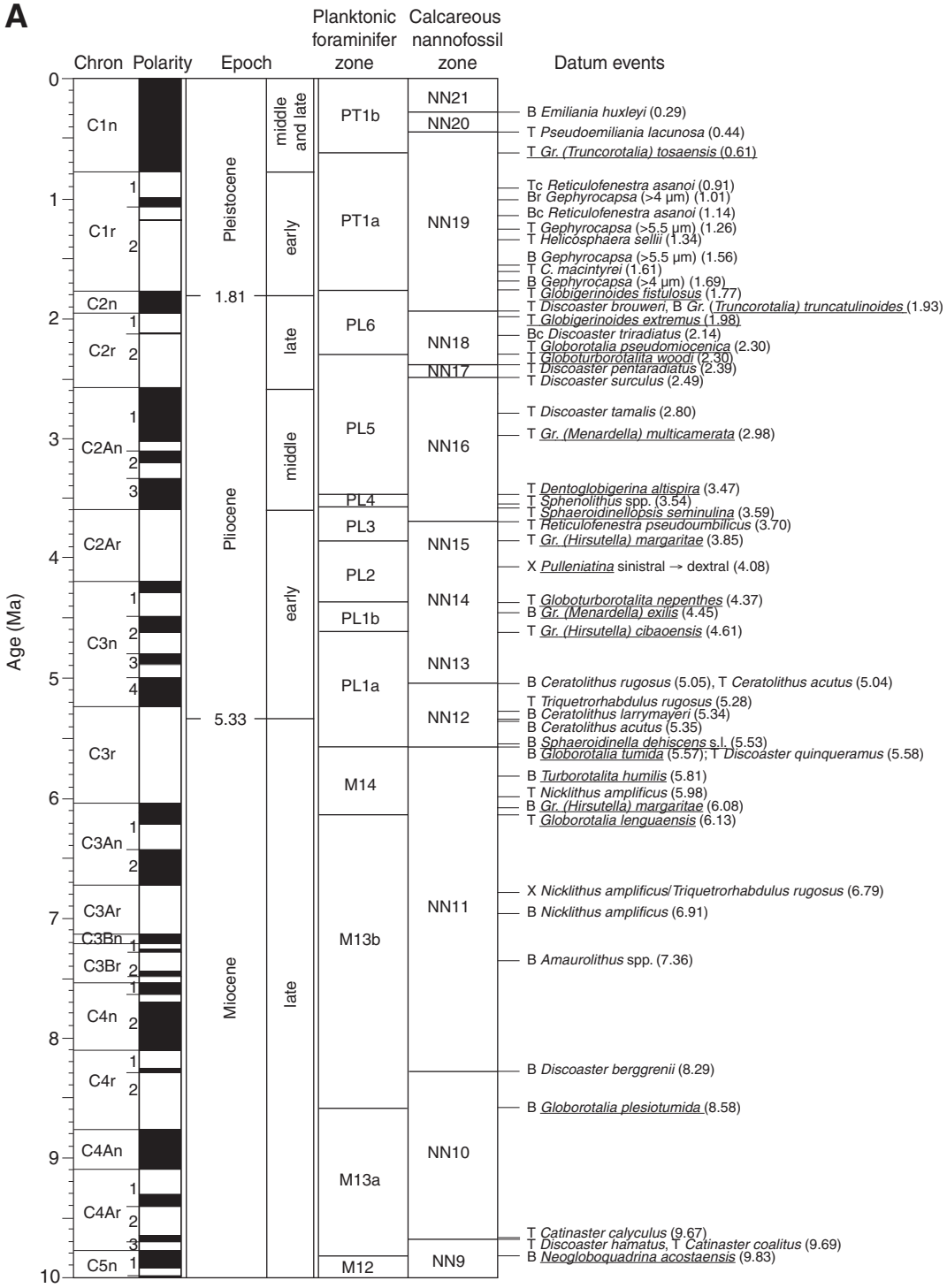

Figure F2 (continued). B. 10–20 Ma. (Continued on next page.)

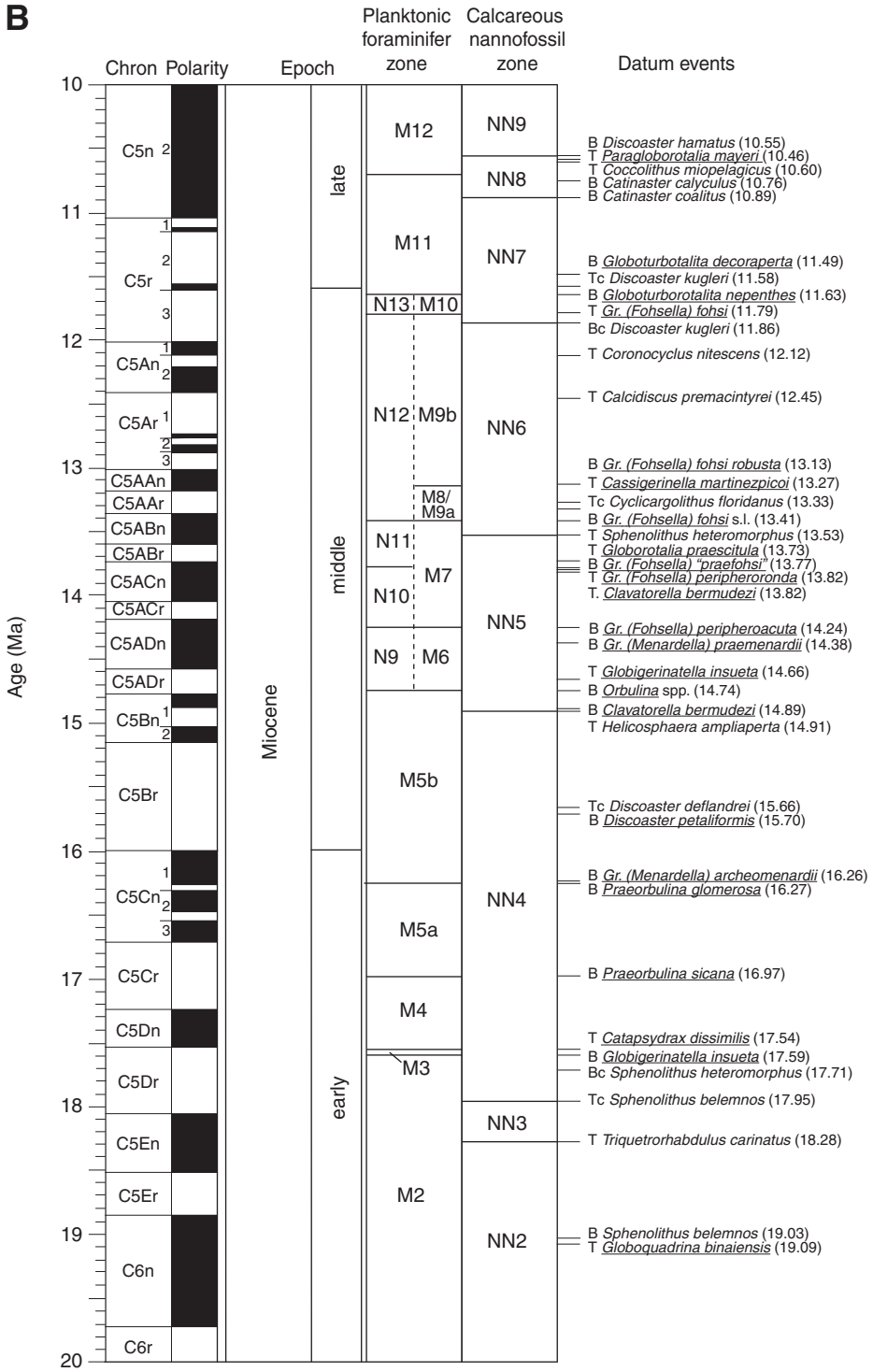

Figure F2 (continued). C. 20–40 Ma. (Continued on next page.)

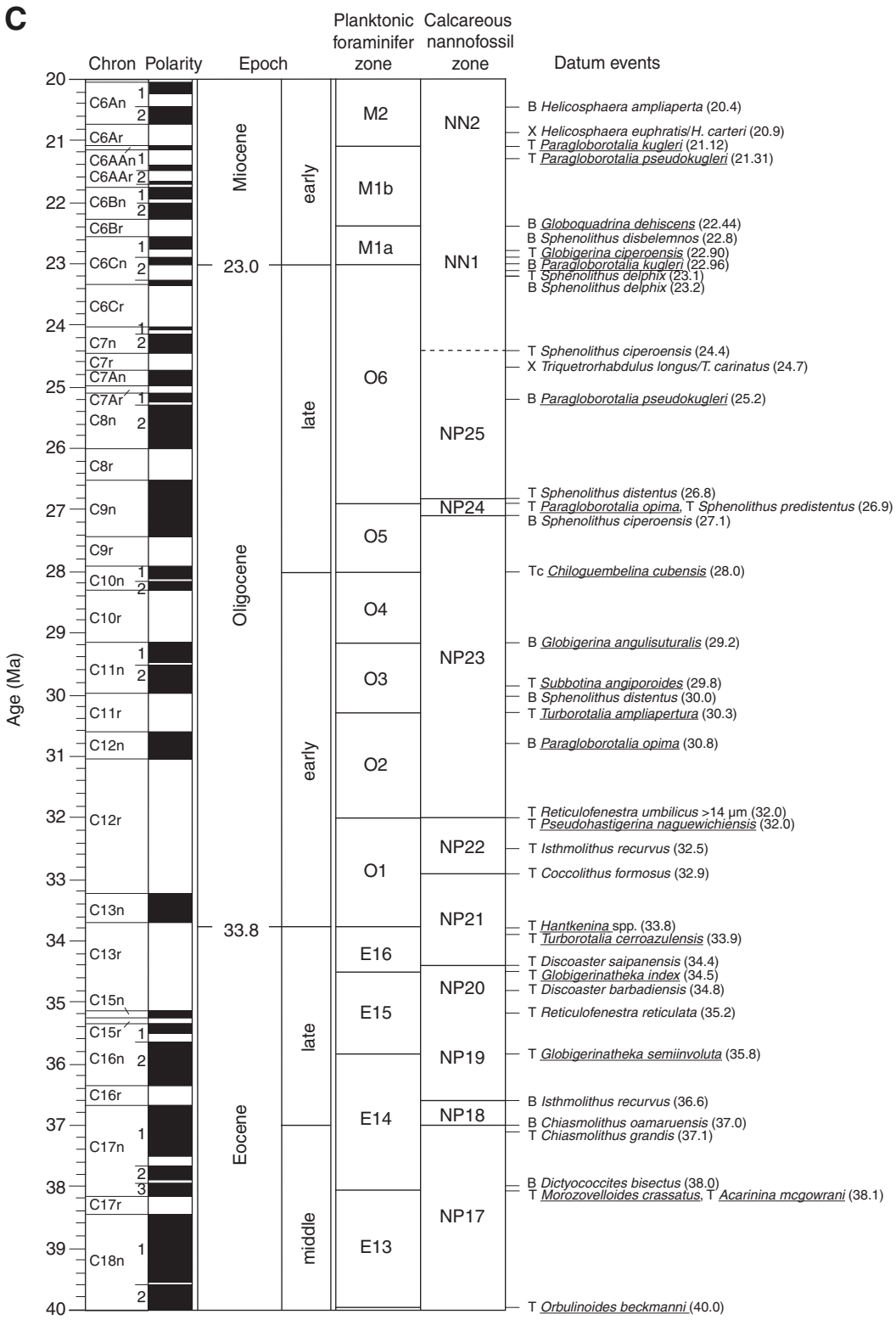

Figure F2 (continued). D. 40–60 Ma.

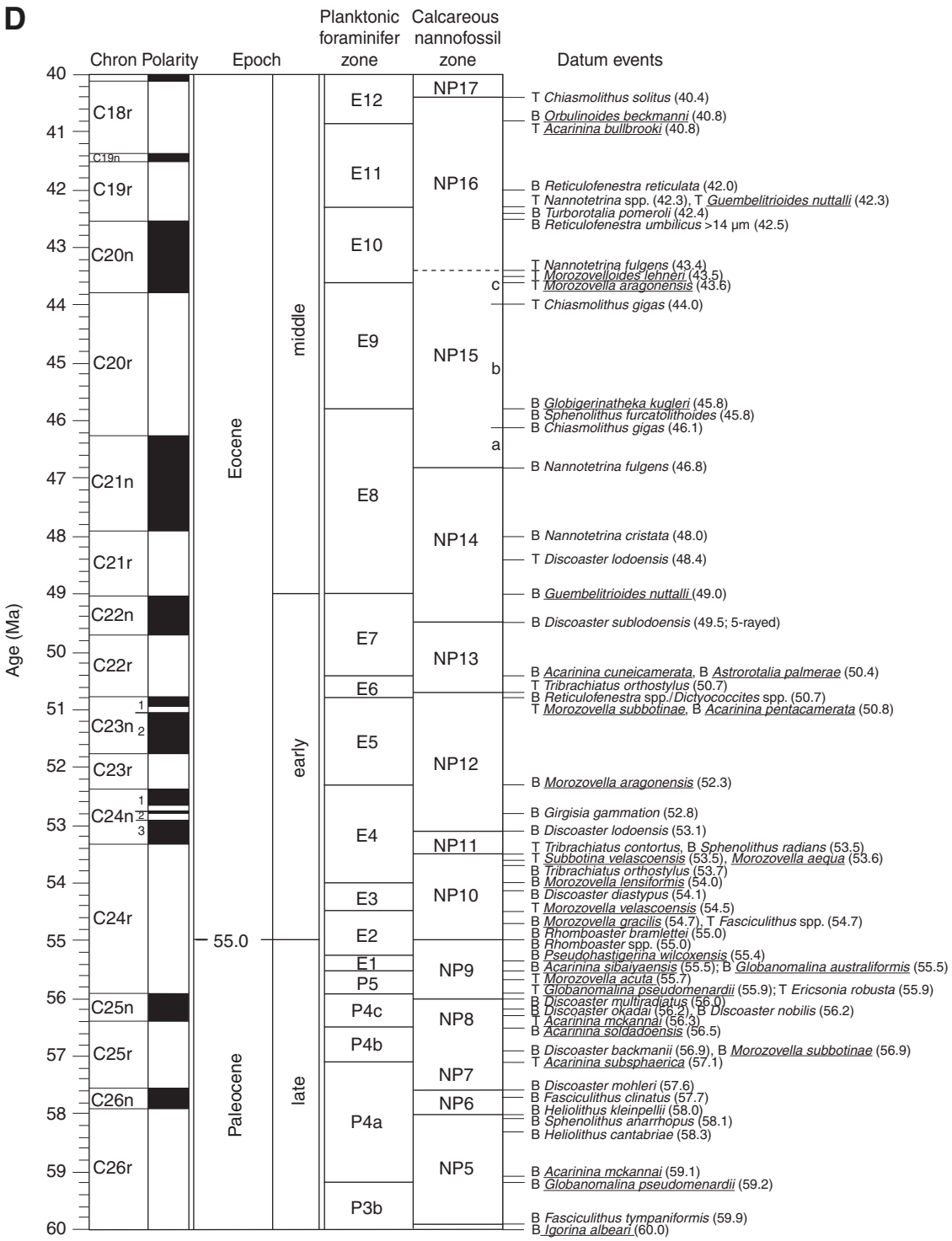

Figure F3. Timescale used for IODP Expedition 320/321 with radiolarian zones and datums through the interval 0 to 60 Ma. Bold face datums define zonal boundaries. B = base, Bc = base common, T = top. **A.** 0–10 Ma. (**Continued on next five pages.**)

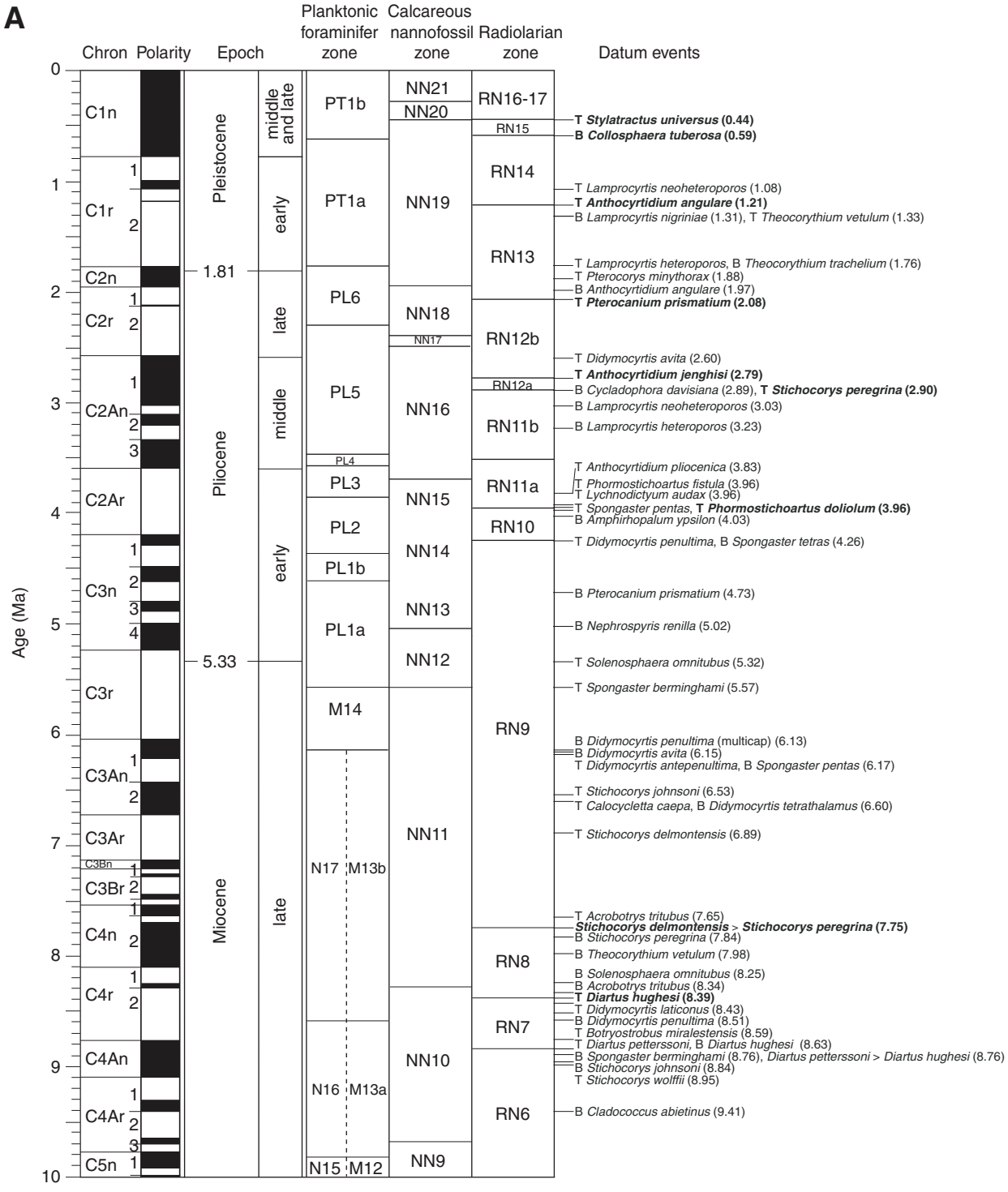

Figure F3 (continued). B. 10–20 Ma. (Continued on next page.)

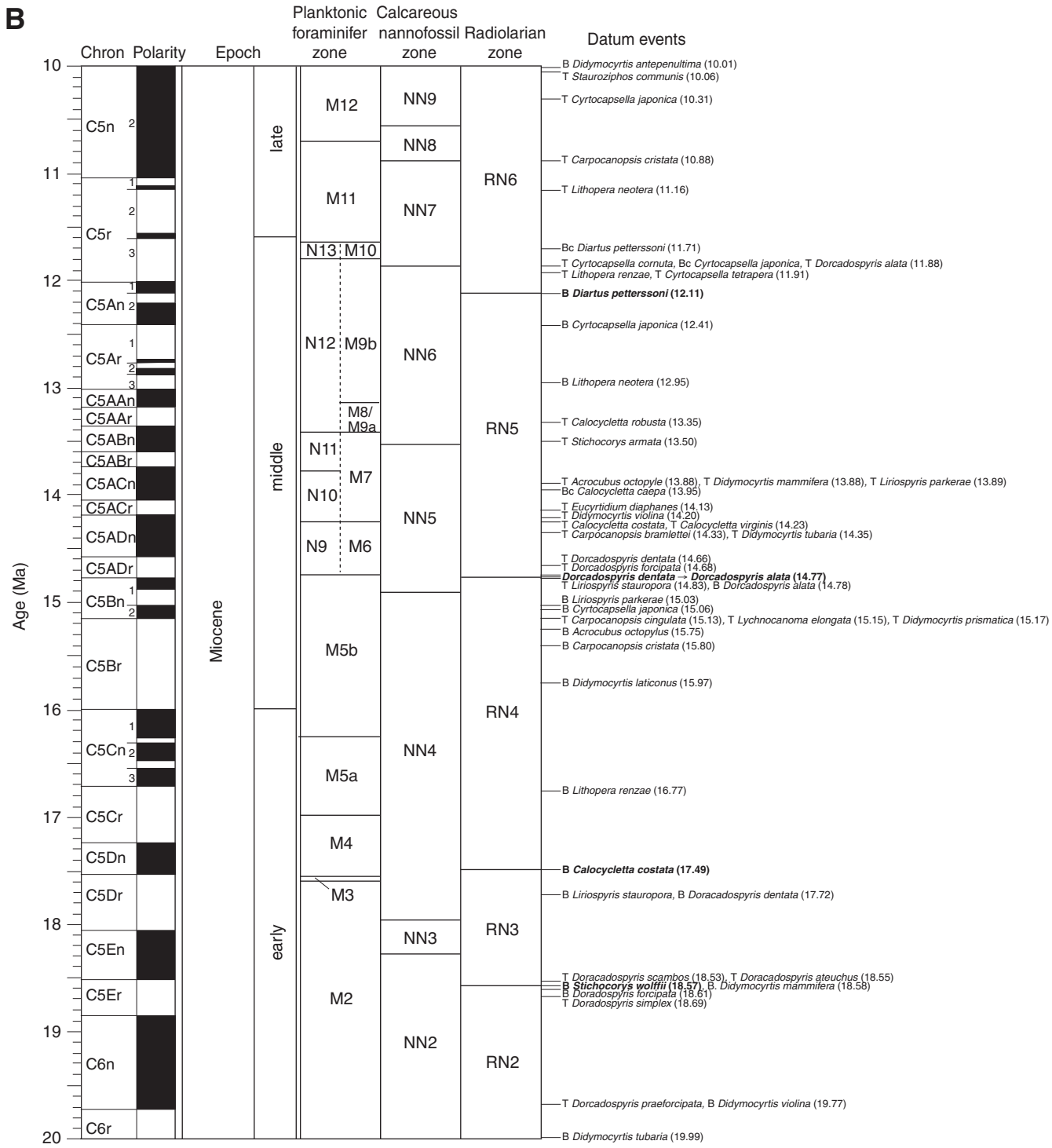

Figure F3 (continued). C. 20–30 Ma. (Continued on next page.)

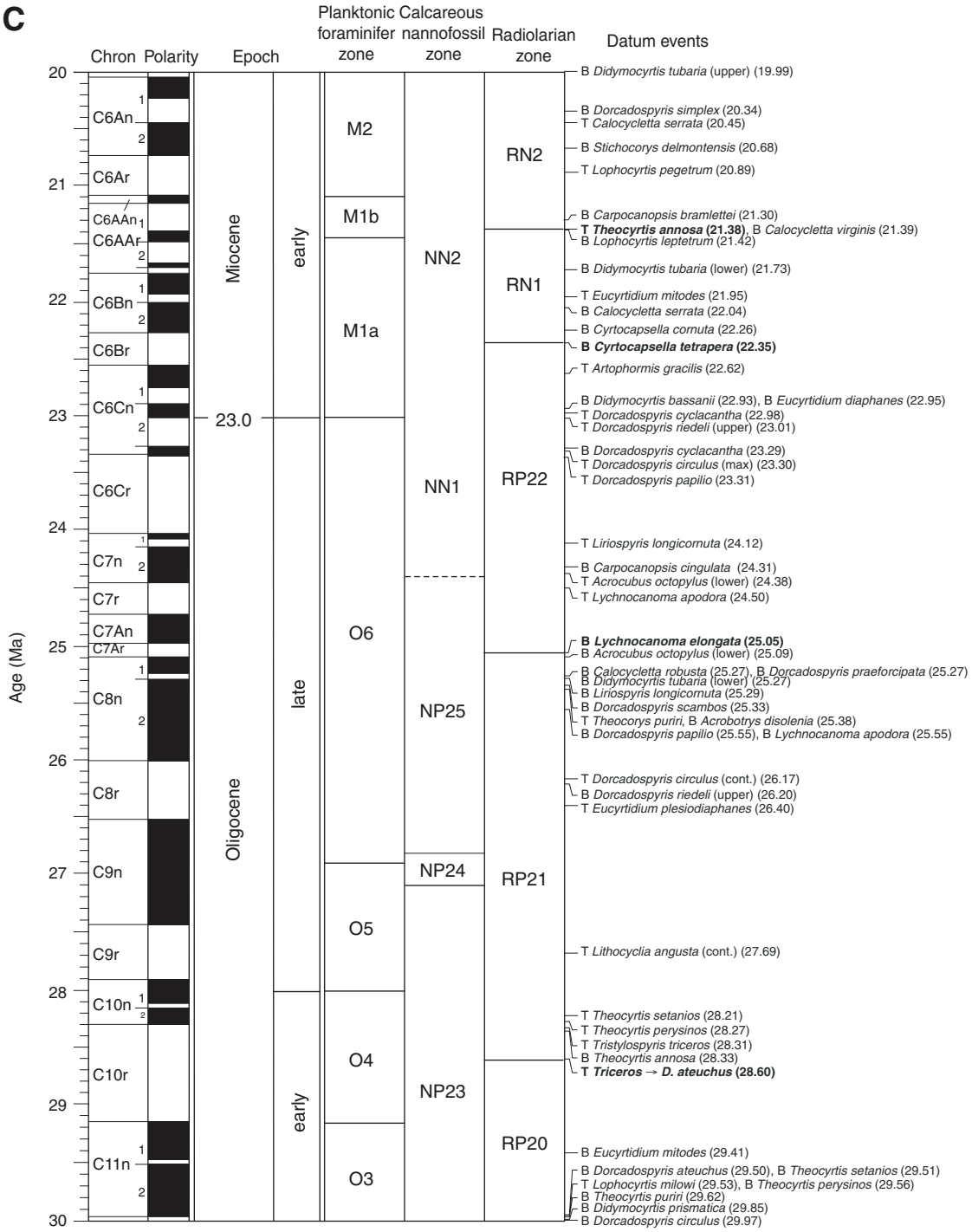

Figure F3 (continued). D. 30–40 Ma. (Continued on next page.)

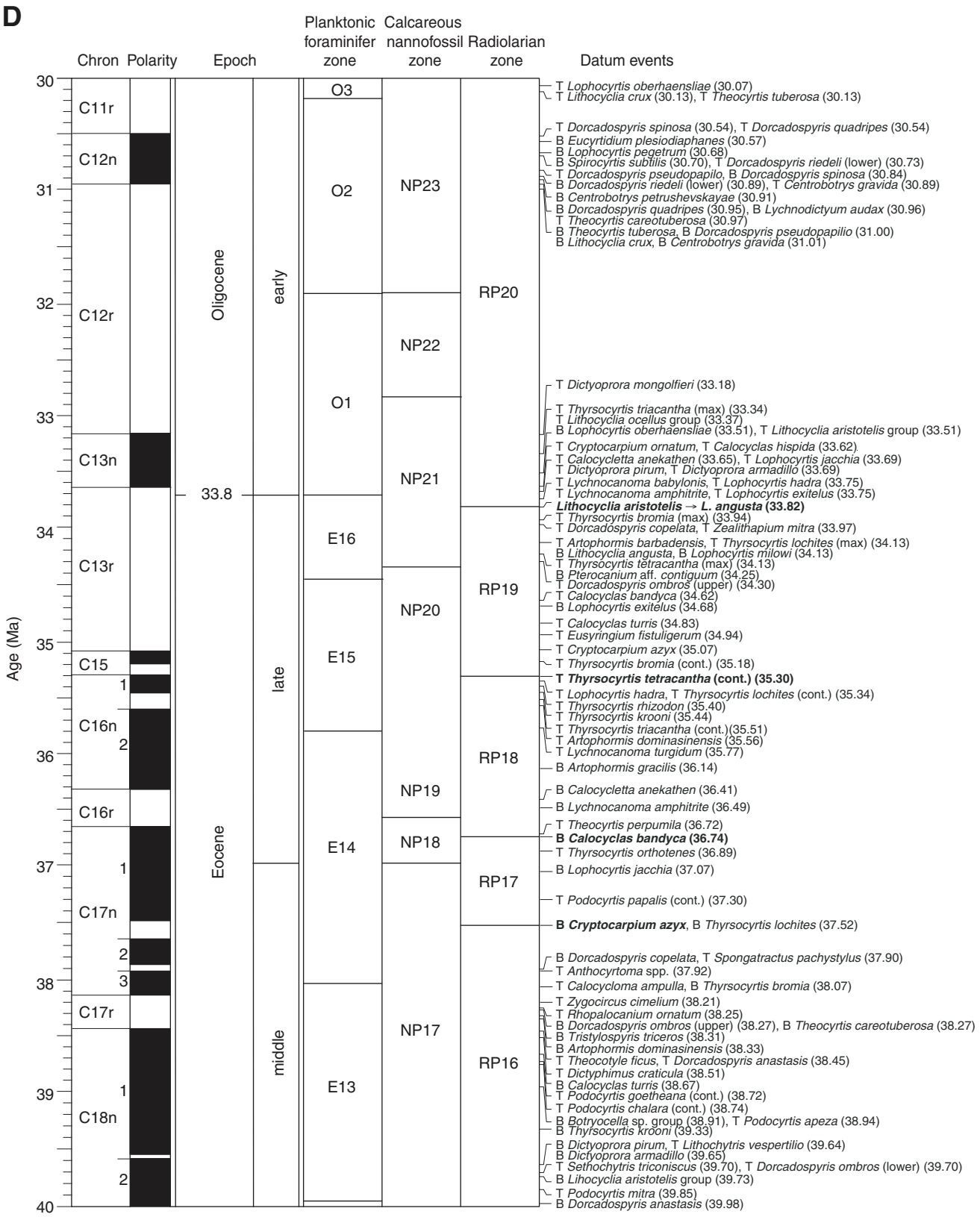

Figure F3 (continued). E. 40–50 Ma. (Continued on next page.)

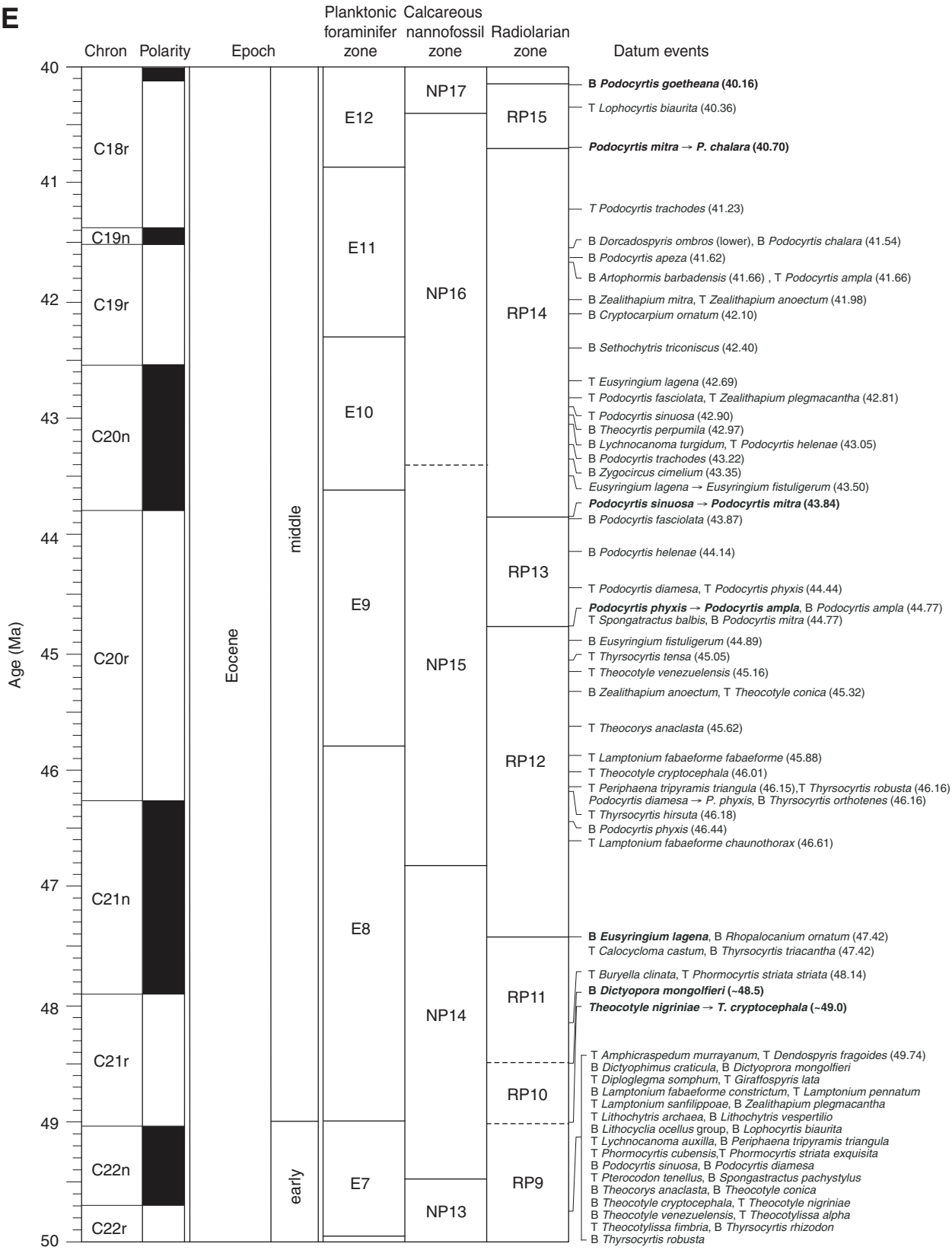

Figure F3 (continued). F. 50–60 Ma.

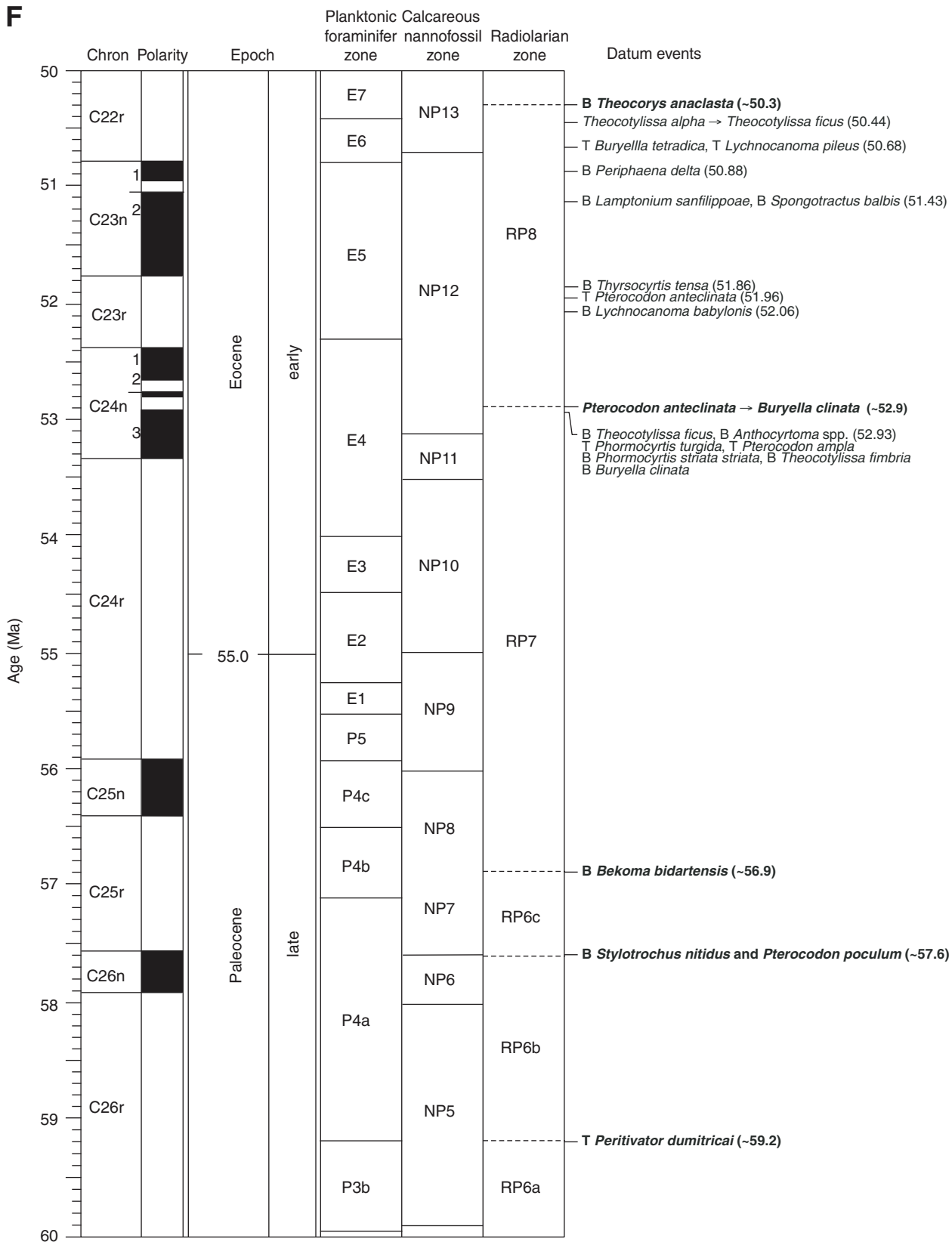

Figure F4. Timescale used for IODP Expedition 320/321 with diatom zones and datums through the interval 0 to 60 Ma. Bold datums define zonal boundaries. B = base, T = top. **A.** 0–10 Ma. (**Continued on next three pages.**)

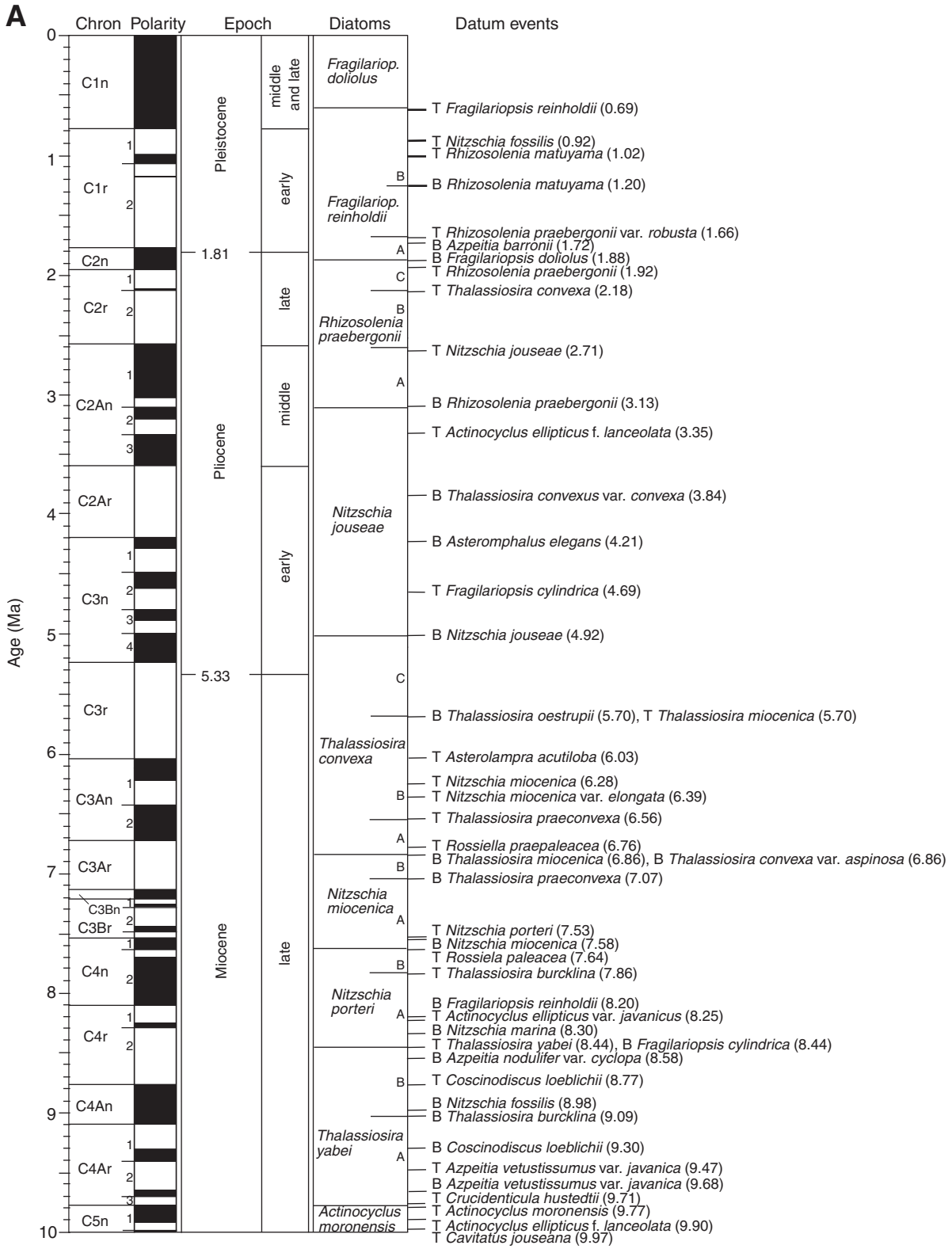

Figure F4 (continued). B. 10–20 Ma. (Continued on next page.)

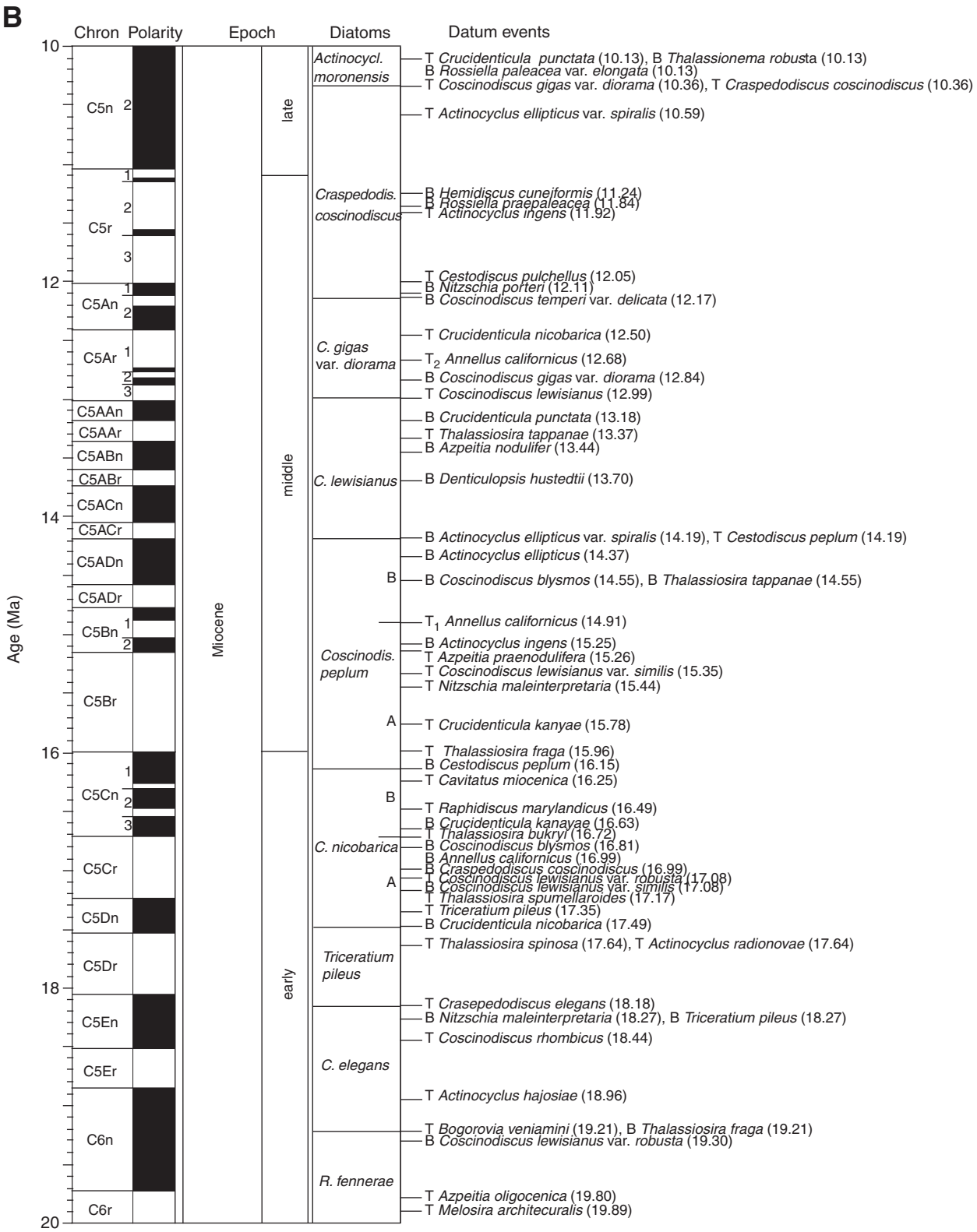

Figure F4 (continued). C. 20–40 Ma. (Continued on next page.)

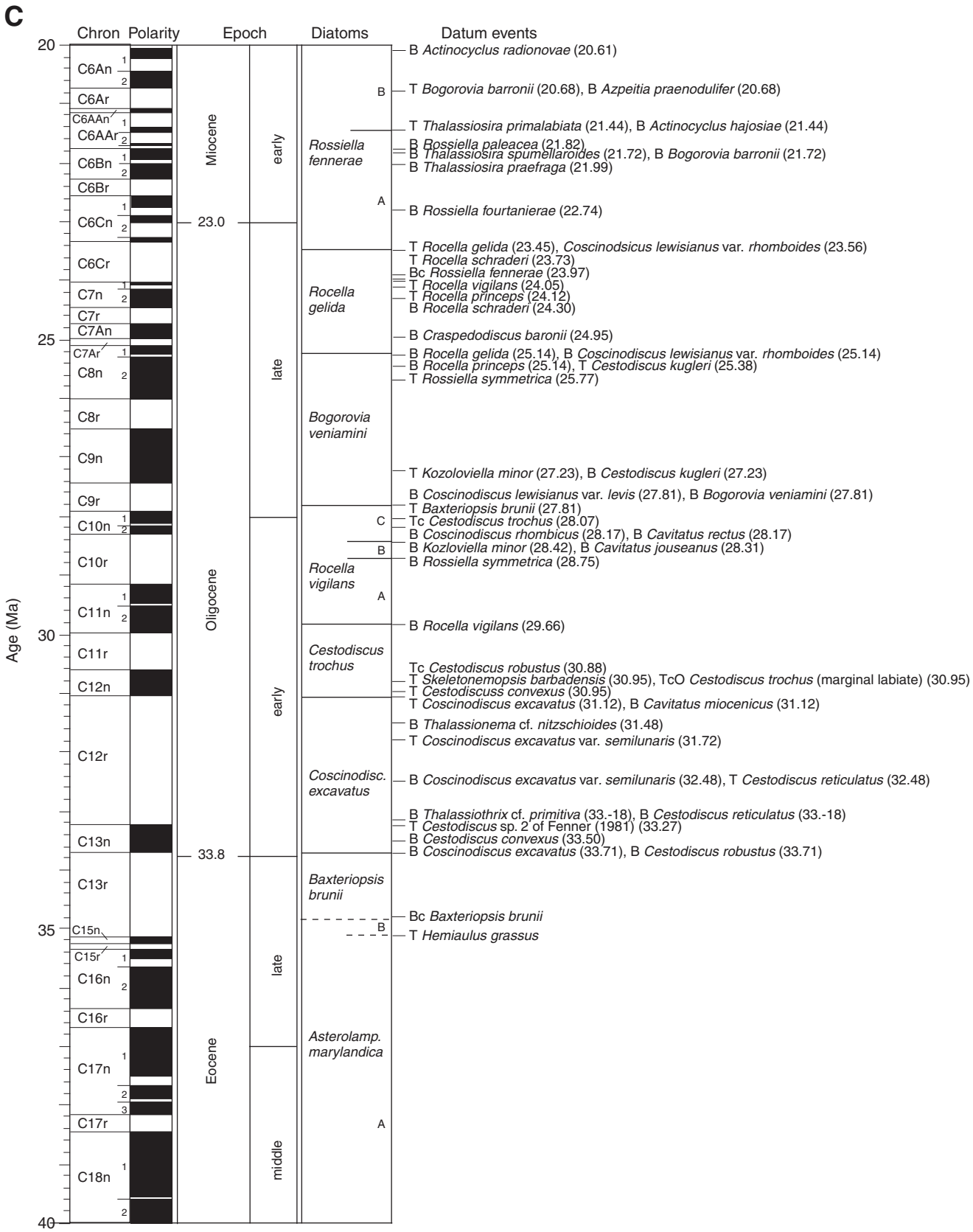

Figure F4 (continued). D. 40–60 Ma.

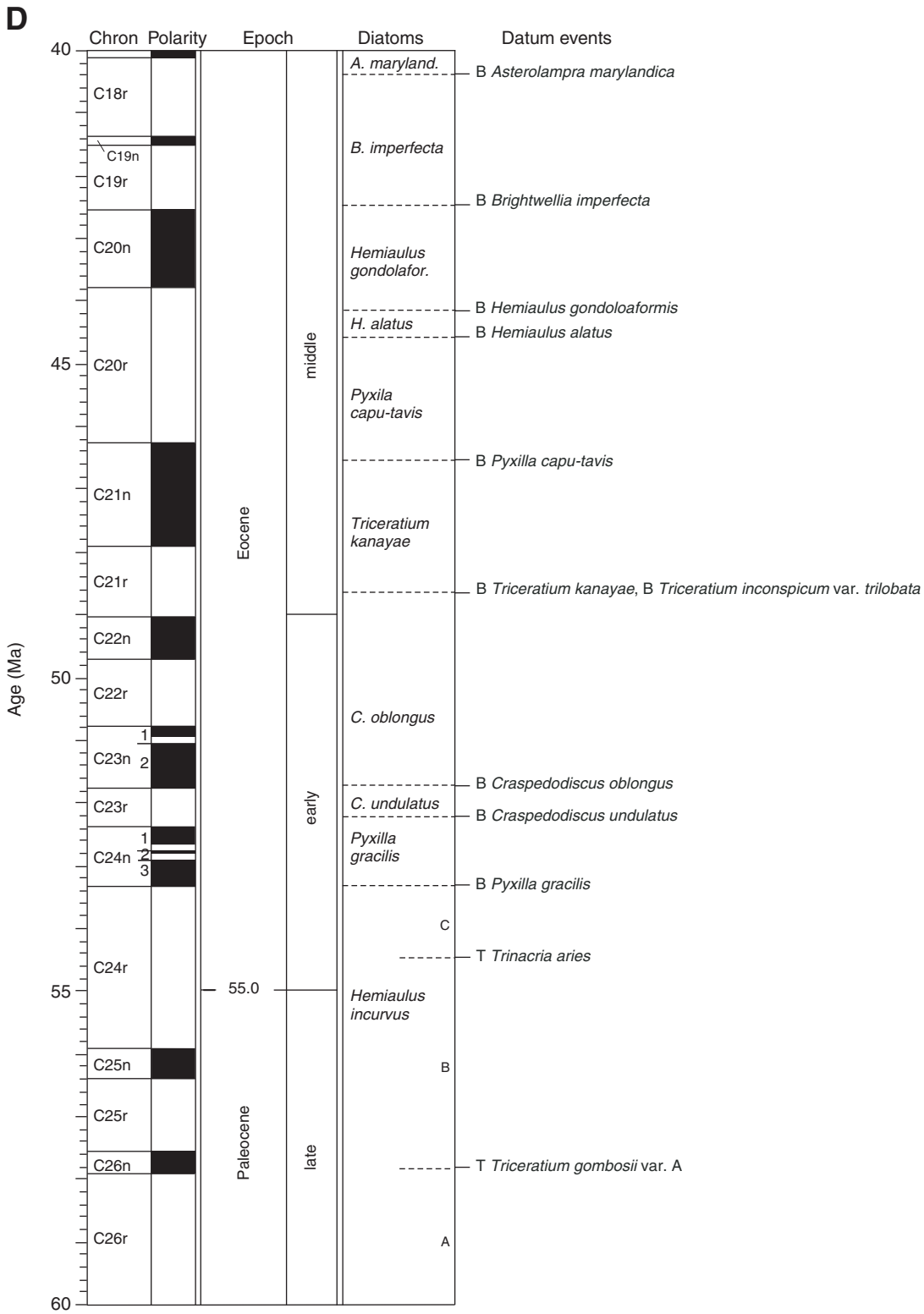

Figure F5. Core description template.

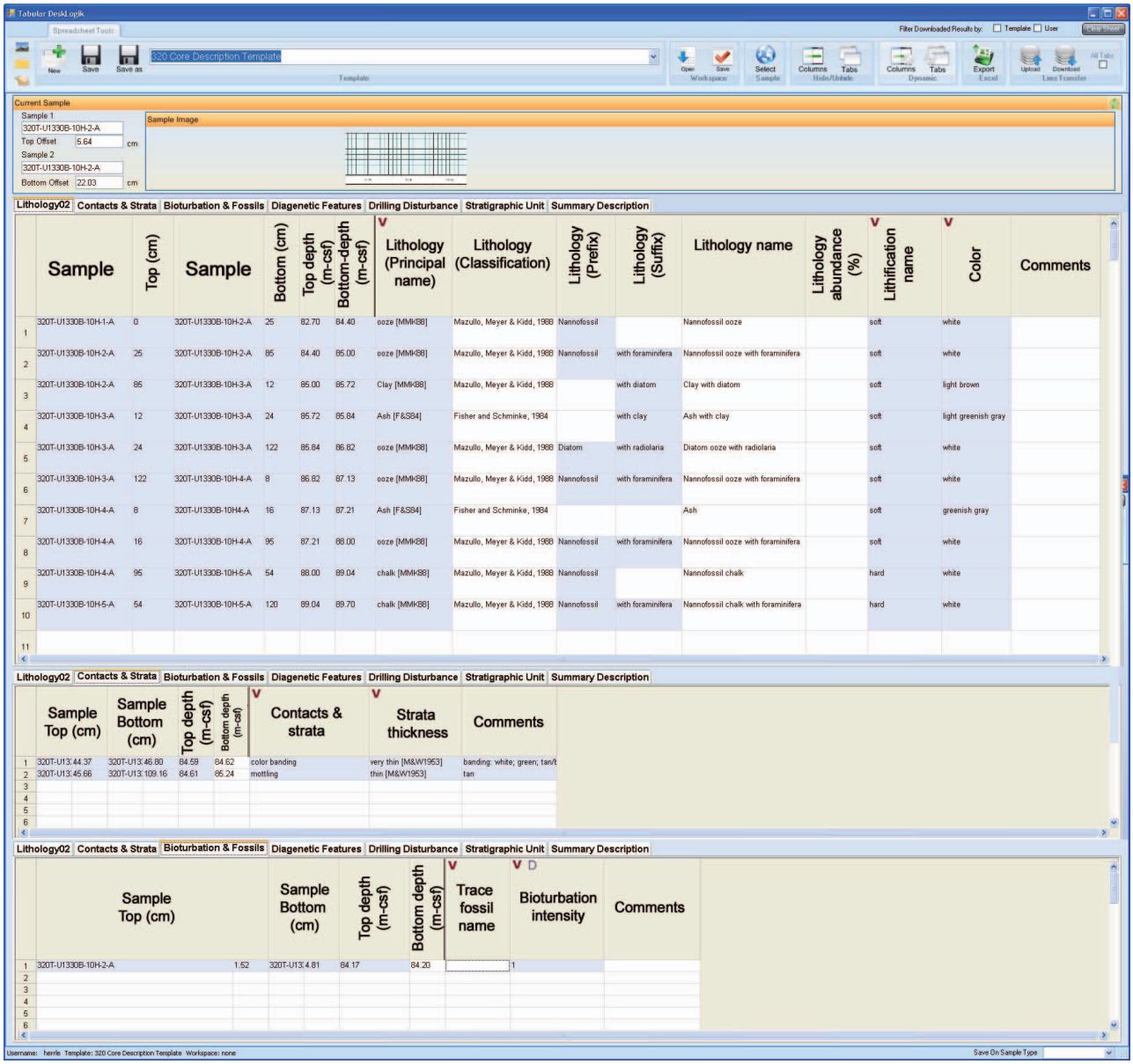

Figure F6. Smear slide template.

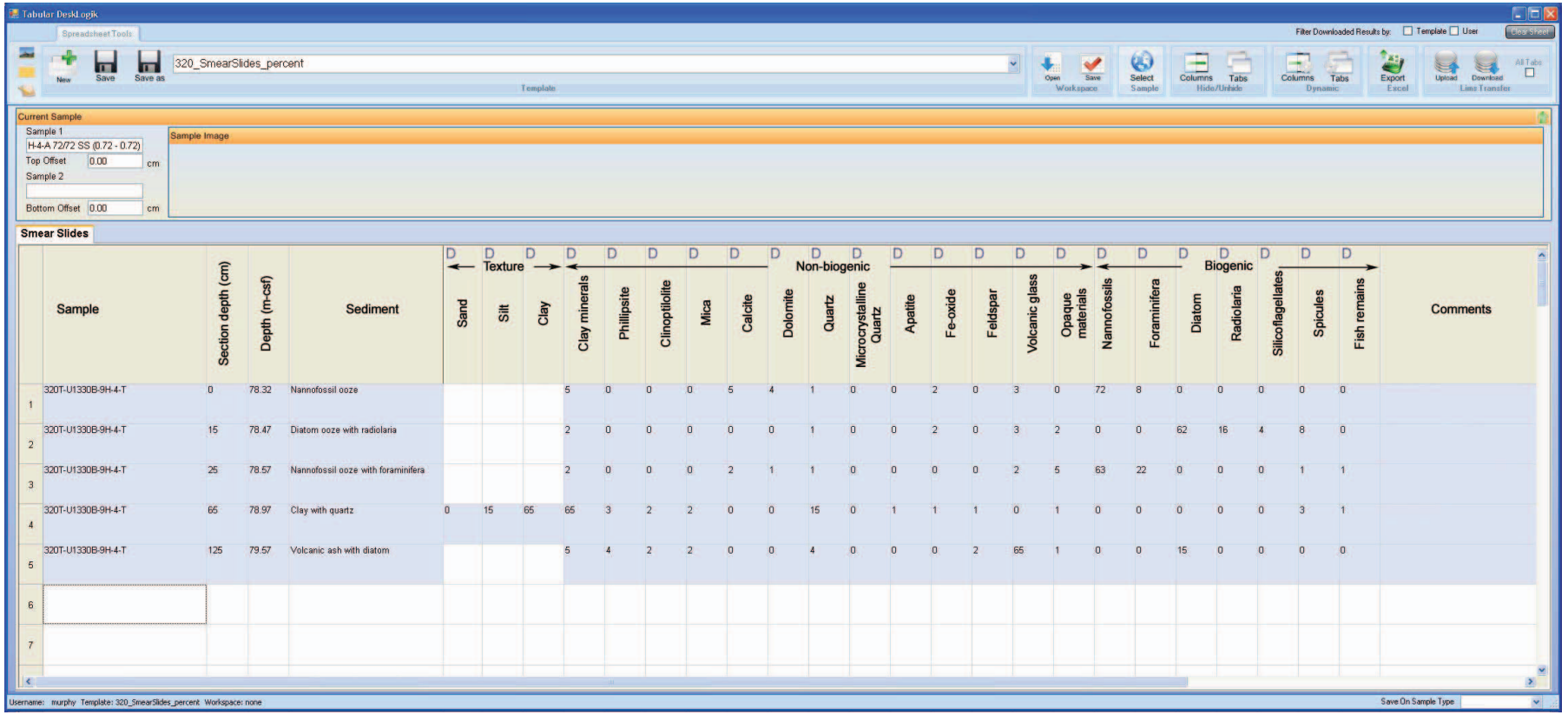

Figure F7. Visual core description example.

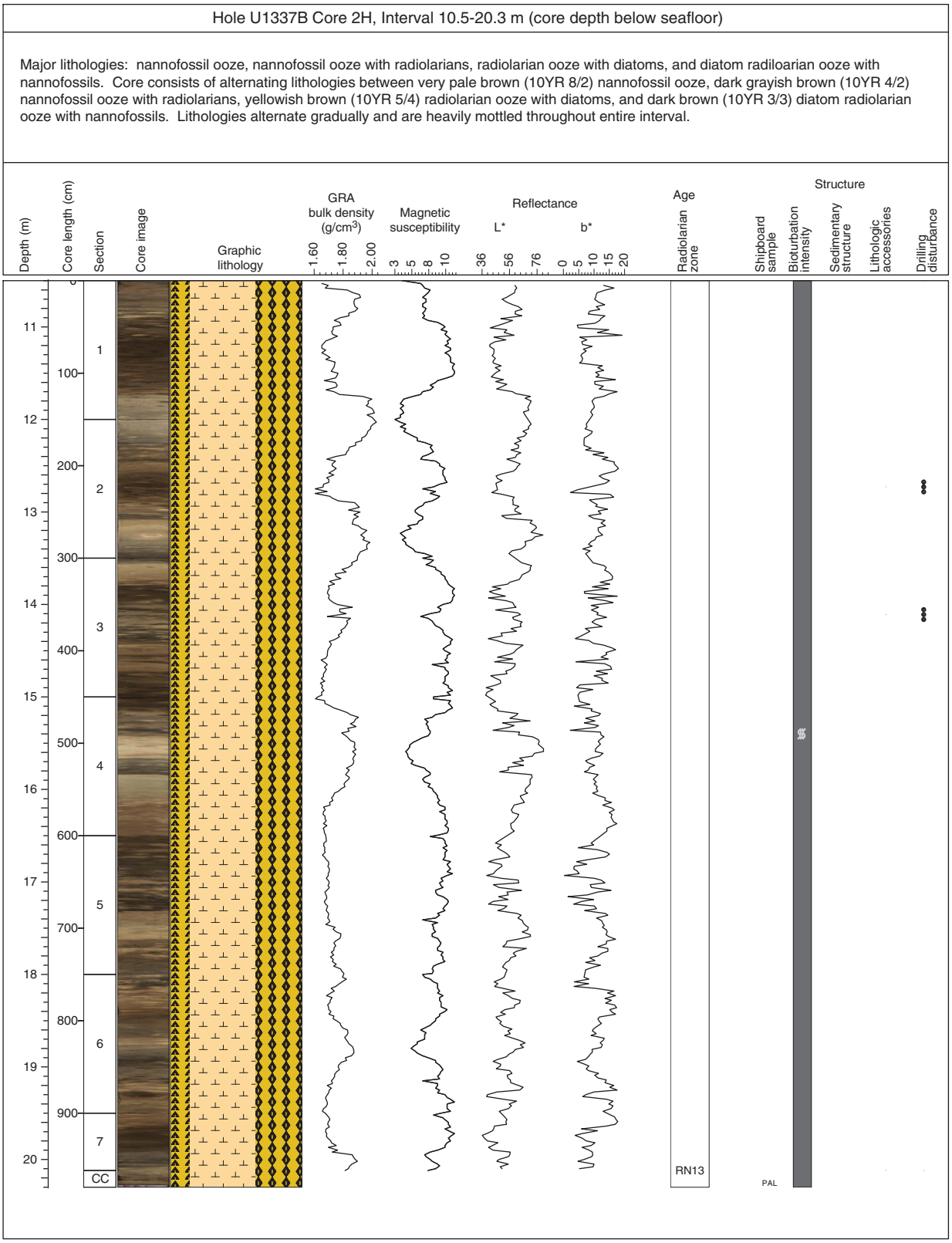

Figure F8. Symbols used on visual core descriptions and lithostratigraphic logs.

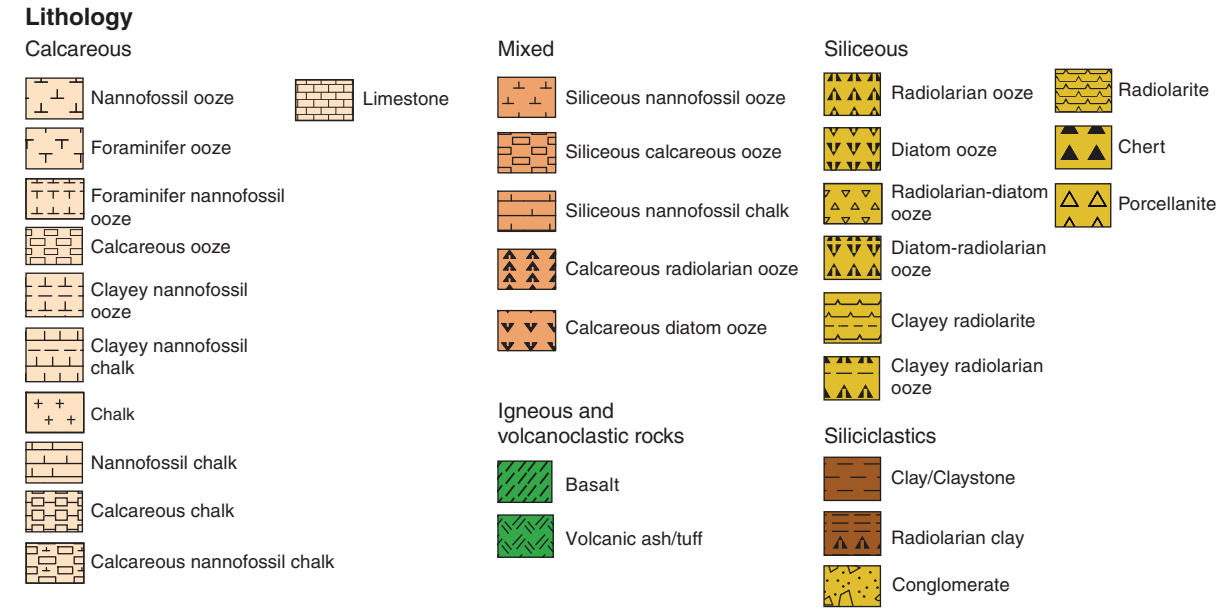

Figure F9. Grain size ternary diagram.

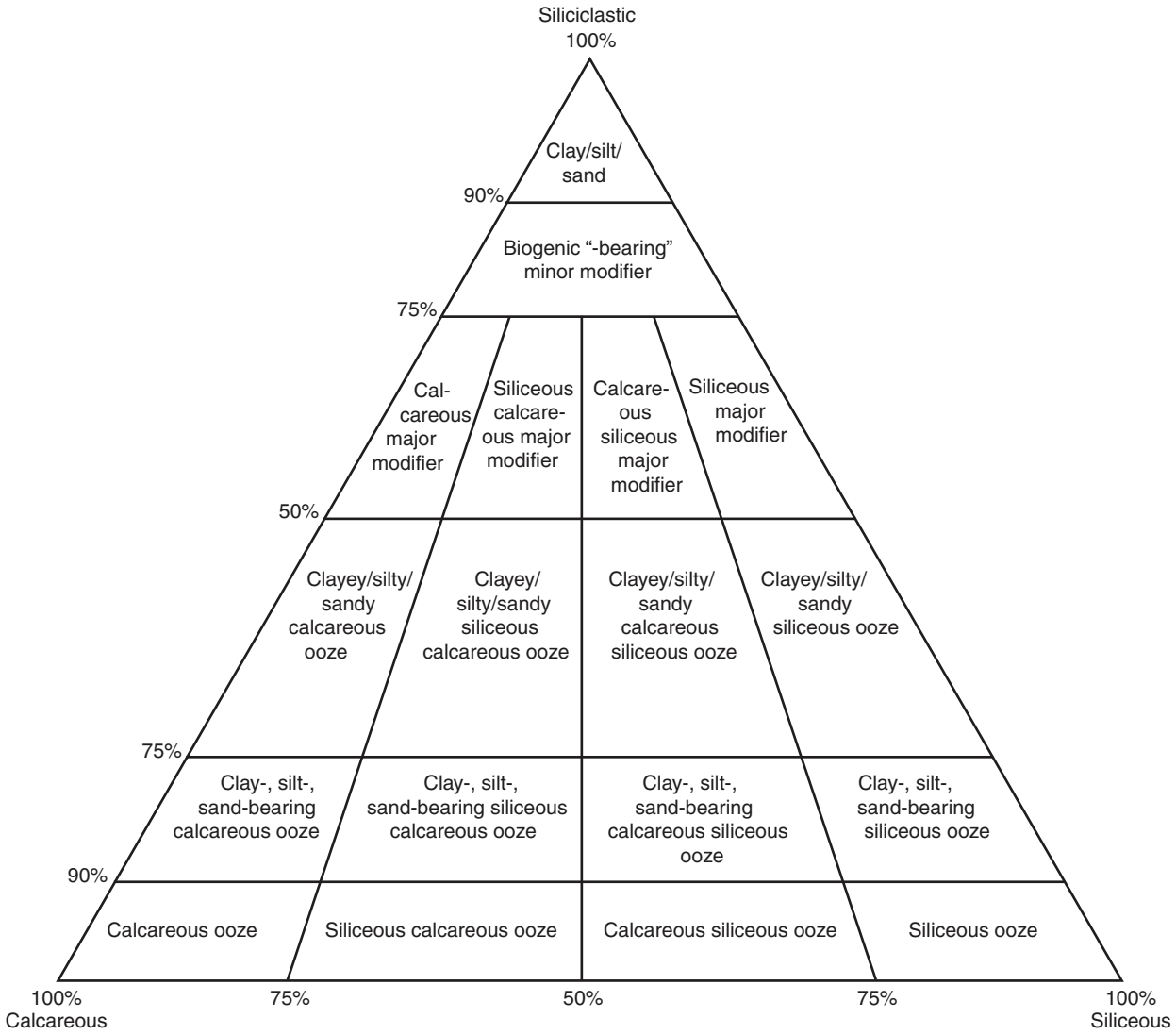

Figure F10. A. Two types of hollow extruders. Discrete paleomagnetic samples were collected by inserting an extruder into soft sediments and then removing it with sediments inside. Excess sediments from the base of the extruder are trimmed with a spatula and the rest of the sediments are extruded into the sample box. **B.** Plastic box with arrow molded into its base used for discrete samples (internal volume = 7 cm^3).

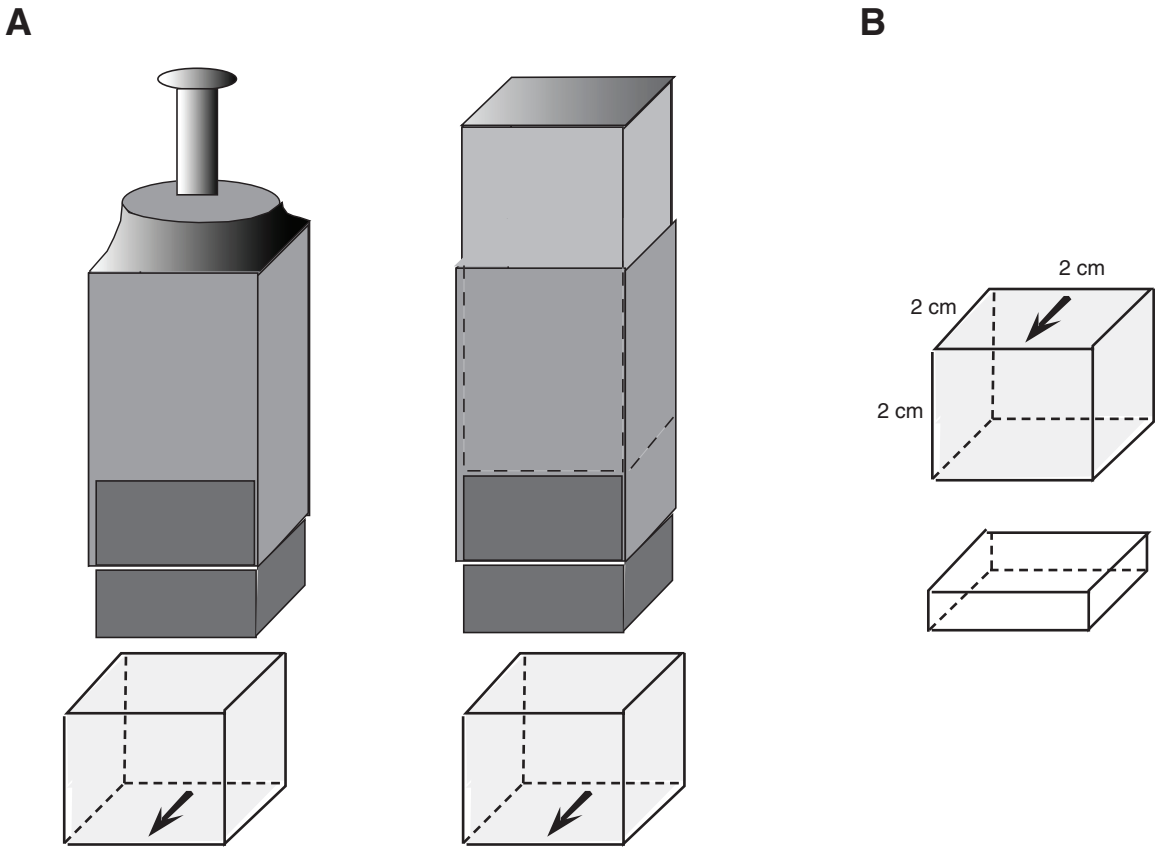

Figure F11. Coordinate systems for archive- and working-half sections and superconducting rock magnetometer.

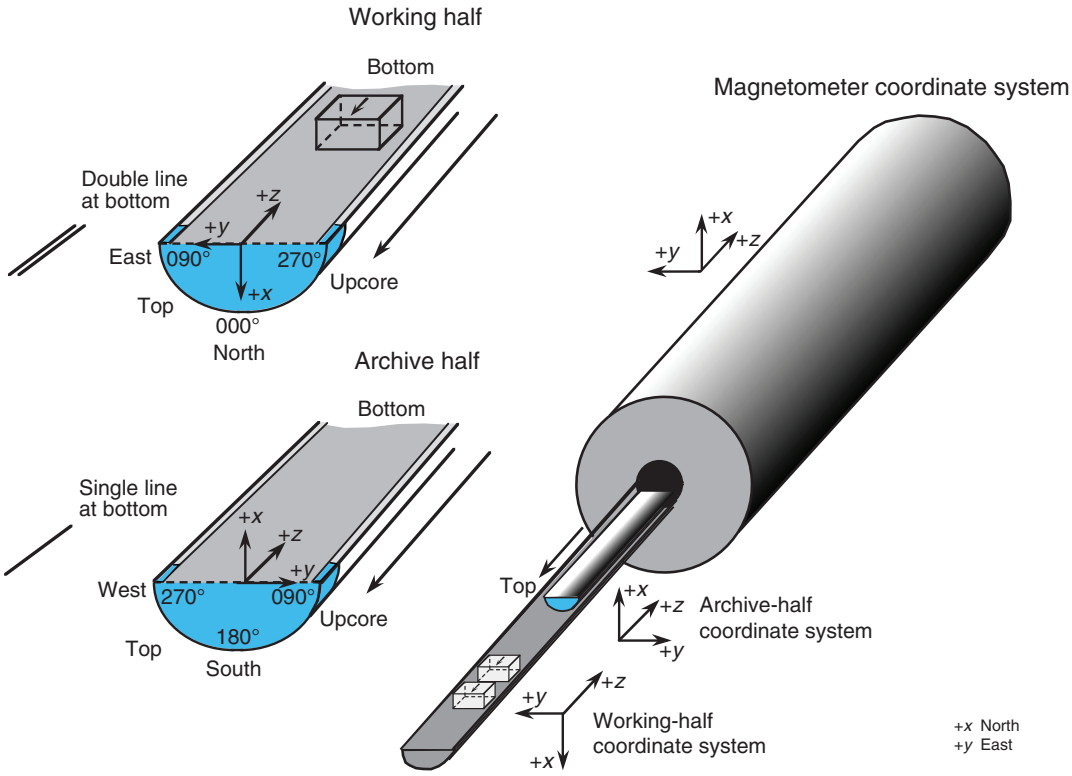

Figure F12. FlexIt tool temperature, total magnetic field, and tool declination data for first tool use, Cores 321-U1331A-1H through 5H. APC = advanced piston corer.

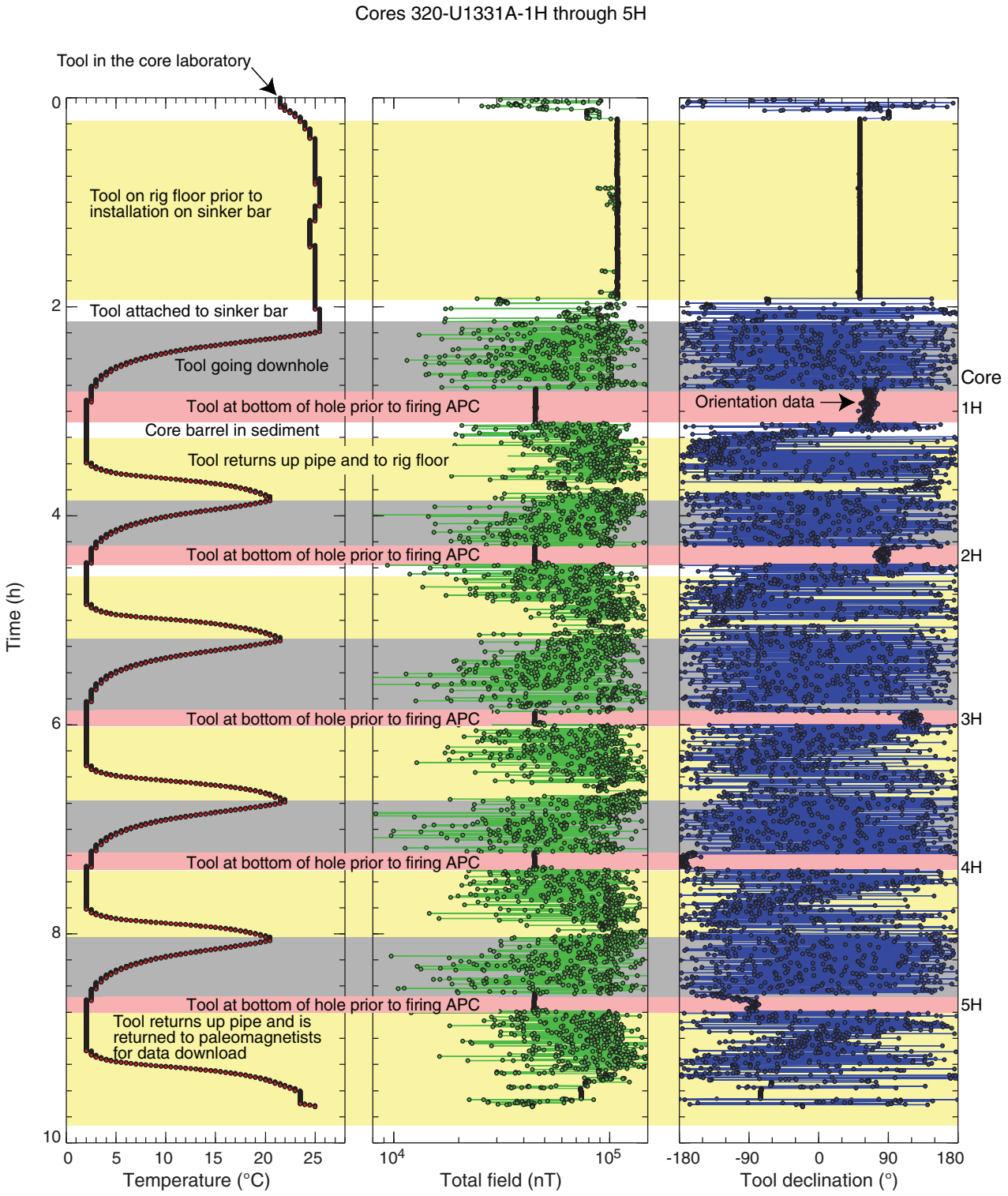

Figure F13. CIELAB color space representing color in terms of three axes, L*, a*, and b* (modified from Hunter Lab, 2008).

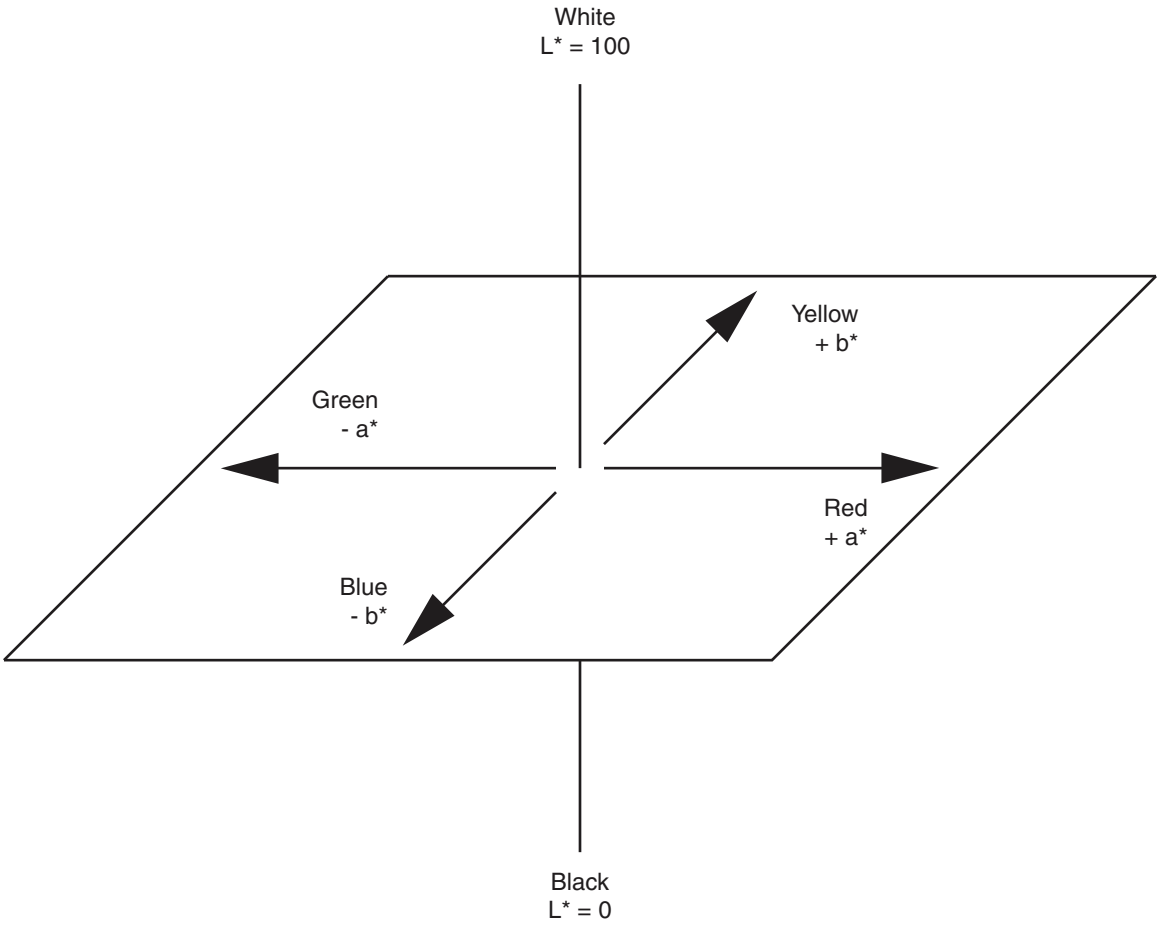

Figure F14. Magnetic susceptibility data, Site U1333. **A.** Core depth below seafloor scale. **B.** Depth-shifted cores on composite depth scale. Magnetic susceptibility data are offset from each other by a constant (300 × 10^{-6} SI) **C.** Spliced section with core breaks (triangles) and hole designations. Red = Hole U1333A, blue = Hole U1333B, green = Hole U1333C.

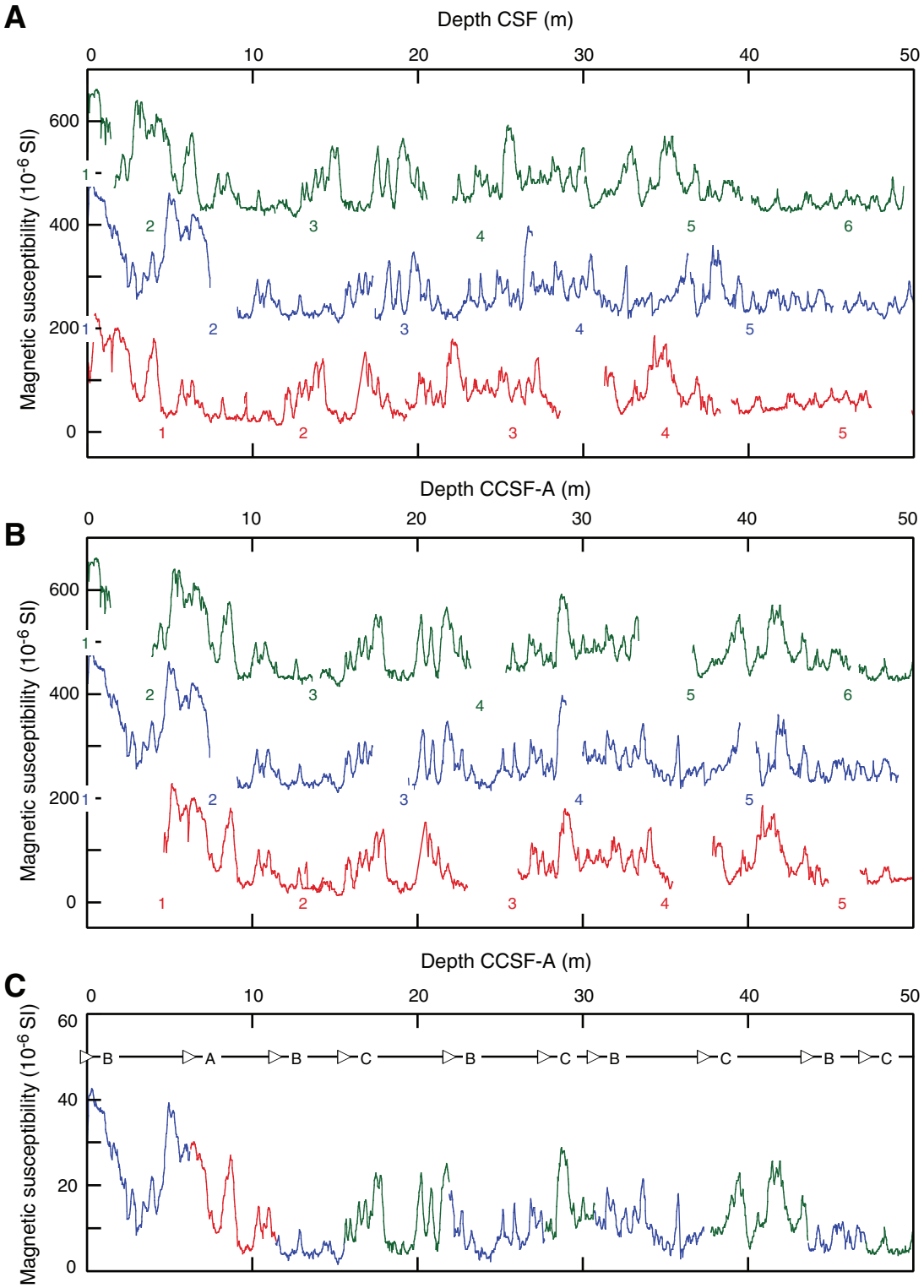

Figure F15. Core depth below seafloor vs. core composite depth below seafloor. Depths are from tops of cores, Site U1333. Growth factor is the slope of the regression line. On average, the CCSF-A depth of the spliced section is 15% greater than the CSF depth in this example.

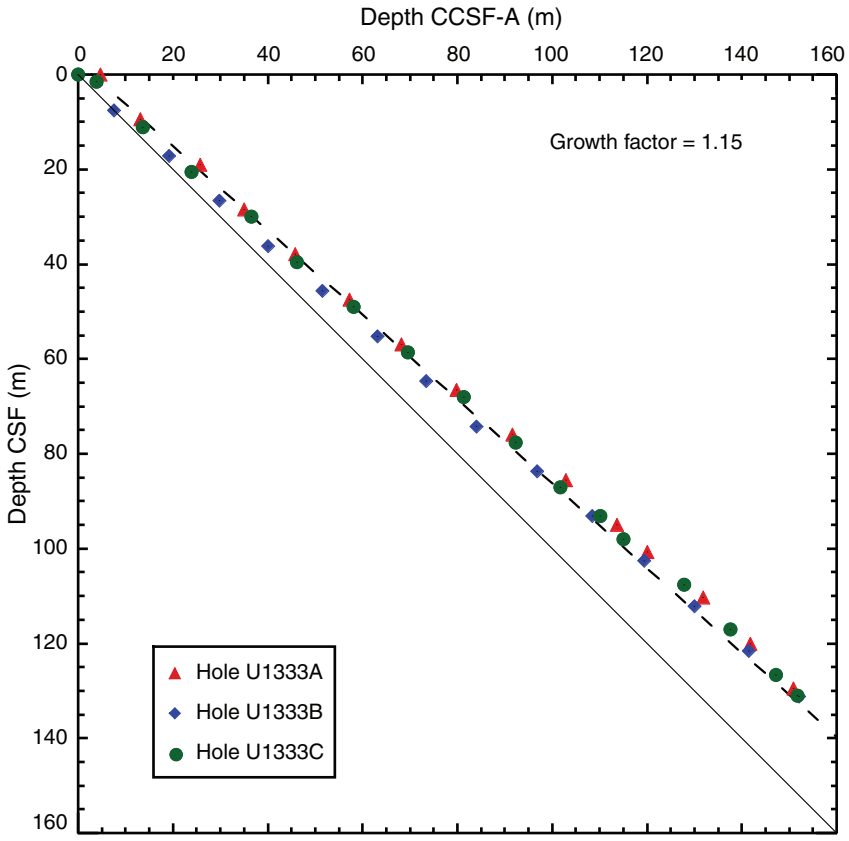

Figure F16. Typical wireline tool strings used during Expedition 320/321. See the site chapters for tool strings deployed at each site. HNGS = Hostile Environment Natural Gamma Ray Sonde, HLDS = Hostile Environment Litho-Density Sonde, MSS = Magnetic Susceptibility Sonde, DSI = Dipole Sonic Imager, GPIT = General Purpose Inclinometer Tool, FMS = Formation MicroScanner, SGT-N = Scintillation Gamma Ray Tool, VSPC = Versatile Seismic power cartridge, VSCC = Versatile Seismic control cartridge.

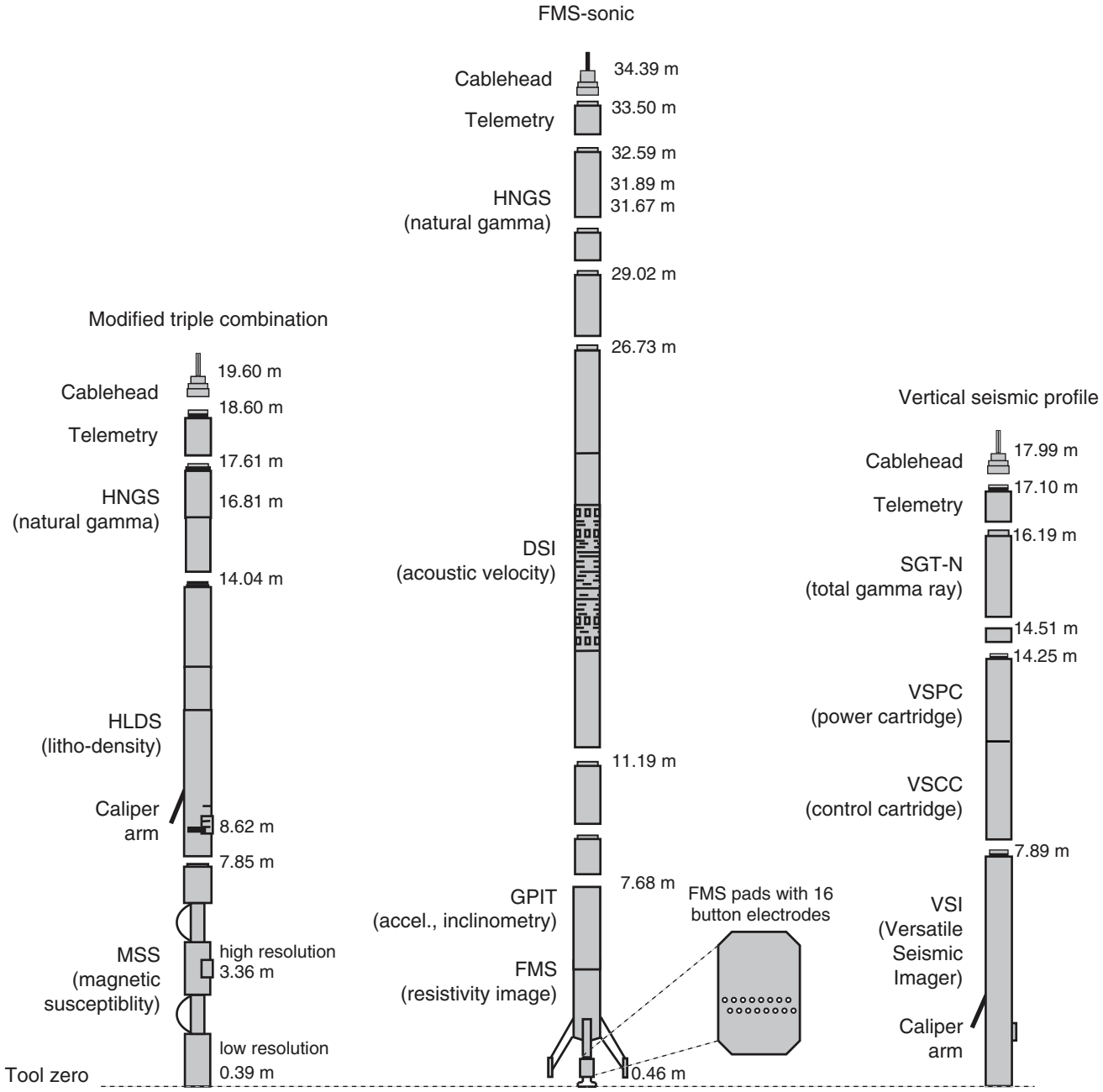

Figure F17. Schematic diagram of Magnetic Susceptibility Sonde (after Robinson et al., 2008).

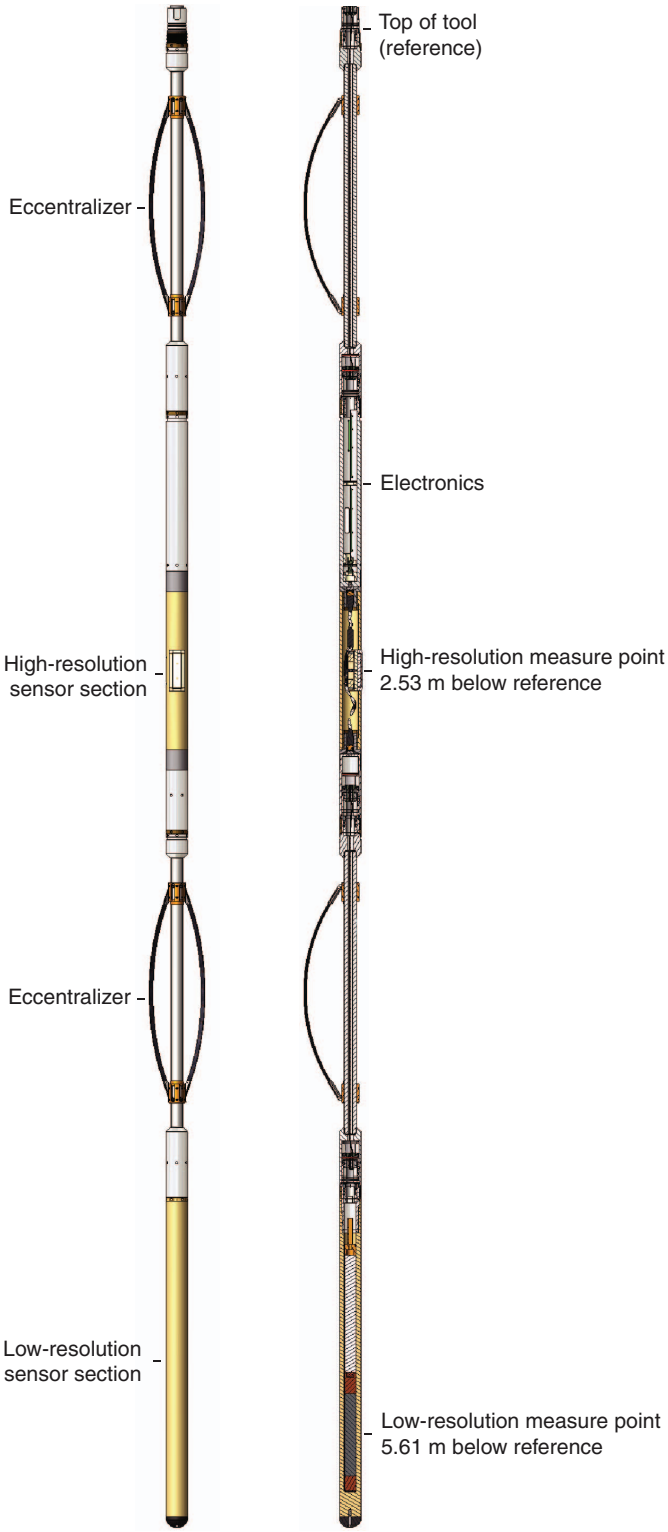

Table T1. Definition of IODP depth scales used during Expedition 320/321. (See table notes.)

Depth scale	Acronym	Origin	Method description	Submethod	Unit	Previous name*	Previous unit*
Drillers depth scale:							
Drilling depth below rig floor	DRF	Drill floor	Add lengths of all drill string components deployed beneath rig floor from bit to point on rig floor where length of deployed portion of last string is measured		m	Depth	mbrf
Drilling depth below seafloor	DSF	Seafloor	Subtract distance between rig floor and sea level from an estimate of seafloor depth at DRF scale using one of the submethods	Mudline core	m	Depth	mbsf
Core depth scale:							
Core depth below seafloor	CSF	Seafloor	Measure core sample or measurement offset below core top and add to core top DSF scale using one of the submethods	Let overlap if long	m	Depth	mbsf
Core composite depth below seafloor	CCSF	Seafloor	Align cores from one hole or multiple adjacent holes based using one of the submethods to create a newly constructed depth scale	A. Append if long B. Scale by factor to approximate CSF	m	Depth	mcd
Wireline depth scale:							
Wireline log depth below rig floor	WRF	Drill floor	Measure length of wireline extended beneath rig floor.		m	Depth	mbrf
Wireline log depth below seafloor	WSF	Seafloor	Subtract distance between rig floor and sea level from an estimate of seafloor depth at WRF scale using one of the submethods.	Seafloor signal	m	Depth	mbsf
Wireline log matched depth below seafloor	WMSF	Seafloor	Pick log data from one run as reference and map other run data using several tie points.	Natural gamma ray logs	m	Depth	mbsf

Notes: * = ODP depth scale conventions. Drillers depth scale is based on length of drill pipe lowered below drill floor. Core depth scale is based on actual length of core recovered and drillers depth, which can vary with time as core expands or contracts. Wireline depth scale is based on wireline length between downhole tool and shipboard winch. See IODP Depth Scale Terminology at www.iodp.org/program-policies/.

Table T2. Age estimates of calcareous nannofossil datum events. (See table notes.) (Continued on next page.)

Species event	Age (Ma)	Zone/ Subzone base	Reference
B *Emiliania huxleyi*	0.29	NN21	Lourens et al., 2004
T *Pseudoemiliania lacunosa*	0.44	NN20	Lourens et al., 2004
Tc *Reticulofenestra asanoi*	0.91		Lourens et al., 2004
Br *Gephyrocapsa* (>4 µm)	1.01		Lourens et al., 2004
Bc *Reticulofenestra asanoi*	1.14		Lourens et al., 2004
T *Gephyrocapsa* (>5.5 µm)	1.26		Lourens et al., 2004
T *Helicosphaera sellii*	1.34		Lourens et al., 2004
B *Gephyrocapsa* (>5.5 µm)	1.56		Lourens et al., 2004
T *Calcidiscus macintyrei*	1.61		Lourens et al., 2004
B *Gephyrocapsa* (>4 µm)	1.69		Lourens et al., 2004
Pliocene/Pleistocene boundary	1.806		Lourens et al., 2004
T *Discoaster brouweri*	1.93	NN19	Lourens et al., 2004
Bc *Discoaster triradiatus*	2.14		Lourens et al., 2004
T *Discoaster pentaradiatus*	2.39	NN18	Lourens et al., 2004
T *Discoaster surculus*	2.49	NN17	Lourens et al., 2004
T *Discoaster tamalis*	2.80		Lourens et al., 2004
T *Sphenolithus* spp.	3.54		Lourens et al., 2004
T *Reticulofenestra pseudoumbilicus*	3.70	NN16	Lourens et al., 2004
T *Ceratolithus acutus*	5.04		Lourens et al., 2004
B *Ceratolithus rugosus*	5.05	NN13	Lourens et al., 2004
T *Triquetrorhabdulus rugosus*	5.28		Lourens et al., 2004
Miocene/Pliocene boundary	5.332		Lourens et al., 2004
B *Ceratolithus larrymayeri*	5.34		Lourens et al., 2004
B *Ceratolithus acutus*	5.35		Lourens et al., 2004
T *Discoaster quinqueramus*	5.58	NN12	Lourens et al., 2004
Tc *Nicklithus amplificus*	5.98		Lourens et al., 2004
X *Nicklithus amplificus*/*T. rugosus*	6.79		Lourens et al., 2004
B *Nicklithus amplificus*	6.91		Lourens et al., 2004
B *Amaurolithus* spp.	7.36		Lourens et al., 2004
B *Discoaster berggrenii*	8.29		Lourens et al., 2004
T *Catinaster calyculus*	9.67		Lourens et al., 2004
T *Discoaster hamatus*	9.69	NN10	Lourens et al., 2004
T *Catinaster coalitus*	9.69		Lourens et al., 2004
B *Discoaster hamatus*	10.55	NN9	Lourens et al., 2004
T *Coccolithus miopelagicus*	10.60		Raffi et al., 2006
B *Catinaster calyculus*	10.76		Lourens et al., 2004
B *Catinaster coalitus*	10.89	NN8	Lourens et al., 2004
Tc *Discoaster kugleri*	11.58		Lourens et al., 2004
Bc *Discoaster kugleri*	11.86	NN7	Lourens et al., 2004
T *Coronocyclus nitescens*	12.12		Lourens et al., 2004
T *Calcidiscus premacintyrei*	12.45		Lourens et al., 2004
Tc *Cyclicargolithus floridanus*	13.33		Lourens et al., 2004
T *Sphenolithus heteromorphus*	13.53	NN6	Lourens et al., 2004
T *Helicosphaera ampliaperta*	14.91	NN5	Lourens et al., 2004
Tc *Discoaster deflandrei*	15.66		Raffi et al., 2006
B *Discoaster petaliformis**	15.70		Raffi et al., 2006
Bc *Sphenolithus heteromorphus*	17.71		Lourens et al., 2004
Tc *Sphenolithus belemnos*	17.95	NN4	Lourens et al., 2004
T *Triquetrorhabdulus carinatus*	18.28	NN3	Lourens et al., 2004
B *Sphenolithus belemnos*	19.03		Lourens et al., 2004
B *Helicosphaera ampliaperta*	20.43		Lourens et al., 2004
X *Helicosphaera euphratis*/*H. carteri*	20.92		Lourens et al., 2004
Tc *Triquetrorhabdulus carinatus*	22.09		Raffi et al., 2006
B *Sphenolithus disbelemnos*	22.76		Lourens et al., 2004
Oligocene/Miocene boundary	23.03		Lourens et al., 2004
T *Sphenolithus delphix*	23.1		Lourens et al., 2004
B *Sphenolithus delphix*	23.2		Lourens et al., 2004
T *Sphenolithus ciperoensis*	24.4	NN1	Blaj et al., 2009
X *Triquetrorhabdulus longus*/*T. carinatus*	24.7		Blaj et al., 2009
Tc *Cyclicargolithus abisectus*	24.7		Lyle et al., 2002
T *Sphenolithus distentus*	26.8	NP25	Blaj et al., 2009
T *Sphenolithus predistentus*	26.9		Blaj et al., 2009
B *Sphenolithus ciperoensis*	27.1	NP24	Blaj et al., 2009
T *Sphenolithus pseudoradians*	28.8		Berggren et al., 1995
B *Sphenolithus distentus*	30.0		Blaj et al., 2009

Table T2 (continued).

Species event	Age (Ma)	Zone/ Subzone base	Reference
T *Reticulofenestra umbilicus* (>14 µm)	32.0	NP23	Blaj et al., 2009
T *Isthmolithus recurvus*	32.5		Villa et al., 2008
T *Coccolithus formosus*	32.9	NP22	Blaj et al., 2009
Eocene/Oligocene boundary	33.8		Pälike et al., 2006
T *Discoaster saipanensis*	34.4	NP21	Blaj et al., 2009
T *Discoaster barbadiensis*	34.8		Blaj et al., 2009
T *Reticulofenestra reticulata*	35.2		Backman, 1987
B *Isthmolithus recurvus*	36.6	NP19	Backman, 1986
B *Chiasmolithus oamaruensis*	37.0	NP18	Berggren et al., 1995
T *Chiasmolithus grandis*	37.1		Backman, 1987
B *Dictyococcites bisectus* (>10 µm)	38.0		Berggren et al., 1995
T *Chiasmolithus solitus*	40.4	NP17	Berggren et al., 1995
B *Reticulofenestra reticulata*	42.0		Berggren et al., 1995
T *Nannotetrina* spp.	42.3		Backman, 1987
B *Reticulofenestra umbilicus* (>14 µm)	42.5		Backman, 1987
T *Nannotetrina fulgens*	43.4		Backman, 1986
T *Chiasmolithus gigas*	44.0	NP15c	Backman, 1986
B *Sphenolithus furcatolithoides*	45.8		Jovane et al., 2007
B *Chiasmolithus gigas*	46.1	NP15b	Agnini et al., 2006
B *Nannotetrina fulgens*	46.8	NP15a	Agnini et al., 2006
B *Nannotetrina cristata*	48.0		Agnini et al., 2006
T *Discoaster lodoensis*	48.4		Agnini et al., 2006
B *Discoaster sublodoensis* (5 rayed)	49.5	NP14	Agnini et al., 2006
B *Dictyococcites/Reticulofenestra*	50.7		Agnini et al., 2006
T *Tribrachiatus orthostylus*	50.7	NP13	Agnini et al., 2006
B *Girgisia gammation*	52.8		Agnini et al., 2007
B *Discoaster lodoensis*	53.1	NP12	Agnini et al., 2007
T *Tribrachiatus contortus*	53.5	NP11	Agnini et al., 2007
B *Sphenolithus radians*	53.5		Agnini et al., 2007
B *Tribrachiatus orthostylus*	53.7		Agnini et al., 2007
B *Discoaster diastypus*	54.1		Agnini et al., 2007
T *Fasciculithus* spp.	54.7		Agnini et al., 2007
B *Rhomboaster bramlettei*	55.0	NP10	Agnini et al., 2007
B *Rhomboaster* spp.	55.0		Agnini et al., 2007
Paleocene/Eocene boundary	55.0		Berggren et al., 1995
T *Ericsonia robusta*	55.9		Agnini et al., 2007
B *Discoaster multiradiatus*	56.0	NP9	Agnini et al., 2007
B *Discoaster okadai*	56.2		Agnini et al., 2007
B *Discoaster nobilis*	56.2		Agnini et al., 2007
B *Discoaster backmanii*	56.9		Agnini et al., 2007
B *Discoaster mohleri*	57.6	NP7	Agnini et al., 2007
B *Fasciculithus clinatus*	57.7		Agnini et al., 2007
B *Heliolithus kleinpellii*	58.0	NP6	Agnini et al., 2007
B *Sphenolithus anarrhopus*	58.1		Agnini et al., 2007
B *Heliolithus cantabriae*	58.3		Agnini et al., 2007
B *Fasciculithus tympaniformis*	59.9	NP5	Agnini et al., 2007

Notes: B = base, T = top, Tc = top common, Bc = base common, Br = base reentrance, X = abundance crossover. * = *Discoaster signus* in Raffi et al., 2006.

Table T3. Age estimates of planktonic foraminifer datum events. (See table notes.) (Continued on next page.)

Species event	Age (Ma)	Zone/Subzone base	Reference
T *Globorotalia (Truncorotalia) tosaensis*	0.61	PT1b	Srinivasan and Sinha, 1992
T *Globigerinoides fistulosus*	1.77	PT1a	Shackleton et al., 1990
Pliocene/Pleistocene boundary	1.81		Lourens et al., 2004
B *Globorotalia (Truncorotalia) truncatulinoides*	1.92		Chaisson and Pearson, 1997
T *Globigerinoides extremus*	1.98		Chaisson and Pearson, 1997
T *Globorotalia pseudomiocenica*	2.30	PL6	Berggren et al., 1995
T *Globoturborotalita woodi*	2.30		Chaisson and Pearson, 1997
T *Globorotalia (Menardella) multicamerata*	2.98		Berggren et al., 1995
T *Dentoglobigerina altispira*	3.47	PL5	Shackleton et al., 1995
T *Sphaeroidinellopsis seminulina*	3.59	PL4	Shackleton et al., 1995
T *Globorotalia (Hirsutella) margaritae*	3.85	PL3	Chaisson and Pearson, 1997
X *Pulleniatina* sinistral → dextral	4.08		Chaisson and Pearson, 1997
T *Globoturborotalita nepenthes*	4.37	PL2	Chaisson and Pearson, 1997
B *Globorotalia (Menardella) exilis*	4.45		Chaisson and Pearson, 1997
T *Globorotalia (Hirsutella) cibaoensis*	4.61	PL1b	Berggren et al., 1995
Miocene/Pliocene boundary	5.33		Lourens et al., 2004
B *Sphaeroidinella dehiscens* s.l.	5.54		Chaisson and Pearson, 1997
B *Globorotalia tumida*	5.57	PL1a	Shackleton et al., 1995
B *Turborotalita humilis*	5.81		Chaisson and Pearson, 1997
B *Globorotalia (Hirsutella) margaritae*	6.08		Chaisson and Pearson, 1997
T *Globorotalia lenguaensis*	6.13	M14	Berggren et al., 1995
B *Globorotalia plesiotumida*	8.58	M13b	Chaisson and Pearson, 1997
B *Neogloboquadrina acostaensis*	9.83	M13a	Chaisson and Pearson, 1997
T *Paragloborotalia mayeri*	10.46	M12	Chaisson and Pearson, 1997
B *Globoturborotalita decoraperta*	11.49		Chaisson and Pearson, 1997
B *Globoturborotalita nepenthes*	11.63	M11	Turco et al., 2002
T *Globorotalia (Fohsella) fohsi* s.l (inc. *lobata* and *robusta*)	11.79	M10/N13	Chaisson and Pearson, 1997
B *Globorotalia (Fohsella) foshi robusta*	13.13	M9b	Chaisson and Pearson, 1997
B *Globorotalia (Fohsella) fohsi* s.l.	13.41	M8/M9a/N12	Chaisson and Pearson, 1997
T *Globorotalia praescitula*	13.73		Turco et al., 2002
B *Globorotalia (Fohsella) "praefohsi"*	13.77	N11	Turco et al., 2002
T *Globorotalia (Fohsella) peripheroronda*	13.80		Turco et al., 2002
T *Clavatorella bermudezi*	13.82		Shackleton et al., 1999
B *Globorotalia (Fohsella) peripheroacuta*	14.24	M7/N10	Pearson and Chaisson, 1997
B *Globorotalia (Menardella) praemenardii*	14.38		Lourens et al., 2004
T *Globigerinatella insueta*	14.66		Pearson and Chaisson, 1997
B *Orbulina* spp.	14.74	M6/N9	Shackleton et al., 1999
B *Clavatorella bermudezi*	14.89		Pearson and Chaisson, 1997
B *Globorotalia (Menardella) archeomenardii*	16.26		Pearson and Chaisson, 1997
B *Praeorbulina glomerosa*	16.27	M5b	Berggren et al., 1995
B *Praeorbulina sicana*	16.97	M5a	Berggren et al., 1995
B *Globorotalia birnageae**	16.69		Berggren et al., 1995
T *Catapsydrax dissimilis*	17.54	M4	Berggren et al., 1995
B *Globigerinatella insueta*	17.59	M3	Pearson and Chaisson, 1997
T *Globoquadrina binaiensis*	19.09		Pearson and Chaisson, 1997
T *Paragloborotalia kugleri*	21.12	M2	Berggren et al., 1995
T *Paragloborotalia pseudokugleri*	21.31		Berggren et al., 1995
B *Globoquadrina dehiscens*	22.44	M1b	Berggren et al., 1995
T *Globigerina ciperoensis*	22.90		Pearson and Chaisson, 1997
B *Paragloborotalia kugleri*	22.96	M1a	Berggren et al., 1995
Oligocene/Miocene boundary	23.03		Lourens et al., 2004
B *Paragloborotalia pseudokugleri*	25.2		Berggren et al., 1995
T *Paragloborotalia opima*	26.9	O6	Wade et al., 2007
Tc *Chiloguembelina cubensis*	28.0	O5	Wade et al., 2007
B *Globigerina angulisuturalis*	29.2	O4	Berggren et al., 1995
T *Subbotina angiporoides*	29.8		Berggren et al., 1995
T *Turborotalia ampliapertura*	30.3	O3	Berggren et al., 1995
B *Paragloborotalia opima*	30.8		Berggren et al., 1995
T *Pseudohastigerina naguewichiensis*	32.0	O2	Berggren et al., 1995
T *Hantkenina* spp.	33.8	O1	Berggren and Pearson, 2005
Eocene/Oligocene boundary	33.8		Pälike et al., 2006
T *Turborotalia cerroazulensis*	33.9		Berggren and Pearson, 2005
T *Globigerinatheka index*	34.5	E16	Berggren and Pearson, 2005
T *Globigerinatheka semiinvoluta*	35.8	E15	Berggren and Pearson, 2005
T *Morozovelloides crassatus*	38.1	E14	Wade, 2004

Table T3 (continued).

Species event	Age (Ma)	Zone/Subzone base	Reference
T *Acarinina mcgowrani*	38.1		Wade, 2004
T *Orbulinoides beckmanni*	40.0	E13	Wade, 2004
B *Orbulinoides beckmanni*	40.8	E12	Berggren et al., 1995
T *Acarinina bullbrooki*	40.8		Berggren et al., 1995
T *Guembelitrinoides nuttalli*	42.3	E11	Berggren and Pearson, 2005
B *Turborotalia pomeroli*	42.4		Berggren et al., 1995
B *Morozovelloides lehneri*	43.5		Berggren et al., 1995
T *Morozovella aragonensis*	43.6	E10	Berggren et al., 1995
B *Globigerinatheka kugleri*	45.8	E9	Berggren et al., 1995
B *Guembelitrinoides nutalli*	49.0	E8	Hancock et al., 2002
B *Acarinina cuneicamerata*	50.4	E7	Hancock et al., 2002
B *Astrorotalia palmerae*	50.4		Berggren et al., 1985
T *Morozovella subbotinae*	50.8	E6	Berggren and Pearson, 2005
B *Acarinina pentacamerata*	50.8		Berggren and Pearson, 2005
B *Morozovella aragonensis*	52.3	E5	Berggren et al., 1995
T *Subbotina velascoensis*	53.5		Berggren et al., 1995
T *Morozovella aequa*	53.6		Berggren et al., 1995
B *Morozovella lensiformis*	54.0	E4	Berggren et al., 1995
T *Morozovella velascoensis*	54.5	E3	Berggren and Pearson, 2005
B *Morozovella gracilis*	54.7		Berggren et al., 1995
B *Pseudohastigerina wilcoxensis*	55.4	E2	Berggren and Pearson, 2005
Paleocene/Eocene boundary	55.0		Berggren et al., 1995
B *Globanomalina australiformis*	55.5		Berggren et al., 1995
B *Acarinina sibaiyaensis*	55.5	E1	Berggren and Pearson, 2005
T *Morozovella acuta*	55.7		Berggren et al., 1995
B *Morozovella subbotinae*	55.9		Berggren et al., 1995
T *Globanomalina pseudomenardii*	55.9	P5	Berggren et al., 1995
T *Acarinina mckannai*	56.3		Berggren et al., 1995
B *Acarinina soldadoensis*	56.5	P4c	Berggren et al., 1995
T *Acarinina subsphaerica*	57.1	P4b	Berggren et al., 1995
B *Acarinina mckannai*	59.1		Berggren et al., 1995
B *Globanomalina pseudomenardii*	59.2	P4a	Berggren et al., 1995
B *Igorina albeari*	60.0	P3b	Berggren et al., 1995

Notes: B = base, T = top, Tc = Top common, X = coiling change. s.l. = sensu lato. * = Zone M4 is not divided into Subzones M4a and M4b because the base of Zone M5, as defined by B *Praeorbulina sicana*, has been recalibrated to 16.97 Ma (Lourens et al., 2004), which is older than B *Globorotalia birnageae* previously used to define the base of Subzone M4b.

Table T4. Age estimates of radiolarian datum events. (See table note.) (Continued on next five pages.)

Species event	Age (Ma)	Zone/ Subzone base	Reference
T *Stylatractus universus*	0.44	RN16	Lourens et al., 2004
B *Collosphaera tuberosa*	0.59	RN15	Lourens et al., 2004
T *Lamprocyrtis neoheteroporos*	1.08		Lourens et al., 2004
T *Anthocyrtidium angulare*	1.21	RN14	Lourens et al., 2004
B *Lamprocyrtis nigriniae*	1.31		Lourens et al., 2004
T *Theocorythium vetulum*	1.33		Lourens et al., 2004
T *Lamprocyrtis heteroporos*	1.76		Lourens et al., 2004
B *Theocorythium trachelium*	1.76		Lourens et al., 2004
Pliocene/Pleistocene boundary	1.81		Lourens et al., 2004
B *Pterocorys minythorax*	1.88		Lourens et al., 2004
B *Anthocyrtidium angulare*	1.97		Lourens et al., 2004
T *Pterocanium prismatium*	2.08	RN13	Lourens et al., 2004
T *Didymocyrtis avita*	2.60		Lourens et al., 2004
T *Anthocyrtidium jenghisi*	2.79	RN12b	Lourens et al., 2004
B *Cycladophora davisiana*	2.89		Lourens et al., 2004
T *Stichocorys peregrina*	2.90	RN12a	Lourens et al., 2004
B *Lamprocyrtis neoheteroporos*	3.03		Lourens et al., 2004
B *Lamprocyrtis heteroporos*	3.23		Lourens et al., 2004
T *Anthocyrtidium pliocenica*	3.83		Lourens et al., 2004
T *Phormostichoartus fistula*	3.96	RN11b	Lourens et al., 2004
T *Lychnodictyum audax*	3.96		Lourens et al., 2004
T *Spongaster pentas*	3.98		Lourens et al., 2004
T *Phormostichoartus doliolum*	4.03	RN11a	Lourens et al., 2004
B *Amphirhopalum ypsilon*	4.10		Lourens et al., 2004
T *Didymocyrtis penultima*	4.26	RN10	Lourens et al., 2004
B *Spongaster tetras*	4.26		Lourens et al., 2004
B *Pterocanium prismatium*	4.73		Lourens et al., 2004
B *Nephrospyris renilla*	5.02		Lourens et al., 2004
T *Solenosphaera omnitubus*	5.32		Lourens et al., 2004
Miocene/Pliocene boundary	5.33		Lourens et al., 2004
T *Spongaster berminghami*	5.57		Lourens et al., 2004
B *Didymocyrtis penultima* (multicap)	6.13		Lourens et al., 2004
B *Didymocyrtis avita*	6.15		Lourens et al., 2004
T *Didymocyrtis antepenultima*	6.17		Lourens et al., 2004
B *Spongaster pentas*	6.17		Lourens et al., 2004
T *Stichocorys johnsoni*	6.53		Lourens et al., 2004
T *Calocycletta caepa*	6.60		Lourens et al., 2004
B *Didymocyrtis tetrathalamus*	6.60		Lourens et al., 2004
T *Stichocorys delmontensis*	6.89		Lourens et al., 2004
T *Acrobotrys tritubus*	7.65		Lourens et al., 2004
Trans *S. delmontensis* > *S. peregrina*	7.75	RN9	Lourens et al., 2004
B *Stichocorys peregrina*	7.84		Lourens et al., 2004
T *Stylosphaera* sp. C	7.95		Lourens et al., 2004
B *Theocorythium vetulum*	7.98		Lourens et al., 2004
B *Solenosphaera omnitubus*	8.25		Lourens et al., 2004
B *Acrobotrys tritubus*	8.34		Lourens et al., 2004
T *Diartus hughesi*	8.39	RN8	Lourens et al., 2004
T *Didymocyrtis laticonus*	8.43		Lourens et al., 2004
B *Didymocyrtis penultima*	8.51		Lourens et al., 2004
T *Botryostrobus miralestensis*	8.59		Lourens et al., 2004
T *Diartus petterssoni*	8.63		Lourens et al., 2004
Trans *D. petterssoni* > *D. hughesi*	8.76	RN7	Lourens et al., 2004
B *Spongaster berminghami*	8.76		Lourens et al., 2004
B *Stichocorys johnsoni*	8.84		Lourens et al., 2004
T *Stichocorys wolffii*	8.95		Lourens et al., 2004
B *Diartus hughesi*	8.99		Lourens et al., 2004
B *Cladococcus abietinus*	9.41		Lourens et al., 2004
B *Didymocyrtis antepenultima*	10.01		Lourens et al., 2004
T *Stauroxiphos communis*	10.06		Lourens et al., 2004
T *Cyrtocapsella japonica*	10.31		Lourens et al., 2004
T *Carpocanopsis cristata*	10.88		Lourens et al., 2004
T *Lithopera neotera*	11.16		Lourens et al., 2004
Bc *Diartus petterssoni*	11.71		Lourens et al., 2004
T *Cyrtocapsella cornuta*	11.86		Lourens et al., 2004
Bc *Cyrtocapsella japonica*	11.86		Lourens et al., 2004
T *Dorcadospyris alata*	11.88		Lourens et al., 2004

Table T4 (continued). (Continued on next page.)

Species event	Age (Ma)	Zone/ Subzone base	Reference
T *Cyrtocapsella tetrapera*	11.91		Lourens et al., 2004
T *Lithopera renzae*	11.91		Lourens et al., 2004
B *Diartus petterssoni*	12.11	RN6	Lourens et al., 2004
B *Cyrtocapsella japonica*	12.41		Lourens et al., 2004
B *Lithopera neotera*	12.95		Lourens et al., 2004
T *Calocycletta robusta*	13.35		Lourens et al., 2004
T *Stichocorys armata*	13.50		Lourens et al., 2004
T *Acrocubus octopyle*	13.88		Lourens et al., 2004
T *Didymocyrtis mammifera*	13.88		Lourens et al., 2004
T *Liriospyris parkerae*	13.89		Lourens et al., 2004
Bc *Calocycletta caepa*	13.95		Lourens et al., 2004
T *Eucyrtidium diaphanes*	14.13		Lourens et al., 2004
T *Didymocyrtis violina*	14.20		Lourens et al., 2004
T *Calocycletta costata*	14.23		Lourens et al., 2004
T *Calocycletta virginis*	14.23		Lourens et al., 2004
T *Carpocanopsis bramlettei*	14.33		Lourens et al., 2004
T *Didymocyrtis tubaria*	14.35		Lourens et al., 2004
T *Dorcadospyris dentata*	14.66		Lourens et al., 2004
T *Dorcadospyris forcipata*	14.68		Lourens et al., 2004
Trans *D. dentata* > *D. alata*	14.78	RN5	Lourens et al., 2004
T *Liriospyris stauropora*	14.83		Lourens et al., 2004
B *Liriospyris parkerae*	15.03		Lourens et al., 2004
B *Cyrtocapsella japonica*	15.06		Lourens et al., 2004
B *Dorcadospyris alata*	15.08		Lourens et al., 2004
T *Carpocanopsis cingulata*	15.13		Lourens et al., 2004
T *Lychnocanoma elongata*	15.15		Lourens et al., 2004
T *Didymocyrtis prismatica*	15.26		Lourens et al., 2004
B *Didymocyrtis laticonus*	15.40		Lourens et al., 2004
B *Acrocubus octopylus*	15.75		Lourens et al., 2004
B *Carpocanopsis cristata*	15.80		Lourens et al., 2004
B *Didymocyrtis laticonus*	15.97		Lourens et al., 2004
B *Lithopera renzae*	16.77		Lourens et al., 2004
B *Calocycletta costata*	17.49	RN4	Lourens et al., 2004
B *Liriospyris stauropora*	17.72		Lourens et al., 2004
B *Dorcadospyris dentata*	17.72		Lourens et al., 2004
T *Dorcadospyris scambos*	18.53		Lourens et al., 2004
T *Dorcadospyris ateuchus*	18.55		Lourens et al., 2004
B *Stichocorys wolffii*	18.57	RN3	Lourens et al., 2004
B *Didymocyrtis mammifera*	18.58		Lourens et al., 2004
B *Dorcadospyris forcipata*	18.61		Lourens et al., 2004
T *Dorcadospyris simplex* s.s.	18.69		Lourens et al., 2004
T *Dorcadospyris praeforcipata*	19.77		Lourens et al., 2004
B *Didymocyrtis violina*	19.77		Lourens et al., 2004
B *Didymocyrtis tubaria*	19.99		Lourens et al., 2004
B *Dorcadospyris simplex* s.s.	20.34		Lourens et al., 2004
T *Calocycletta serrata*	20.45		Lourens et al., 2004
B *Stichocorys delmontensis*	20.68		Lourens et al., 2004
T *Lophocyrtis pegetrum*	20.89		Lourens et al., 2004
B *Carpocanopsis bramlettei*	21.30		Lourens et al., 2004
T *Theocyrtis annosa*	21.38	RN2	Lourens et al., 2004
B *Calocycletta virginis*	21.39		Lourens et al., 2004
B *Lophocyrtis leptetrum*	21.42		Lourens et al., 2004
B *Didymocyrtis tubaria*	21.73		Lourens et al., 2004
T *Eucyrtidium mitodes*	21.95		Lourens et al., 2004
B *Calocycletta serrata*	22.04		Lourens et al., 2004
B *Cyrtocapsella cornuta*	22.26		Lourens et al., 2004
B *Cyrtocapsella tetrapera*	22.35	RN1	Lourens et al., 2004
T *Artophormis gracilis*	22.62		Lourens et al., 2004
B *Anthocyrtidium marieae*	22.74		Lourens et al., 2004
B *Didymocyrtis bassanii*	22.93		Lourens et al., 2004
B *Eucyrtidium diaphanes*	22.95		Lourens et al., 2004
T *Dorcadospyris cyclacantha*	22.98		Lourens et al., 2004
T *Dorcadospyris riedeli*	23.01		Lourens et al., 2004
Oligocene/Miocene boundary	23.03		Lourens et al., 2004
B *Dorcadospyris cyclacantha*	23.29		Lourens et al., 2004
T *Dorcadospyris circulus*	23.30		Lourens et al., 2004
T *Dorcadospyris papilio*	23.31		Lourens et al., 2004

Table T4 (continued). (Continued on next page.)

Species event	Age (Ma)	Zone/ Subzone base	Reference
T *Liriospyris longicornuta*	24.12		Pälike et al., 2006
B *Carpocanopsis cingulata*	24.31		Pälike et al., 2006
T *Acrocubus octopylus*	24.38		Pälike et al., 2006
T *Lychnocanoma apodora*	24.50		Pälike et al., 2006
B *Lychnocanoma elongata*	25.05	RP22	Pälike et al., 2006
B *Acrocubus octopylus*	25.09		Pälike et al., 2006
B *Didymocyrtis tubaria*	25.27		Pälike et al., 2006
B *Calocycletta robusta*	25.27		Pälike et al., 2006
B *Dorcadospyris praeforcipata*	25.27		Pälike et al., 2006
B *Liriospyris longicornuta*	25.29		Pälike et al., 2006
B *Dorcadospyris scambos*	25.33		Pälike et al., 2006
T *Theocorys puriri*	25.38		Pälike et al., 2006
B *Acrobotrys disolenia*	25.38		Pälike et al., 2006
B *Dorcadospyris papilio*	25.55		Pälike et al., 2006
B *Lychnocanoma apodora*	25.55		Pälike et al., 2006
T *Dorcadospyris circulus*	26.17		Pälike et al., 2006
B *Dorcadospyris riedeli*	26.20		Pälike et al., 2006
T *Eucyrtidium plesiodiaphanes*	26.40		Pälike et al., 2006
T *Lithocyclia angusta*	27.69		Pälike et al., 2006
T *Theocyrtis setanios*	28.21		Pälike et al., 2006
T *Theocyrtis perysinos*	28.27		Pälike et al., 2006
T *Tristylospyris triceros*	28.31		Pälike et al., 2006
B *Theocyrtis annosa*	28.33		Pälike et al., 2006
Trans *T. triceros* > *D. ateuchus*	28.60	RP21	Pälike et al., 2006
B *Eucyrtidium mitodes*	29.41		Pälike et al., 2006
B *Dorcadospyris ateuchus*	29.50		Pälike et al., 2006
B *Theocyrtis setanios*	29.51		Pälike et al., 2006
T *Lophocyrtis milowi*	29.53		Pälike et al., 2006
B *Theocyrtis perysinos*	29.56		Pälike et al., 2006
B *Theocorys puriri*	29.62		Pälike et al., 2006
B *Didymocyrtis prismatica*	29.85		Pälike et al., 2006
B *Dorcadospyris circulus*	29.97		Pälike et al., 2006
T *Lophocyrtis oberhaensliae*	30.07		Pälike et al., 2006
T *Theocyrtis tuberosa*	30.13		Pälike et al., 2006
T *Lithocyclia crux*	30.13		Pälike et al., 2006
T *Dorcadospyris spinosa*	30.54		Pälike et al., 2006
T *Dorcadospyris quadripes*	30.54		Pälike et al., 2006
B *Eucyrtidium plesiodiaphanes*	30.57		Pälike et al., 2006
B *Lophocyrtis pegetrum*	30.68		Pälike et al., 2006
B *Spirocyrtis subtilis*	30.70		Pälike et al., 2006
T *Dorcadospyris riedeli*	30.73		Pälike et al., 2006
T *Dorcadospyris pseudopapilio*	30.84		Pälike et al., 2006
B *Dorcadospyris spinosa*	30.84		Pälike et al., 2006
T *Centrobotrys gravida*	30.89		Pälike et al., 2006
B *Dorcadospyris riedeli*	30.90		Pälike et al., 2006
B *Centrobotrys petrushevskayae*	30.91		Pälike et al., 2006
B *Dorcadospyris quadripes*	30.95		Pälike et al., 2006
B *Lychnodictyum audax*	30.96		Pälike et al., 2006
T *Theocyrtis careotuberosa*	30.97		Pälike et al., 2006
B *Theocyrtis tuberosa*	31.00		Pälike et al., 2006
B *Dorcadospyris pseudopapilio*	31.00		Pälike et al., 2006
B *Lithocyclia crux*	31.01		Pälike et al., 2006
B *Centrobotrys gravida*	31.01		Pälike et al., 2006
T *Dictyoprora mongolfieri*	33.18		Pälike et al., 2006
T *Thyrsocyrtis triacantha* (max)	33.34		Pälike et al., 2006
T *Lithocyclia ocellus* gr.	33.37		Pälike et al., 2006
B *Lophocyrtis oberhaensliae*	33.51		Pälike et al., 2006
T *Lithocyclia aristotelis* gr.	33.51		Pälike et al., 2006
T *Cryptocarpium ornatum*	33.62		Pälike et al., 2006
T *Calocyclas hispida*	33.62		Pälike et al., 2006
T *Calocycletta anekathen*	33.65		Pälike et al., 2006
T *Lophocyrtis jacchia*	33.69		Pälike et al., 2006
T *Dictyoprora pirum*	33.69		Pälike et al., 2006
T *Dictyoprora armadillo*	33.69		Pälike et al., 2006
T *Lychnocanoma babylonis*	33.75		Pälike et al., 2006
T *Lophocyrtis hadra*	33.75		Pälike et al., 2006
T *Lychnocanoma amphitrite*	33.75		Pälike et al., 2006
T *Lophocyrtis exitelus*	33.75		Pälike et al., 2006

Table T4 (continued). (Continued on next page.)

Species event	Age (Ma)	Zone/ Subzone base	Reference
Eocene/Oligocene boundary	33.80		Pälike et al., 2006
Trans *L. aristotelis* > *L. angusta*	33.82	RP20	Pälike et al., 2006
T *Dorcadospyris copelata*	33.84		Pälike et al., 2006
T *Thyrsocyrtis bromia* (max)	33.94		Pälike et al., 2006
T *Zealithapium mitra*	33.97		Pälike et al., 2006
T *Artophormis barbadensis*	33.97		Pälike et al., 2006
T *Thyrsocyrtis lochites* (max)	34.13		Pälike et al., 2006
B *Lithocyclia angusta*	34.13		Pälike et al., 2006
B *Lophocyrtis milowi*	34.13		Pälike et al., 2006
T *Thyrsocyrtis tetracantha* (max)	34.13		Pälike et al., 2006
B *Pteropilium* sp. aff. *Pterocanium contiguum*	34.25		Pälike et al., 2006
T *Dorcadospyris ombros* (upper)	34.30		Pälike et al., 2006
T *Calocyclas bandyca*	34.62		Pälike et al., 2006
B *Lophocyrtis exitelus*	34.68		Pälike et al., 2006
T *Calocyclas turris*	34.83		Pälike et al., 2006
T *Eusyringium fistuligerum*	34.94		Pälike et al., 2006
T *Cryptocarpium azyx*	35.07		Pälike et al., 2006
T *Thyrsocyrtis bromia* (continuous)	35.18		Pälike et al., 2006
T *Thyrsocyrtis tetracantha* (continuous)	35.30	RP19	Pälike et al., 2006
B *Lophocyrtis hadra*	35.34		Pälike et al., 2006
T *Thyrsocyrtis lochites* (continuous)	35.34		Pälike et al., 2006
T *Thyrsocyrtis rhizodon*	35.40		Pälike et al., 2006
T *Thyrsocyrtis krooni*	35.44		Pälike et al., 2006
T *Thyrsocyrtis triacantha* (continuous)	35.51		Pälike et al., 2006
T *Artophormis dominasinensis*	35.56		Pälike et al., 2006
T *Lychnocanoma turgidum*	35.77		Pälike et al., 2006
B *Artophormis gracilis*	36.14		Pälike et al., 2006
B *Calocycletta anekathen*	36.41		Pälike et al., 2006
B *Lychnocanoma amphitrite*	36.49		Pälike et al., 2006
T *Theocyrtis perpumila*	36.72		Pälike et al., 2006
B *Calocyclas bandyca*	36.74	RP18	Pälike et al., 2006
T *Thyrsocyrtis orthotenes*	36.89		Pälike et al., 2006
B *Lophocyrtis jacchia*	37.07		Pälike et al., 2006
T *Podocyrtis papalis* (continuous)	37.30		Pälike et al., 2006
B *Cryptocarpium azyx*	37.52	RP17	Pälike et al., 2006
B *Thyrsocyrtis lochites*	37.52		Pälike et al., 2006
B *Dorcadospyris copelata*	37.90		Pälike et al., 2006
T *Spongatractus pachystylus*	37.90		Pälike et al., 2006
T *Anthocyrtoma* spp.	37.92		Pälike et al., 2006
T *Calocycloma ampulla*	38.07		Pälike et al., 2006
B *Thyrsocyrtis bromia*	38.07		Pälike et al., 2006
B *Thyrsocyrtis tetracantha*	38.12		Pälike et al., 2006
T *Zygocircus cimelium*	38.21		Pälike et al., 2006
T *Rhopalocanium ornatum*	38.25		Pälike et al., 2006
B *Theocyrtis careotuberosa*	38.27		Pälike et al., 2006
B *Dorcadospyris ombros* (upper)	38.27		Pälike et al., 2006
B *Tristylospyris triceros*	38.31		Pälike et al., 2006
B *Artophormis dominasinensis*	38.33		Pälike et al., 2006
T *Theocotyle ficus*	38.45		Pälike et al., 2006
T *Dorcadospyris anastasis*	38.45		Pälike et al., 2006
T *Dictyophimus craticula*	38.51		Pälike et al., 2006
B *Calocyclas turris*	38.67		Pälike et al., 2006
T *Podocyrtis goetheana* (continuous)	38.72		Pälike et al., 2006
T *Podocyrtis chalara* (continuous)	38.74		Pälike et al., 2006
B *Botryocella* sp. gr.	38.91		Pälike et al., 2006
T *Podocyrtis apeza*	38.95		Pälike et al., 2006
B *Thyrsocyrtis krooni*	39.34		Pälike et al., 2006
B *Dictyoprora pirum*	39.65		Pälike et al., 2006
T *Lithochytris vespertilio*	39.65		Pälike et al., 2006
B *Dictyoprora armadillo*	39.65		Pälike et al., 2006
T *Sethochytris triconiscus*	39.70		Pälike et al., 2006
T *Dorcadospyris ombros* (lower)	39.70		Pälike et al., 2006
B *Lithocyclia aristotelis* gr.	39.73		Pälike et al., 2006
T *Podocyrtis mitra*	39.85		Pälike et al., 2006
B *Dorcadospyris anastasis*	39.98		Pälike et al., 2006
B *Podocyrtis goetheana*	40.16	RP16	Pälike et al., 2006
T *Lophocyrtis biaurita*	40.36		Pälike et al., 2006
Trans *P. mitra* > *P. chalara*	40.70	RP15	Pälike et al., 2006

Table T4 (continued). (Continued on next page.)

Species event	Age (Ma)	Zone/ Subzone base	Reference
T *Podocyrtis trachodes*	41.28		Cande and Kent, 1995
B *Podocyrtis chalara*	41.54		Cande and Kent, 1995
B *Dorcadospyris ombros* (lower)	41.54		Cande and Kent, 1995
B *Podocyrtis apeza*	41.63		Cande and Kent, 1995
B *Artophormis barbadensis*	41.66		Cande and Kent, 1995
T *Podocyrtis ampla*	41.67		Cande and Kent, 1995
B *Zealithapium mitra*	41.98		Cande and Kent, 1995
T *Zealithapium anoectum*	41.98		Cande and Kent, 1995
B *Cryptocarpium ornatum*	42.10		Cande and Kent, 1995
B *Sethochytris triconiscus*	42.40		Cande and Kent, 1995
T *Eusyringium lagena*	42.69		Cande and Kent, 1995
T *Podocyrtis fasciolata*	42.81		Cande and Kent, 1995
T *Zealithapium plegmacantha*	42.81		Cande and Kent, 1995
T *Podocyrtis sinuosa*	42.90		Cande and Kent, 1995
B *Theocyrtis perpumila*	42.97		Cande and Kent, 1995
T *Podocyrtis helenae*	43.05		Cande and Kent, 1995
B *Lychnocanoma turgidum*	43.05		Cande and Kent, 1995
B *Podocyrtis trachodes*	43.22		Cande and Kent, 1995
B *Zygocircus cimelium*	43.35		Cande and Kent, 1995
Trans *P. sinuosa* > *P. mitra*	43.84	RP14	Cande and Kent, 1995
B *Podocyrtis fasciolata*	43.87		Cande and Kent, 1995
B *Podocyrtis helenae*	44.15		Cande and Kent, 1995
T *Podocyrtis diamesa*	44.44		Cande and Kent, 1995
T *Podocyrtis phyxis*	44.44		Cande and Kent, 1995
T *Spongatractus balbis*	44.77		Cande and Kent, 1995
Trans *P. phyxis* > *P. ampla*	44.77	RP13	Cande and Kent, 1995
B *Podocyrtis mitra*	44.77		Cande and Kent, 1995
B *Podocyrtis ampla*	44.77		Cande and Kent, 1995
B *Eusyringium fistuligerum*	44.89		Cande and Kent, 1995
T *Thyrsocyrtis tensa*	45.06		Cande and Kent, 1995
T *Theocotyle venezuelensis*	45.16		Cande and Kent, 1995
B *Zealithapium anoectum*	45.32		Cande and Kent, 1995
T *Theocotyle conica*	45.32		Cande and Kent, 1995
T *Lamptonium fab. constrictum*	45.62		Cande and Kent, 1995
T *Lamptonium fab. fabaeforme*	45.88		Cande and Kent, 1995
T *Theocotyle cryptocephala*	46.01		Cande and Kent, 1995
T *Periphaena tripyramis triangula*	46.16		Cande and Kent, 1995
B *Thyrsocyrtis orthotenes*	46.16		Cande and Kent, 1995
T *Thyrsocyrtis robusta*	46.16		Cande and Kent, 1995
T *Thyrsocyrtis hirsuta*	46.19		Cande and Kent, 1995
B *Podocyrtis phyxis*	46.44		Cande and Kent, 1995
T *Lamptonium fab. chaunothorax*	46.61		Cande and Kent, 1995
T *Periphaena delta*	46.74		Cande and Kent, 1995
T *Theocorys anaclasta*	45.62		Cande and Kent, 1995
T *Calocycloma castum*	47.42		Cande and Kent, 1995
B *Thyrsocyrtis triacantha*	47.42		Cande and Kent, 1995
B *Rhopalocanium ornatum*	47.42		Cande and Kent, 1995
B *Eusyringium lagena*	47.42	RP12	Cande and Kent, 1995
T *Buryella clinata*	48.14		Cande and Kent, 1995
T *Phormocyrtis striata striata*	48.14		Cande and Kent, 1995
B *Dictyoprora mongolfieri*	~48.50	RP11	Cande and Kent, 1995
T *Amphicraspedum murrayanum*	49.74		Cande and Kent, 1995
T *Dendrospyris fragoides*	49.74		Cande and Kent, 1995
B *Dictyophimus craticula*	49.74		Cande and Kent, 1995
T *Diploplegma somphum*	49.74		Cande and Kent, 1995
T *Giraffospyris lata*	49.74		Cande and Kent, 1995
B *Lamptonium fab. constrictum*	49.74		Cande and Kent, 1995
T *Lamptonium pennatum*	49.74		Cande and Kent, 1995
T *Lamptonium sanfilippoae*	49.74		Cande and Kent, 1995
B *Zealithapium plegmacantha*	49.74		Cande and Kent, 1995
T *Lithochytris archaea*	49.74		Cande and Kent, 1995
B *Lithochytris vespertilio*	49.74		Cande and Kent, 1995
B *Lithocyclia ocellus* gr.	49.74		Cande and Kent, 1995
B *Lophocyrtis biaurita*	49.74		Cande and Kent, 1995
T *Lychnocanoma auxilla*	49.74		Cande and Kent, 1995
B *Periphaena tripyramis triangula*	49.74		Cande and Kent, 1995
T *Phormocyrtis cubensis*	49.74		Cande and Kent, 1995
T *Phormocyrtis striata exquisita*	49.74		Cande and Kent, 1995

Table T4 (continued).

Species event	Age (Ma)	Zone/ Subzone base	Reference
B *Podocyrtis sinuosa*	49.74		Cande and Kent, 1995
B *Podocyrtis diamesa*	49.74		Cande and Kent, 1995
T *Pterocodon tenellus*	49.74		Cande and Kent, 1995
B *Spongatractus pachystylus*	49.74		Cande and Kent, 1995
B *Theocotyle conica*	49.74		Cande and Kent, 1995
B *Theocotyle cryptocephala*	49.74		Cande and Kent, 1995
Trans *T. nigriniae* > *T. cyrptocephala*	~49.00	RP10	Cande and Kent, 1995
T *Theocotyle nigriniae*	49.74		Cande and Kent, 1995
B *Theocotyle venezuelensis*	49.74		Cande and Kent, 1995
T *Theocotylissa alpha*	49.74		Cande and Kent, 1995
T *Theocotylissa fimbria*	49.74		Cande and Kent, 1995
B *Thyrsocyrtis rhizodon*	49.74		Cande and Kent, 1995
B *Thyrsocyrtis robusta*	49.74		Cande and Kent, 1995
B *Theocorys anaclasta*	~50.00	RP9	Cande and Kent, 1995
T *Buryella tetradica* s.s.	50.68		Cande and Kent, 1995
T *Lychnocanoma pileus*	50.68		Cande and Kent, 1995
B *Periphaena delta*	50.88		Cande and Kent, 1995
B *Lamptonium sanfilippoae*	51.44		Cande and Kent, 1995
B *Spongatractus balbis*	51.44		Cande and Kent, 1995
B *Thyrsocyrtis tensa*	51.86		Cande and Kent, 1995
T *Pterocodon anteclinata*	51.96		Cande and Kent, 1995
B *Lychnocanoma babylonis*	52.06		Cande and Kent, 1995
Trans *P. anteclinata* > *B. clinata*	~52.90	RP8	Cande and Kent, 1995
B *Theocotylissa ficus*	52.94		Cande and Kent, 1995
B *Anthocyrtoma* spp.	52.94		Cande and Kent, 1995
T *Phormocyrtis turgida*	52.94		Cande and Kent, 1995
T *Pterocodon ampla*	52.94		Cande and Kent, 1995
B *Phormocyrtis striata striata*	52.94		Cande and Kent, 1995
B *Theocotylissa fimbria*	52.94		Cande and Kent, 1995
B *Buryella clinata*	52.94		Cande and Kent, 1995

Note: B = base, Bc = bottom common, T = top, Trans = transitional forms.

Table T5. Age estimates of diatom datum events. (See table notes.) (Continued on next two pages.)

Species event	Age (Ma)	Zone base	Reference
T *Fragilariopsis reinholdii*	0.69	*Fragilariopsis doliolus*	Burckle, 1972
T *Nitzschia fossilis*	0.92		Barron, 1983; Baldauf and Iwai, 1995
T *Rhizosolenia matuyamai*	1.02		Burckle, 1978
B *Rhizosolenia matuyamai*	1.20		
T *Rhizosolenia praebergonii* var. *robusta*	1.66	A/B boundary	
B *Azpeitia barronii*	1.72		Barron, 1983
B *Fragilariopsis doliolus*	1.88	*Fragilariopsis reinholdii*	Burckle, 1978
T *Rhizosolenia praebergonii*	1.92		Burckle, 1978; Baldauf and Iwai, 1995
T *Thalassiosira convexa*	2.18	B/C boundary	Burckle, 1978
T *Nitzschia jouseae*	2.71	A/B boundary	Burckle, 1978; Baldauf and Iwai, 1995
B *Rhizosolenia praebergonii*	3.13	*Rhizosolenia praebergonii*	Burckle, 1978; Baldauf and Iwai, 1995
T *Actinocyclus ellipticus* f. *lanceolata*	3.35		Barron, 1983
B *Thalassiosira convexa* var. *convexa*	3.84		Burckle and Trainer, 1979; Baldauf and Iwai, 1995
B *Asteromphalus elegans*	4.21		Burckle, 1978
T *Fragilariopsis cylindrica*	4.69		Burckle, 1978
B *Nitzschia jouseae*	4.92	*Nitzschia jouseae*	Burckle, 1978
B *Thalssiosira oestrupii*	5.70		Burckle, 1978
T *Thalssiosira miocenica*	5.70	B/C boundary	Burckle, 1978
T *Asterolampra acutiloba*	6.03		Burckle, 1978
T *Nitzschia miocenica*	6.28		Burckle, 1978
T *Nitzschia miocenica* var. *elongata*	6.39		
T *Thalssiosira praeconvexa*	6.56	A/B boundary	Burckle, 1978
T *Rossiella praepaleacea*	6.76		
B *Thalassiosira miocenica*	6.86		
B *Thalassiosira convexa*	6.86	*Thalassirosira convexa*	Burckle, 1978
B *Thalassiosira praeconvexa*	7.07	A/B boundary	Burckle, 1978
T *Nitzschia porteri*	7.53		Burckle, 1978
B *Nitzschia miocenica*	7.58	*Nitzschia miocenica*	Burckle, 1978
T *Rossiella paleacea*	7.64		Burckle, 1978
T *Thalssiosira burckliana*	7.86	A/B boundary	Burckle, 1978
B *Fragilariopsis reinholdii*	8.20		Barron, 1983
T *Actinocyclus ellipticus* var. *javanicus*	8.25		
B *Nitzschia marina*	8.30		Barron, 1983
T *Thalssiosira yabei*	8.44	*Nitzschia porteri*	Burckle, 1978
B *Fragilariopsis cyclindrica*	8.44		Burckle, 1978
B *Azpeitia nodulifer* var. *cyclopa*	8.58		
T *Coscinodiscus loeblichii*	8.77		
B *Nitzschia fossilis*	8.98		Barron, 1983
B *Thalassiosira burcklina*	9.09	A/B boundary	Barron, 1983
B *Cosdinodiscus loeblichii*	9.30		Barron, 1983
T *Azpeitia vetustissimus* var. *javanica*	9.47		Burckle, 1978
B *Azpeitia vetustissimus* var. *javanica*	9.68		Burckle, 1978
T *Crucidenticula hustedtii*	9.71		Burckle, 1978
T *Actinocyclus moronensis*	9.77	*Thalassiosira yabei*	Burckle, 1978
B *Actinocyclus ellipticus* f. *lanceolata*	9.90		Barron, 1983
T *Cavitatus jouseanus*	9.97		Barron, 1983
T *Crucidenticula punctata*	10.13		
B *Rossiella paleacea* var. *elongata*	10.13		Barron, 1983
B *Thalassionema robusta*	10.13		Barron, 1983
T *Coscinodsicus gigas* var. *diorama*	10.36	*Actinocyclus moronensis*	Barron, 1983
T *Crasepedodicus coscinodiscus*	10.36		Barron et al., 1985a
T *Actinocyclus ellipticus* var. *spiralis*	10.59		Barron, 1983
B *Hemidiscus cuneiformis*	11.24		Burckle, 1978
B *Rossiella praepaleacea*	11.84		Barron, 1983
T *Actinocyclus ingens*	11.92		Barron, 1983
T *Cestodiscus pulchellus*	12.05		Barron, 1983
B *Nitzschia porteri*	12.11		Barron, 1983
B *Coscinodiscus temperi* var. *delicata*	12.17	*Craspedodiscus coscinodiscus*	Burckle et al., 1982
T *Crucidenticula nicobarica*	12.50		Barron, 1983
T2 *Annellus californicus*	12.68		Barron, 1983
B *Coscinodiscus gigas* var. *diorama*	12.84		Barron, 1983
T *Coscinodiscus lewisianus*	12.99	*Coscinodiscus gigas* var. *diorama*	Burckle, 1972; Barron et al., 1985b
B *Crucidenticula punctata*	13.18		
T *Thalassiosira tappanae*	13.37		Burckle, 1978; Barron, 1983
B *Azpeitia nodulifer*	13.44		Burckle, 1978
B *Triceratium cinnamomeum*	13.52		
B *Denticulopsis hustedtii*	13.70		Burckle, 1978
B *Actinocyclus ellipticus* var. *spiralis*	14.19	*Coscinodiscus lewisianus*	Barron, 1983
T *Cestodiscus peplum*	14.19		Burckle, 1978

Table T5 (continued). (Continued on next page.)

Species event	Age (Ma)	Zone base	Reference
B *Actinocyclus ellipticus*	14.37		Barron, 1983
B *Coscinodiscus blysmos*	14.55		Barron, 1983
B *Thalassirosira tappanae*	14.55		
T1 *Annellus californicus*	14.91	A/B boundary	Burckle, 1978
T *Azpeitia praenodulifera*	15.26		Barron, 1983
B *Actinocyclus ingens*	15.25		Barron, 1983
T *Coscinodiscus lewisianus* var. *simillis*	15.35		Barron, 1983
T *Nitzschia maleinterpretaria*	15.44		Barron, 1983
T *Crucidenticula kanayae*	15.78		Barron, 1983
T *Thalassirosira fraga*	15.96		Barron, 1983
B *Cestodiscus pepulum*	16.15	*Cestodiscus peplum*	Barron et al., 1985a
T *Cavitatus miocenica*	16.25		
T *Raphidiscus marylandicus*	16.49		
B *Crucidenticula kanayae*	16.63		
T *Thalassirosira bukryi*	16.72	A/B boundary	Barron et al., 1985a
B *Coscinodiscus blysmos*	16.81		
B *Annellus californicus*	16.99		
B *Craspedodicus coscinodiscus*	16.99		
T *Coscinodiscus lewisianus* var. *robusta*	17.08		
B *Coscinodiscus lewisianus* var. *similis*	17.08		
T *Thalassirosira spumellaroides*	17.17		
T *Triceratium pileus*	17.35		
B *Crucidenticula nicobarica*	17.49	*Crucidenticula nicobarica*	Barron et al., 1985a
T *Thalassirosira spinosa*	17.64		
T *Actinocyclus radionovae*	17.64		Barron et al., 1985a
T *Craspedodiscus elegans*	18.18	*Triceratium pileus*	Barron et al., 1985a
B *Nitzschia maleinterpretaria*	18.27		
B *Triceratium pileus*	18.27		Barron, 1983
T *Coscinodiscus rhombicus*	18.44		Barron, 1983
T *Actinocyclus hajosiae*	18.96		Barron, 1983
T *Bogorovia veniamini*	19.21	*Craspedodiscus elegans*	Barron et al., 1985a
B *Thalassirosira fraga*	19.21		Barron, 1983
B *Coscinodiscus lewisianus* var. *robustus*	19.30		
T *Azpeitia oligocenica*	19.80		Barron et al., 1985b
T *Melosira architecturalis*	19.89		
B *Actinocyclus radionovae*	20.61		Barron et al., 2006
T *Bogorovia barronii*	20.68		Barron et al., 2006
B *Azpeitia praenodulifera*	20.68		Barron et al., 2006
B *Rossiella paleacea*	20.96		Barron et al., 2006
T *Thalassirosira primalabiata*	21.44		Barron et al., 1985b; Burckle, 1972
B *Actinocyclus hajosiae*	21.44	A/B boundary	Barron et al., 2006
B *Thalassiosira spumellaroides*	21.72		Barron et al., 2006
B *Bogorovia barronii*	21.72		Barron et al., 2006
B *Thalassirosira praefraga*	21.99		Barron et al., 2006
B *Rossiella fourtanierae*	22.74		Barron et al., 2006
T *Rocella gelida*	23.45	*Rossiella fennerae*	Barron et al., 2006
T *Coscinodiscus lewisianus* var. *rhomboides*	23.45		Barron et al., 2006
T *Rocella schraderi*	23.73		Barron et al., 2006
Bc *Rossiella fennerae*	23.97		Barron et al., 2006
T *Rocella vigilans*	24.05		Barron et al., 2006
T *Rocella princeps*	24.12		Barron et al., 2006
B *Rocella schraderi*	24.30		Barron et al., 2006
B *Craspedodiscus barronii*	24.95		Barron et al., 2006
B *Rocella gelida*	25.14	*Rocella gelida*	Barron et al., 2006
B *Coscinodiscus lewisianus* var. *rhomboides*	25.14		Barron et al., 2006
B *Rocella princeps*	25.38		Barron et al., 2006
T *Cestodiscus kugleri*	25.38		Barron et al., 2006
T *Rossiella symmetrica*	25.77		Barron et al., 2006
T *Kozloviella minor*	27.23		Barron et al., 2006
B *Cestodiscus kugleri*	27.23		Barron et al., 2006
B *Coscinodiscus lewisianus* var. *levis*	27.81		Barron et al., 2006
B *Bogorovia veniamini*	27.81	*Bogorovia veniamini*	Barron et al., 2006
T *Baxteriopsis brunii*	27.81		Barron et al., 2006
Tc *Cestodiscus trochus*	28.07		Barron et al., 2006
B *Coscinodiscus rhombicus*	28.17		Barron et al., 2006
B *Cavitatus rectus*	28.17		Barron et al., 2006
B *Kozloviella minor*	28.31		Barron et al., 2006
B *Cavitatus jouseanus*	28.31	B/C boundary	Barron et al., 2006
B *Rossiella symmetrica*	28.75	A/B boundary	Barron et al., 2006

Table T5 (continued).

Species event	Age (Ma)	Zone base	Reference
B *Rocella vigilans*	29.66	*Rocella vigilins*	Barron et al., 2006
Tc *Cestodiscus robustus*	30.78		Barron et al., 2006
T *Skeletonemopsis barbadiensis*	30.95		Barron et al., 2006
T *Cestodiscus trochus*, marginal labiate processes	30.95		Barron et al., 2006
T *Cestodiscus convexus*	30.95		Barron et al., 2006
T *Coscinodiscus excavatus*	31.12	*Cestodiscus trochus*	Barron et al., 2006
B *Cavitatus miocenicus*	21.12		Barron et al., 2006
B *Thalassionema* cf. *nitzschioides*	31.48		Barron et al., 2006
T *Coscinodiscus excavatus* var. *semilunaris*	31.72		Barron et al., 2006
B *Coscinodiscus excavatus* var. *semilunaris*	32.48		Barron et al., 2006
T *Cestodiscus reticulatus*	32.48		Barron et al., 2006
B *Thalassiothrix* cf. *primitiva*	33.18		Barron et al., 2006
B *Cestodiscus reticulatus*	33.18		Barron et al., 2006
T *Cestodiscus* sp. 2 of Fenner 1981	33.27		Barron et al., 2006
B *Cestodiscus convexus*	33.50		Barron et al., 2006
B *Coscinodiscus excavatus*	33.71	*Coscinodiscus excavatus*	Barron et al., 2006
B *Cestodiscus robustus*	33.71		Barron et al., 2006
B *Baxteriopsis brunii*	—	*Baxteriopsis brunii*	Fenner, 1985
B *Asterolampra marylandica*	—	*Asterolampra marylandica*	Fenner, 1985
B *Brightwellia imperfecta*	—	*Brightwellia imperfecta*	Fenner, 1985
T *Pyxilla caput-avis*	—		Fenner, 1985
B *Hemiaulus gondolaformis*	—	*Hemiaulus gondolaformis*	Fenner, 1985
B *Hemiaulus lyriformis*	—		Fenner, 1985
B *Hemiaulus exiguus*	—		Fenner, 1985
B *Hemiaulus alatus*	—	*Hemiaulus alatus*	Fenner, 1985
B *Pyxilla caput-avis*	—	*Pyxilla caput-avis*	Fenner, 1985
B *Triceratium inconspicum* var. *trilobata*	—		Fenner, 1985
B *Triceratium kanayae*	—	*Triceratium kanayae*	Fenner, 1985

Notes: T = top, B = bottom, T1 = lowermost top, T2 = uppermost top, Bc = bottom common occurrence, Tc = top common occurrence. A/B and B/C in Zone column = subzonal boundary.

Table T6. Normal polarity intervals of the Expedition 320/321 geomagnetic polarity timescale. (**Continued on next page.**)

Normal polarity interval age (Ma)		Polarity chron	Cryptochron	Reference
Top	Bottom			
0.000	0.781	C1n, Brunhes	C1n-1n	Lourens et al., 2004
0.988	1.072	C1r.1n, Jaramillo		Lourens et al., 2004
1.173	1.185	C1r.2n, Cobb Mountain		Lourens et al., 2004
			C1r.2r-1n	Lourens et al., 2004
1.778	1.945	C2n, Olduvai		Lourens et al., 2004
2.128	2.148	C2r.1n, Reunion		Lourens et al., 2004
			C2r.2r-1	Lourens et al., 2004
2.581	3.032	C2An.1n, Gauss		Lourens et al., 2004
3.116	3.207	C2An.2n		Lourens et al., 2004
3.330	3.596	C2An.3n		Lourens et al., 2004
4.187	4.300	C3n.1n, Cochiti		Lourens et al., 2004
4.493	4.631	C3n.2n, Nunivak		Lourens et al., 2004
4.799	4.896	C3n.3n, Sidufjall		Lourens et al., 2004
4.997	5.235	C3n.4n, Thvera		Lourens et al., 2004
6.033	6.252	C3An.1n		Lourens et al., 2004
6.436	6.733	C3An.2n		Lourens et al., 2004
7.140	7.212	C3Bn		Lourens et al., 2004
7.251	7.285	C3Br.1n		Lourens et al., 2004
7.454	7.489	C3Br.2n		Lourens et al., 2004
7.528	7.642	C4n.1n		Lourens et al., 2004
7.695	8.108	C4n.2n		Lourens et al., 2004
8.254	8.300	C4r.1n		Lourens et al., 2004
			C4r.2r-1	Lourens et al., 2004
8.769	9.098	C4An		Lourens et al., 2004
9.312	9.409	C4Ar.1n		Lourens et al., 2004
9.656	9.717	C4Ar.2n		Lourens et al., 2004
9.779	9.934	C5n.1n		Lourens et al., 2004
9.987	11.040	C5n.2n	C5n-2n-1, 2, 3	Lourens et al., 2004
11.118	11.154	C5r.1n		Lourens et al., 2004
11.554	11.614	C5r.2n		Lourens et al., 2004
12.014	12.116	C5An.1n		Lourens et al., 2004
12.207	12.415	C5An.2n		Lourens et al., 2004
12.730	12.765	C5Ar.1n		Lourens et al., 2004
12.820	12.878	C5Ar.2n		Lourens et al., 2004
13.015	13.183	C5AAn		Lourens et al., 2004
13.369	13.605	C5ABn		Lourens et al., 2004
13.734	14.095	C5ACn		Lourens et al., 2004
14.194	14.581	C5ADn		Lourens et al., 2004
14.784	14.877	C5Bn.1n		Lourens et al., 2004
15.032	15.160	C5Bn.2n		Lourens et al., 2004
15.974	16.268	C5Cn.1n		Lourens et al., 2004
16.303	16.472	C5Cn.2n		Lourens et al., 2004
16.543	16.721	C5Cn.3n		Lourens et al., 2004
17.235	17.533	C5Dn		Lourens et al., 2004
			C5Dr-1	Lourens et al., 2004
18.056	18.524	C5En		Lourens et al., 2004
18.748	19.722	C6n		Lourens et al., 2004
20.040	20.213	C6An.1n		Lourens et al., 2004
20.439	20.709	C6An.2n		Lourens et al., 2004
21.083	21.159	C6AAn		Lourens et al., 2004
21.403	21.483	C6AAr.1n		Lourens et al., 2004
21.659	21.688	C6AAr.2n		Lourens et al., 2004
21.767	21.936	C6Bn.1n		Lourens et al., 2004
21.992	22.268	C6Bn.2n		Lourens et al., 2004
22.564	22.754	C6Cn.1n		Lourens et al., 2004
22.902	23.030	C6Cn.2n		Lourens et al., 2004
23.278	23.340	C6Cn.3n		Pälike, 2006
			C6r-1	Pälike, 2006
24.022	24.062	C7n.1n		Pälike, 2006
24.147	24.459	C7n.2n		Pälike, 2006
			C7r-1	Pälike, 2006
24.756	24.984	C7An		Pälike, 2006
25.110	25.248	C8n.1n		Pälike, 2006
25.306	26.032	C8n.2n	C8n.2n-1	Pälike, 2006
26.508	27.412	C9n	C9n-1, 2	Pälike, 2006
			C9r-1	Pälike, 2006

Table T6 (continued).

Normal polarity interval age (Ma)		Polarity chron	Cryptochron	Reference
Top	Bottom			
27.886	28.126	C10n.1n		Pälike, 2006
28.164	28.318	C10n.2n		Pälike, 2006
			C10r-1, 2	Pälike, 2006
29.166	29.467	C11n.1n		Pälike, 2006
29.536	29.957	C11n.2n		Pälike, 2006
			C11r.1	Pälike, 2006
30.617	31.021	C12n		Pälike, 2006
			C12r-1, 2, 3, 4, 5, 6, 7, 8	Pälike, 2006
33.232	33.705	C13n	C13n-1	Pälike, 2006
			C13r-1, 2, 3, 4	Pälike, 2006
35.126	35.254	C15n		Pälike, 2006
35.328	35.554	C16n.1n		Pälike, 2006
35.643	36.355	C16n.2n		Pälike, 2006
36.668	37.520	C17n.1n		Pälike, 2006
37.656	37.907	C17n.2n		Pälike, 2006
37.956	38.159	C17n.3n		Pälike, 2006
38.449	39.554	C18n.1n		Pälike, 2006
39.602	40.084	C18n.2n		Pälike, 2006
41.358	41.510	C19n		Pälike, 2006
42.536	43.789	C20n		Cande and Kent, 1995
46.264	47.906	C21n		Cande and Kent, 1995
49.037	49.714	C22n		Cande and Kent, 1995
50.778	50.946	C23n.1n		Cande and Kent, 1995
51.047	51.743	C23n.2n		Cande and Kent, 1995
52.364	52.663	C24n.1n		Cande and Kent, 1995
52.757	52.801	C24n.2n		Cande and Kent, 1995
52.903	53.347	C24n.3n		Cande and Kent, 1995
			C24r-1, 2, 3, 4, 5, 6, 7, 8, 9, 10, 11	Cande and Kent, 1995
55.904	56.391	C25n		Cande and Kent, 1995
			C25r-1, 2, 3, 4, 5	Cande and Kent, 1995
57.554	57.911	C26n		Cande and Kent, 1995
			C26r-1, 2, 3, 4, 5, 6, 7	Cande and Kent, 1995
60.920	61.276	C27n		Cande and Kent, 1995
62.499	63.634	C28n		Cande and Kent, 1995
			C28r-1	Cande and Kent, 1995
63.976	64.745	C29n		Cande and Kent, 1995

Table T7. Shipboard paleomagnetism laboratory equipment. (See table note.)

Equipment	Status	Quality assessment
2G Enterprises 760R superconducting rock magnetometer	Used and functional	Magnetic moments for a 150 cm blank (air) after tray and background corrections is $<2 \times 10^{-10}$ Am^2. Magnetic field in sensor region is <8 nT.*
AGICO KappaBridge KLY-4S susceptibility meter	Used and functional	Used to measure bulk susceptibilities.
DTECH D-2000 alternating-field (AF) demagnetizer	Not used	Undetermined.
Schonstedt TSD-1 thermal demagnetizer	Used and functional	Thermal demagnetization experiments were conducted on 13 discrete samples.
ASC IM-10 impulse magnetizer (Serial 01971)	Tested and functional	Undetermined.
Applied Physics portable fluxgate magnetometer (model 520)	Tested and functional	Resolution <1 nT.*
Molspin minispin magnetometers (two)	Not used	Undetermined.

Note: * = from survey of the magnetic field inside the instrument and around the laboratory, completed during Expedition 320T.

Table T8. Mean values for reference interstitial water samples and IAPSO seawater. (See table notes.)

Sample	Value	Li^+ (μM)	B (μM)	Mg^{2+} (mM)	H_4SiO_4 (μM)	K^+ (mM)	Ca^{2+} (mM)	Mn^{2+} (μM)	Fe^{2+} (μM)	Sr^{2+} (μM)	Ba^{2+} (μM)
320-U1336B-2H-5	Expedition 320 value	23.2	440	49.0	325	ND	10.6	BD	BD	93.8	BD
	Expedition 321 mean (N = 3)	23.3	450	ND	558	ND	ND	BD	BD	103.5	BD
	Standard deviation	0.35	41.6		15.0					0.70	
	% RSD (1σ)	1.51	9.25		2.69					0.67	
320-U1336B-8H-3	Expedition 320 value	17.50	430.5	43.5	607	9.9	16.0	6.29	BD	177	BD
	Expedition 321 mean (N = 3)	16.56	453.4	ND	767	ND	ND	6.57	BD	208	BD
	Standard deviation	0.45	10.1		16.0			0.58		10.2	
	% RSD (1σ)	2.74	2.22		2.08			8.82		4.89	
320-U1336B-19H-3	Expedition 320 value	8.13	404.5	29.2	853	8.2	28.7	1.77	11.7	404	BD
	Expedition 321 mean (N = 2)	7.35	403	ND	985	ND	ND	1.98	11.6	462	BD
	Standard deviation	0.31	81		0.355			0.16	0.38	9.23	
	% RSD (1σ)	4.24	20		0.036			8.23	3.27	2.00	
IAPSO seawater	Expedition 321 mean (N = 7)	26.4	439	55.1	37.9	10.4	11.0	BD	BD	86.2	BD
	Standard deviation	1.15	36.3	1.51	2.81	0.08	0.16			1.32	
	% RSD (1σ)	4.34	8.27	2.75	7.42	0.82	1.50			1.53	

Notes: IAPSO = International Association for the Physical Sciences of the Ocean. RSD = relative standard deviation. ND = not determined, BD = below detection.

Table T9. Standards used for major and minor element bulk sediment geochemistry. (See table notes.)

Standard	Wavelength (nm)	BHVO-2-1	BIR-1-3	JR-2-3	NIST1C-1	SCO-1-3	STM-1-1
Major element oxide (%):							
SIO_2	251.611	49.85	47.77	75.65	6.84	62.78	59.64
Al_2O_3	308.215	13.53	15.35	12.82	1.3	13.67	18.39
Fe_2O_3 T	259.94	12.34	11.26	0.86	0.55	5.14	5.22
MnO_2	257.61	0.2	0.171	0.11	0.025	0.05	0.22
MgO	285.213	7.23	9.68	0.05	0.42	2.72	0.101
CaO	393.366 or 317.933	11.43	13.24	0.45	50.3	2.62	1.09
Na_2O	589.592	2.22	1.75	4.03	0.02	0.9	8.94
K_2O	766.491	0.52	0.027	4.45	0.28	2.77	4.28
TiO_2	337.28	2.73	0.96	0.09	0.07	0.628	0.135
P_2O_5	214.914	0.27	0.046	0.01	0.04	0.206	0.158
Trace element (ppm):							
Ba	455.403	130	*7*	39	*78*	570	560
Cr	267.716	289	382	2.6	*17.4*	68	4.3
Cu	324.754	136	126	1.4		28.7	4.6
Sc	361.383	31.8	44	5.57		10.8	0.61
Sr	421.552 or 407.771	389	108	8	254	174	700
V	292.401	317	0.01			131	8.7
Y	360.073	27.6	16	51.3		26	46
Zr	339.198	179	15.5	97.2	26	160	1210

Notes: Standard values from Govindaraju (1994) or GeoREM database (italic). During Expedition 321, wavelengths Ca 317.933 nm and Sr 407.771 nm were used for their larger linear dynamic ranges.

Table T10. Mean values for limestone reference materials analyzed by $LiBO_2$ flux method, Expedition 321. (See table notes.)

Analyte	Wavelength (nm)	CRM 393 reference value	CRM 393 mean (*N* = 7)	CRM 393 standard deviation	CRM 393 RSD % (1σ)	NIST 1c reference value	NIST 1c mean (*N* = 10)	NIST 1c standard deviation	NIST 1c RSD % (1σ)
Major element oxide (%):									
SiO_2	251.611	0.7	0.528	0.0124	2.36	6.84	7.93	0.366	4.62
Al_2O_3	308.215	0.12	0.152	0.00496	3.26	1.3	1.26	0.0184	1.46
Fe_2O_3 T	259.94	0.045	BD			0.55	0.675	0.0749	11.1
MnO_2	257.61	0.01	0.00792	0.000505	6.37	0.025	0.0223	0.00468	21.0
MgO	285.213	0.15	0.137	0.00446	3.25	0.42	0.383	0.00997	2.60
CaO	317.933	55.4	53.9	0.839	1.56	50.3	50.3	1.70	3.39
Na_2O	589.592					0.02	BD		
K_2O	769.897	0.02	BD			0.28	0.285	0.0252	8.85
TiO_2	337.28	0.009	BD			0.07	0.0320	0.0150	46.7
P_2O_5	214.914	0.006	BD			0.04	0.0488	0.0195	39.9
Trace element (ppm):									
Ba	455.403	53	BD			78	BD		
Cr	267.716					17.4	BD		
Sr	407.771	160	155	2.91	1.88	258	273	5.45	2.00
Y	360.073					4.1	BD		
Zr	339.198	2.4	BD			23	27.5	4.14	15.1

Notes: Reference values are certified or preferred values from GeoREM database. RSD = relative standard deviation. BD = below detection.

Table T11. Element/Ca ratios measured for NIST 1c limestone. (See table notes.)

	Ratio (mM/M)		
	Mg/Ca	Mn/Ca	Fe/Ca
Mean Expedition 321 (*N* = 7)	5.58	0.261	1.66
Standard deviation (1σ)	0.09	0.004	0.07
RSD %	1.68	1.69	4.17
Kryc et al. (2003)	Not available	0.218	1.28

Notes: RSD = relative standard deviation. NIST = National Institute of Standards and Technology (U.S.).

Table T12. Wireline tool string downhole measurements, Expedition 320/321. (See table notes.)

Tool string	Tool	Measurement	Sampling interval (cm)	Approximate vertical resolution (cm)
Triple combination and paleo combination	HNGS	Spectral gamma ray	15	51
	GPIT	Tool orientation	0.25 and 15	NA
	HLDS	Bulk density	2.5 and 15	38/46
	DIT*	Resistivity	15	200/150/76
	MSS*	Magnetic susceptibility	5	40/10
Formation MicroScanner-sonic	HNGS	Spectral gamma ray	15	51
	GPIT	Tool orientation	0.25 and 15	NA
	FMS	Microresistivity	1.25	0.5
	DSI	Acoustic velocity	15	107
Versatile Seismic Imager	VSI	Seismic waveforms	Stations at 15 m	NA
	SGT-N	Total gamma ray	15	30

Notes: All tool and tool string names (except MSS) are trademarks of Schlumberger. * = not included in every logging run. NA = not applicable. For definitions of tool acronyms, see Table T13.

Table T13. Acronyms and units used for downhole wireline tools and measurements. (See table notes.)

Tool	Output	Explanation	Unit
DIT-E		Dual Induction Tool	
	IDPH	Deep induction resistivity	Ω·m
	IMPH	Medium induction resistivity	Ω·m
	SFLU	Spherically focused resistivity	Ω·m
DSI		Dipole Sonic Imager	
	DTCO	Compressional wave delay time (Δt)	ms/ft
	DTSM	Shear wave delay time (Δt)	ms/ft
	DTST	Stoneley wave delay time (Δt)	ms/ft
FMS		Formation MicroScanner	
	C_1, C_2	Orthogonal hole diameters	inch
	P1AZ	Pad 1 azimuth	°
		Spatially oriented resistivity images of borehole wall	
GPIT		General Purpose Inclinometer Tool	
	DEVI	Hole deviation	°
	HAZI	Hole azimuth	°
	F_x, F_y, F_z	Earth's magnetic field (three orthogonal components)	Oe
	A_x, A_y, A_z	Acceleration (three orthogonal components)	m/s^2
HLDS		Hostile Environment Litho-Density Sonde	
	RHOM	Bulk density	g/cm^3
	PEFL	Photoelectric effect	b/e^-
	LCAL	Caliper (measure of borehole diameter)	inch
	DRH	Bulk density correction	g/cm^3
HNGS		Hostile Environment Gamma Ray Sonde	
	HSGR	Standard (total) gamma ray	gAPI
	HCGR	Computed gamma ray (HSGR minus uranium contribution)	gAPI
	HFK	Potassium (K)	wt%
	HTHO	Thorium (Th)	ppm
	HURA	Uranium (U)	ppm
MGT		Multi-Sensor Spectral Gamma Ray Tool	
	GR	Total gamma radiation	gAPI
MSS		Magnetic Susceptibility Sonde	
	MSSLSUS	Magnetic susceptibility, low resolution	SI units
	MSSHSUS	Magnetic susceptibility, high resolution	SI units
	MSSLCON	Electrical conductivity	SI units
SGT-N		Scintillation Gamma Ray Tool	
	GR	Total gamma ray	gAPI
	ECGR	Environmentally corrected gamma ray	gAPI
	EHGR	High-resolution environmentally corrected gamma ray	gAPI

Notes: For the complete list of acronyms used in IODP and for additional information about tool physics, consult IODP-USIO Science Services, LDEO, at iodp.ldeo.columbia.edu/TOOLS_LABS/tools.html.